Fracture Mechanics

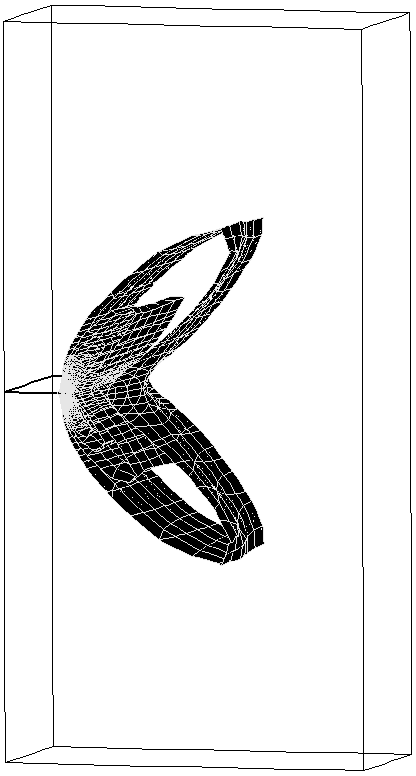

Dr.ir. P.J.G. Schreurs

Mechanical Engineering

Fracture Mechanics

Lecture notes - course 4A780

Dr.ir. P.J.G. Schreurs

Eindhoven University of Technology
Department of Mechanical Engineering
Materials Technology
August 28, 2014

Contents

Chapter 1

Introduction

Important aspects of technological and biological structures are stiffness and strength. Requirements on stiffness, being the resistance against reversible deformation, may vary over a wide range. Strength, the resistance against irreversible deformation, is always required to be high, because this deformation may lead to loss of functionality and even global failure.

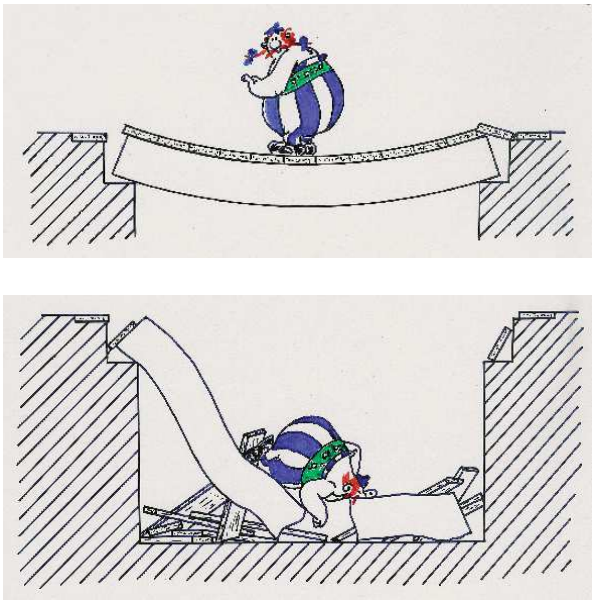

Fig. 1.1 : *Stiffness and strength.*

Continuum mechanics

When material properties and associated mechanical variables can be assumed to be continuous functions of spatial coordinates, analysis of mechanical behavior can be done with *Continuum Mechanics*. This may also apply to permanent deformation, although this is associated with structural changes, e.g. phase transformation, dislocation movement, molecular slip and breaking of atomic bonds. The only requirement is that the material behavior is studied on a scale, large enough to allow small scale discontinuities to be averaged out.

When a three-dimensional continuum is subjected to external loads it will deform. The strain components, which are derived from the displacements u_i $(i = 1, 2, 3)$ by differentiation – $(\ )_{,j}$ – with respect to spatial coordinates x_j $(j = 1, 2, 3)$, are related by the compatibility relations.

The stress components σ_{ij} $(i, j = 1, 2, 3)$ must satisfy the equilibrium equations – partial differential equations – and boundary conditions.

In most cases the equilibrium equations are impossible to solve without taking into account the material behavior, which is characterized by a material model, relating stress components σ_{ij} to strain components ε_{kl} $(k, l = 1, 2, 3)$.

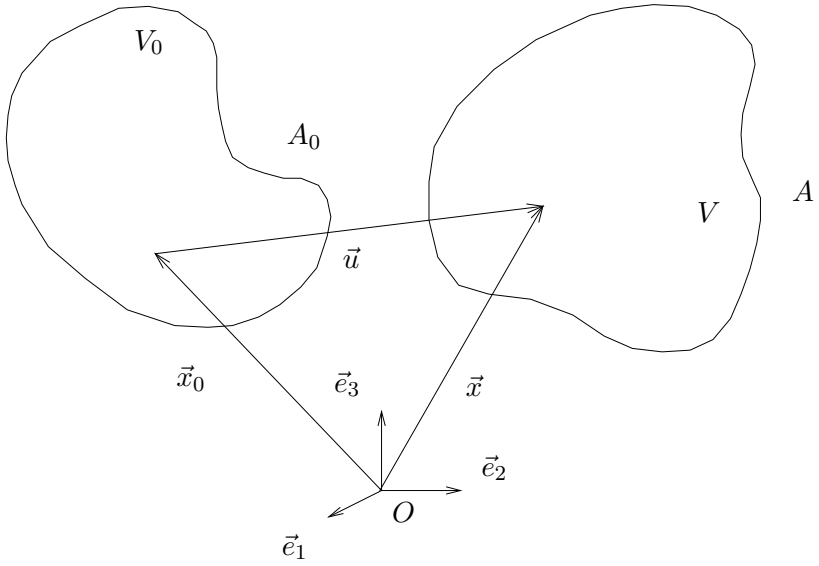

Fig. 1.2 : *Deformation of a continuum.*

- volume / area $V_0, V \ / \ A_0, A$
- base vectors $\{\vec{e}_1, \vec{e}_2, \vec{e}_3\}$
- position vector $\vec{x}_0, \vec{x}$

- displacement vector $\vec{u}$
- strains $\varepsilon_{kl} = \frac{1}{2}(u_{k,l} + u_{l,k})$
- compatibility relations

- equilibrium equations $\sigma_{ij,j} + \rho q_i = 0 \quad ; \quad \sigma_{ij} = \sigma_{ji}$
- density ρ
- load/mass q_i
- boundary conditions $p_i = \sigma_{ij} n_j$

- material model $\sigma_{ij} = N_{ij}(\varepsilon_{kl})$

Material behavior

To investigate, model and characterize the material behavior, it is necessary to do experiments. The most simple experiment is the tensile/compression loading of a tensile bar.

Strain-time and stress-time curves reveal much information about the material behavior, which can be concluded to be elastic : reversible, time-independent; visco-elastic : reversible, time-dependent; elasto-plastic : irreversible, time-independent; visco-plastic : irreversible, time-dependent; damage : irreversible, decreasing properties.

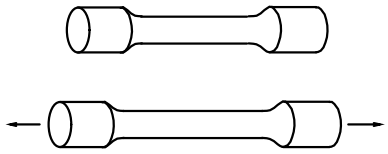

Fig. 1.3 : *Tensile test.*

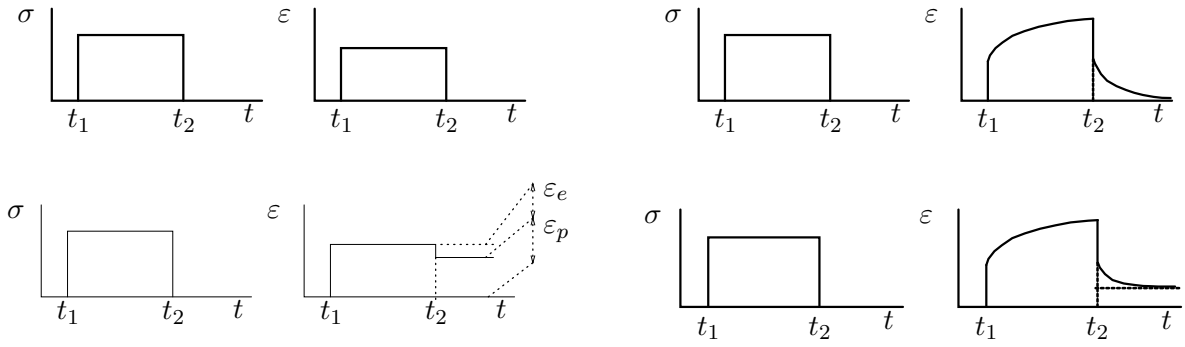

Fig. 1.4 : *Stress excitation and strain response as function of time: elastic, visco-elastic, elasto-plastic, visco-plastic.*

Stress-strain curves may show linear, nonlinear, hardening and softening behavior.

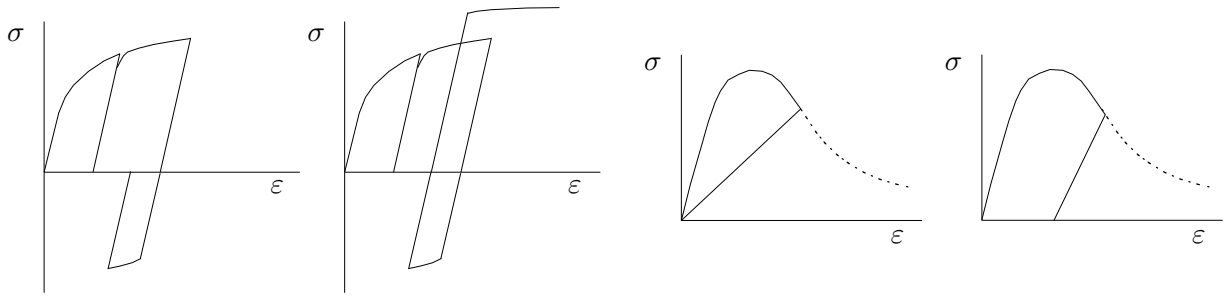

Fig. 1.5 : *Stress-strain curves for hardening (left) and softening (right) material behavior.*

Fracture

When material damage like micro-cracks and voids grow in size and become localized, the averaging procedure can no longer be applied and discontinuities must be taken into account. This localization results in a macroscopic crack, which may grow very fast, resulting in global failure.

Although early approaches have striven to predict fracture by analyzing the behavior of atomic bonds, Griffith has shown in 1921 that attention should be given to the behavior of an existing crack.

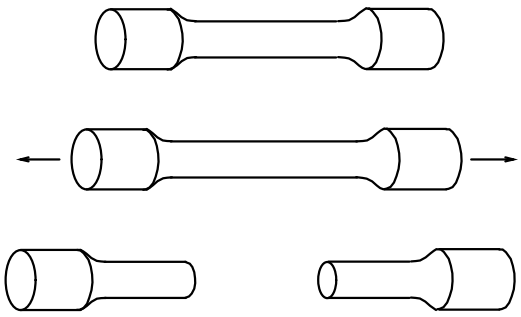

Fig. 1.6 : *Tensile test with axial elongation and fracture.*

Fracture mechanics

In fracture mechanics attention is basically focused on a single crack. Theoretical concepts and experimental techniques have been and are being developed, which allow answers to questions like:

- Will a crack grow under the given load ?
- When a crack grows, what is its speed and direction ?
- Will crack growth stop ?
- What is the residual strength of a construction (part) as a function of the (initial) crack length and the load ?
- What is the proper inspection frequency ?
- When must the part be repaired or replaced ?

Several fields of science are involved in answering these questions : material science and chemistry, theoretical and numerical mathematics, experimental and theoretical mechanics. As a result, the field of fracture mechanics can be subdivided in several specializations, each with its own concepts, theory and terminology.

Fig. 1.7 : *Crack in a bicycle crank.*
(Source: internet)

Experimental fracture mechanics

Detection of cracks is done by experimental techniques, ranging from simple and cheap to sophisticated and expensive. *Experimental Fracture Mechanics* (EFM) is about the use and development of hardware and procedures, not only for crack detection, but, moreover, for the accurate determination of its geometry and loading conditions.

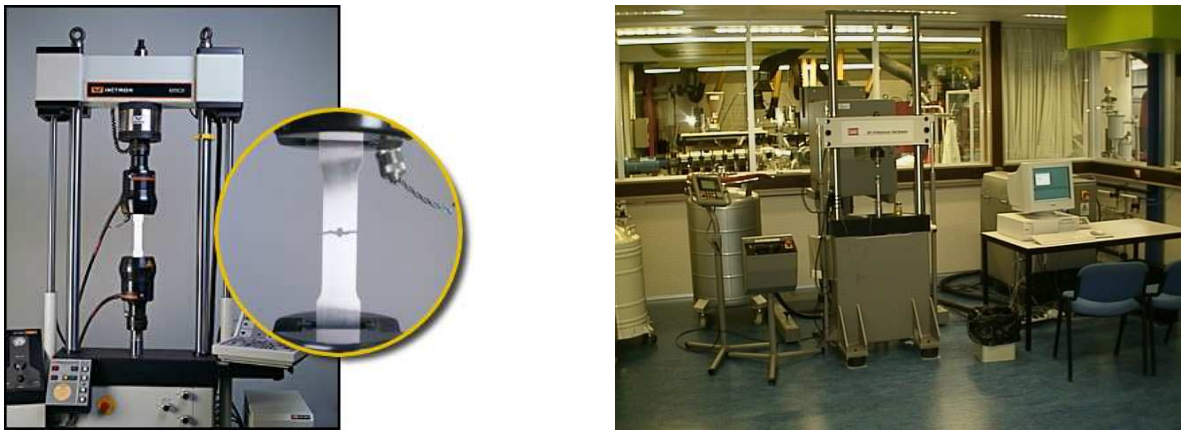

Fig. 1.8 : *Experimental tensile equipment.*
(Source: Internet)

Linear elastic fracture mechanics

A large field of fracture mechanics uses concepts and theories in which linear elastic material behavior is an essential assumption. This is the case for *Linear Elastic Fracture Mechanics* (LEFM).

Prediction of crack growth can be based on an energy balance. The *Griffith criterion* states that "crack growth will occur, when there is enough energy available to generate new

crack surface." The *energy release rate* is an essential quantity in energy balance criteria. The resulting crack growth criterion is referred to as being *global*, because a rather large volume of material is considered.

The crack growth criterion can also be based on the stress state at the crack tip. This stress field can be determined analytically. It is characterized by the *stress intensity factor*. The resulting crack growth criterion is referred to as *local*, because attention is focused at a small material volume at the crack tip.

Assumption of linear elastic material behavior leads to infinite stresses at the crack tip. In reality this is obviously not possible: plastic deformation will occur in the crack tip region. Using yield criteria (Von Mises, Tresca), the crack tip plastic zone can be determined. When this zone is small enough (*Small Scale Yielding*, SSY), LEFM concepts can be used.

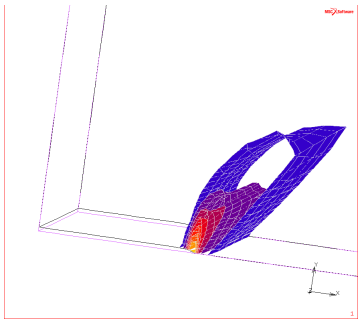

Fig. 1.9 : *Plastic strain zone at the crack tip.*

Dynamic fracture mechanics

It is important to predict whether a crack will grow or not. It is also essential to predict the speed and direction of its growth. Theories and methods for this purpose are the subject of *Dynamic Fracture Mechanics* (DFM).

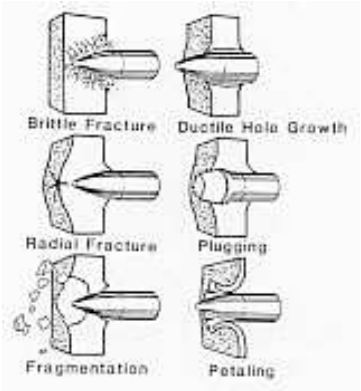

Fig. 1.10 : *Impact of a bullet in a plate [39].*

Nonlinear fracture mechanics

When the plastic crack tip zone is too large, the stress and strain fields from LEFM are not valid any more. This is also the case when the material behavior is nonlinear elastic (e.g. in polymers and composites). Crack growth criteria can no longer be formulated with the stress intensity factor.

In *Elastic-Plastic Fracture Mechanics* (EPFM) or *Non-Linear Fracture Mechanics* (NLFM) criteria are derived, based on the *Crack Tip Opening Displacement*. Its calculation is possible using models of Irwin or Dugdale-Barenblatt for the crack tip zone.

Another crack growth parameter, much used in NLFM, is the *J-integral*, which characterizes the stress/deformation state in the crack tip zone.

Numerical techniques

Analytical calculation of relevant quantities is only possible for some very simple cases. For more practical cases numerical techniques are needed. Numerical calculations are mostly done using the *Finite Element Method* (FEM). Special *quarter-point crack tip elements* must be used to get accurate results.

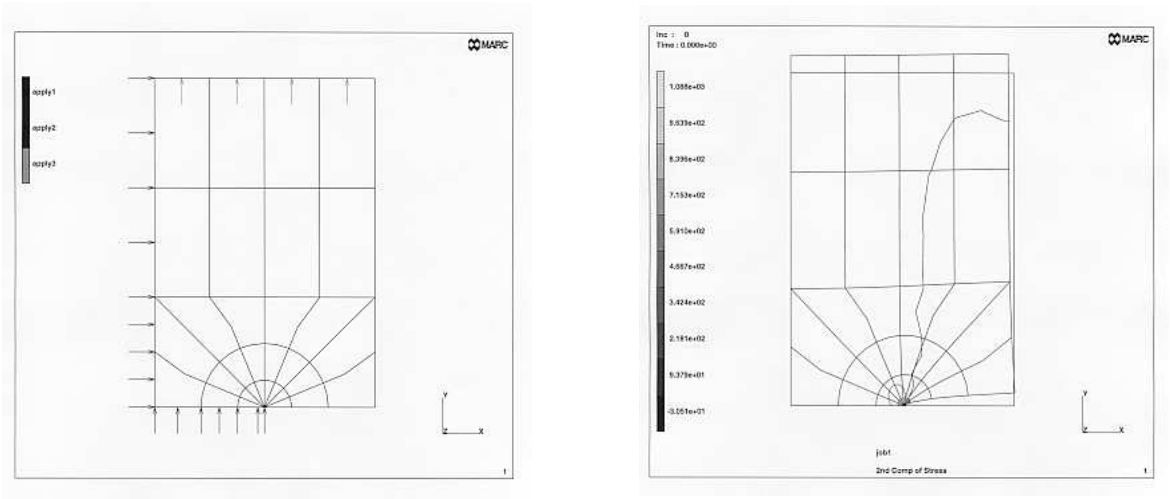

Fig. 1.11 : *Loading and deformation of a cracked plate.*
(A quarter of the plate is modeled and shown.)

Fatigue

When a crack is subjected to a time-dependent load, be it harmonic or random, the crack will gradually grow, although the load amplitude is very small. This phenomenon is called *Fatigue Crack Propagation* (FCP) and may unexpectedly and suddenly result in *Fatigue Failure.*

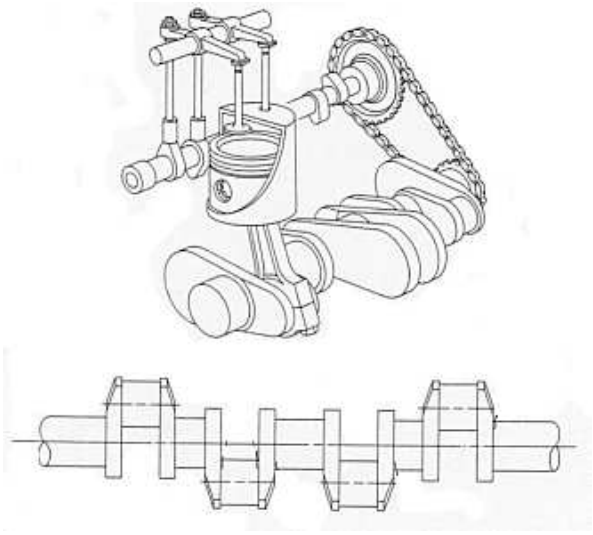

Fig. 1.12 : *Engine and crank axis.*

Outline

Many books and papers on fracture mechanics and fatigue exist, a lot of which are rather intimidating for a first reader, because they are either too specialized and/or lack a proper introduction of concepts and variables. This is partly due to the fact that Fracture Mechanics has developed into many specialized subjects, all focused on different applications. In this course a number of these subjects are discussed, with an emphasis on a clear introduction of concepts and derivation of variables. The main goal is to give an overview of the whole field. For more detail, the reader is referred to the specialized publications, some of which can be found in the *References*.

Chapter 2

Fracture mechanics

In this chapter we first discuss some mechanisms, which can be recognized after fracture has occurred. They are generally related to the amount of dissipated energy during crack growth and therefore to ductile or brittle fracture. The theoretical strength of a material can be predicted from the maximum bond strength between atoms. The result of these very approximating calculations appears to be not in accordance with experimental findings. Griffith was the first to recognize that attention must be focused to imperfections like already existing cracks. Fracture Mechanics is thus started with the experimental studies by Griffith in 1921 and has since then developed in various directions.

2.1 Fracture mechanisms

The way a crack propagates through the material is indicative for the fracture mechanism. Visual inspection of the fracture surface gives already valuable information. The next mechanisms are generally distinguished.

- shear fracture
- cleavage fracture
- fatigue fracture
- crazing
- de-adhesion

2.1.1 Shearing

When a crystalline material is loaded, dislocations will start to move through the lattice due to local shear stresses. Also the number of dislocations will increase. Because the internal structure is changed irreversibly, the macroscopic deformation is permanent (plastic). The dislocations will coalesce at grain boundaries and accumulate to make a void. These voids will grow and one or more of them will transfer in a macroscopic crack. One or more cracks may then grow and lead to failure.

Because the origin and growth of cracks is provoked by shear stresses, this mechanism is referred to as *shearing*. Plastic deformation is essential, so this mechanism will generally be observed in FCC crystals, which have many closed-packed planes.

The fracture surface has a 'dough-like' structure with dimples, the shape of which indicate the loading of the crack. For some illustrative pictures, we refer to the book of Broek [10].

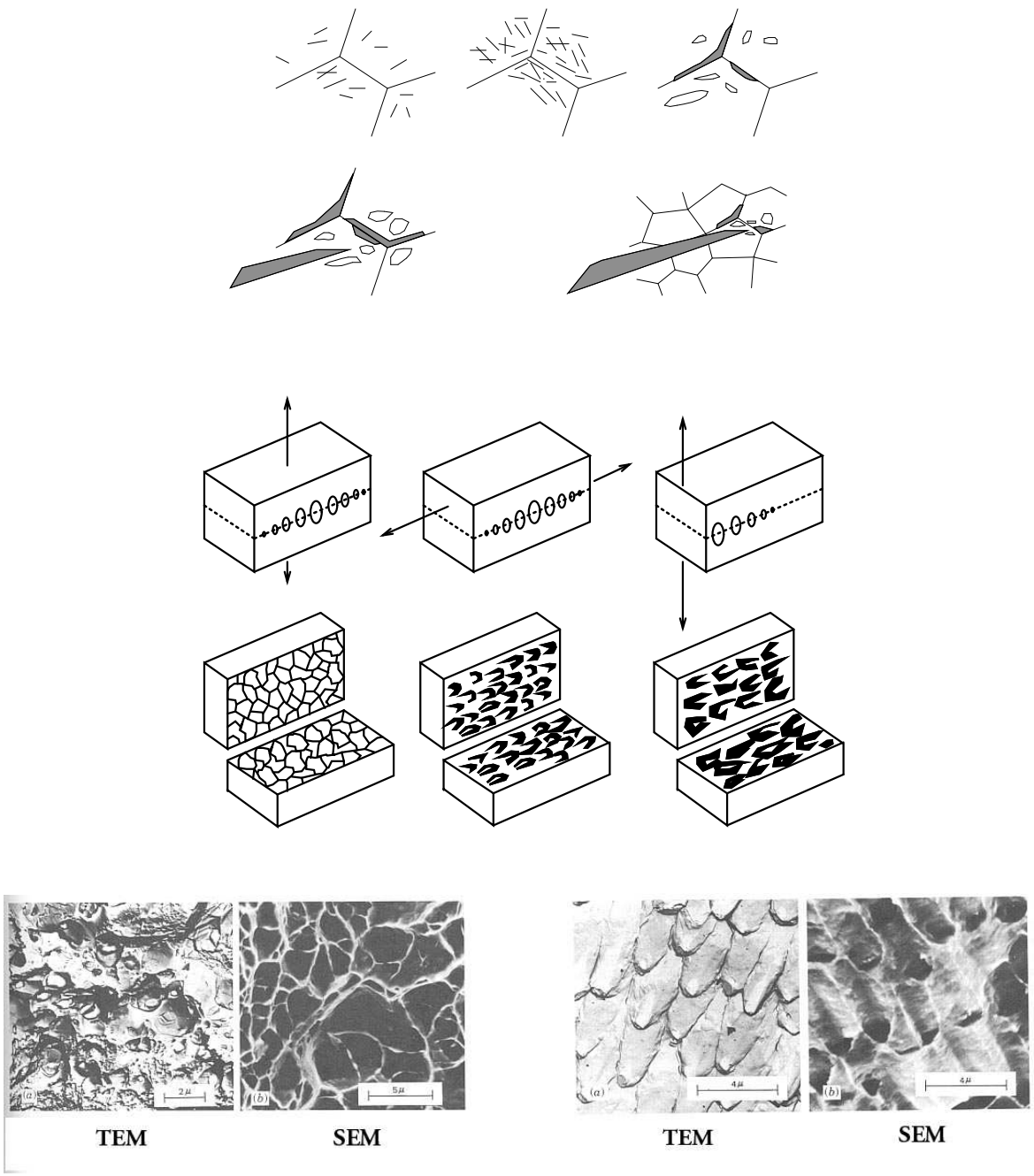

Fig. 2.1 : *Dislocation movement and coalescence into grain boundary voids, resulting in dimples in the crack surface [30].*

2.1.2 Cleavage

When plastic deformation at the crack tip is prohibited, the crack can travel through grains by splitting atom bonds in lattice planes. This is called *intra- or trans-granular cleavage*. When the crack propagates along grain boundaries, it is referred to as *inter-granular cleavage*.

This cleavage fracture will prevail in materials with little or no closed-packed planes, having HCP or BCC crystal structure. It will also be observed when plastic deformation is prohibited due to low temperature or high strain rate. As will be described later, a three-dimensional stress state may also result in this mechanism.

Inter-granular cleavage will be found in materials with weak or damaged grain boundaries. The latter can be caused by environmental influences like hydrogen or high temperature.

The crack surface has a 'shiny' appearance. The discontinuity of the lattice orientations in neighboring grains will lead to so-called cleavage steps, which resemble a 'river pattern'. Nice pictures can be found in [11].

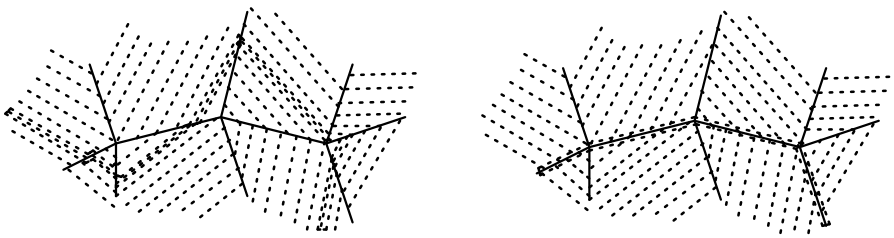

Fig. 2.2 : *Inter- and intra-granular cleavage fracture.*

2.1.3 Fatigue

When a crack is subjected to cyclic loading, the crack tip will travel a very short distance in each loading cycle, provided that the stress is high enough, but not too high to cause sudden global fracture. With the naked eye we can see a 'clam shell' structure in the crack surface. Under a microscope 'striations' can be seen, which mark the locations of the crack tip after each individual loading cycle.

This mechanism is referred to as *fatigue*. Because crack propagation is very small in each individual load cycle, a large number of cycles is needed before total failure occurs. The number of cycles to failure N_f is strongly related to the stress amplitude $\Delta\sigma = \frac{1}{2}(\sigma_{max} - \sigma_{min})$ and the average stress $\sigma_m = \frac{1}{2}(\sigma_{max} + \sigma_{min})$.

Nice pictures of macroscopic and microscopic fatigue crack surfaces can again be found in [11].

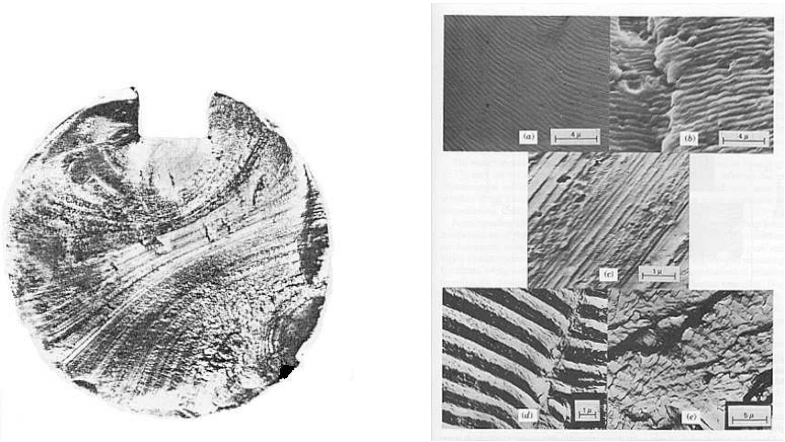

Fig. 2.3 : *Clam shell fatigue crack surface and striations [30].*

2.1.4 Crazing

In a polymer material sub-micrometer voids may initiate when a critical load level is exceeded. Sometimes, one or a limited number of these *crazes* grow locally to generate a large and fatal crack. In other circumstances the crazes spread out over a larger area. This is indicated as "stress whitening", because the crazes refract the light, resulting in a white colored appearance. Some nice pictures of crazes can be found in [29].

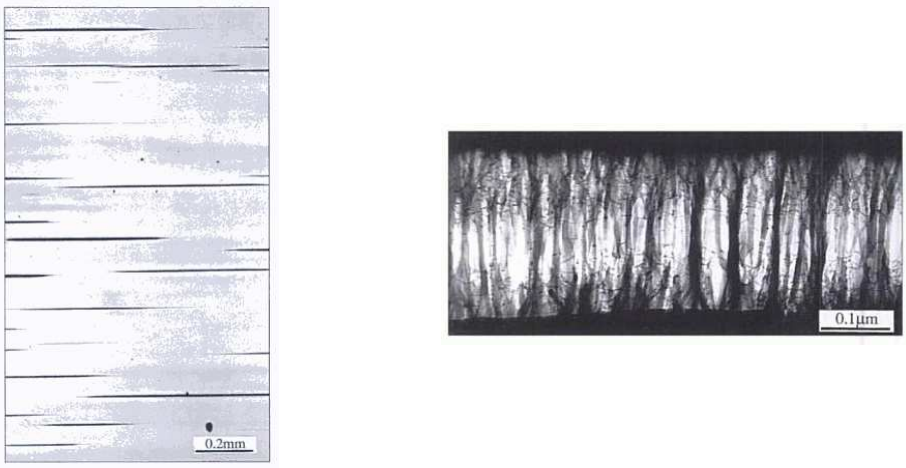

Fig. 2.4 : *Crazes in polystyrene on a macroscopic and microscopic scale. (Source: Internet)*

2.1.5 De-adhesion

Adhesion refers to bonding between atoms of different materials, while cohesion refers to bonding between atoms of one and the same material. Applications include the joining of two different entities such as structural parts and the adhesion of a generally thin layer on a generally thicker substrate. In the latter case the thin layer is also often referred to as surface layer, thin film or coating.

Surface layers may be metallic – metals (M) and their nitrides (MNx) or oxides (MOx) –, anorganic – oxides, carbides, diamond – or organic – polymers. Thicknesses vary from several nanometers to hundreds of micrometers. Substrates can also be metallic – metals and alloys –, anorganic – ceramics, glass – and organic.

The adhesion of the layer to the substrate is determined by chemical bond strength and highly influenced by initial stresses and damage in the surface layer and the roughness of the substrate. Initial residual stresses can be classified as thermal , due to solidification and cooling , and mechanical , due to volume mismatch (penetration) and plastic strain (impact). The adhesion strength can be characterized by the maximum normal strength, the maximum tangential strength or the work needed for separation. Many experimental techniques are available to determine these parameters. Modeling of the adhesion strength is often done with *cohesive zone* (CZ) models, where the mentioned parameters play an important role.

2.2 Ductile - brittle behavior

When a crack propagates, new free surface is generated, having a specific surface energy γ, which for solid materials is typically 1 [Jm^{-2}]. This energy is provided by the external load and is also available as stored elastic energy. Not all available energy, however, is used for the generation of new crack surfaces. It is also transformed into other energies, like kinetic energy or dissipative heat. When a lot of available energy is used for crack growth, the fracture is said to be *brittle*. When a lot of energy is transformed into other energies, mainly due to dissipative mechanisms, the fracture is indicated to be *ductile*.

Although boundary and environmental conditions are of utmost importance, it is common practice to say that a certain material is brittle or ductile. A first indication of this follows from the stress-strain curve, registered in a tensile test up to fracture of the tensile bar. The area under the curve is a measure for the dissipated energy before failure. Tensile curves for a variety of materials are shown in the figure.

Because dissipation is associated with plastic deformation, shear fracture is often found in materials which show ductile fracture. When plastic deformation and thus dissipation is less, fracture is more brittle.

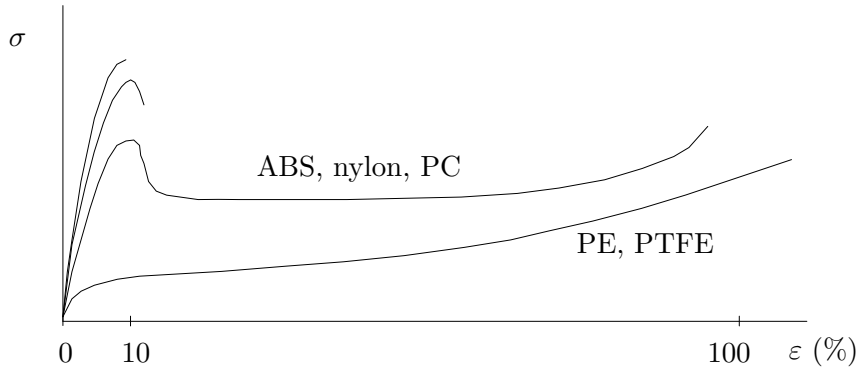

Fig. 2.5 : *Tensile test up to fracture and various stress-strain curves.*

2.2.1 Charpy v-notch test

Although the tensile stress-strain curve already provides an indication for brittle/ductile failure, the standard experiment to investigate this is the Charpy V-notch test. The main advantage of this test is that it provides a simple measure for the dissipated energy during fast crack propagation.

The specimen is a beam with a 2 mm deep V-shaped notch, which has a 90^o angle and a 0.25 mm root radius. It is supported and loaded as in a three-point bending test. The load is provided by the impact of a weight at the end of a pendulum. A crack will start at the tip of the V-notch and runs through the specimen. The material deforms at a strain rate of typically 10^3 s^{-1}. The energy which is dissipated during fracture can be calculated easily from the height of the pendulum weight, before and after impact. The dissipated energy is the *Impact Toughness* C_v [J].

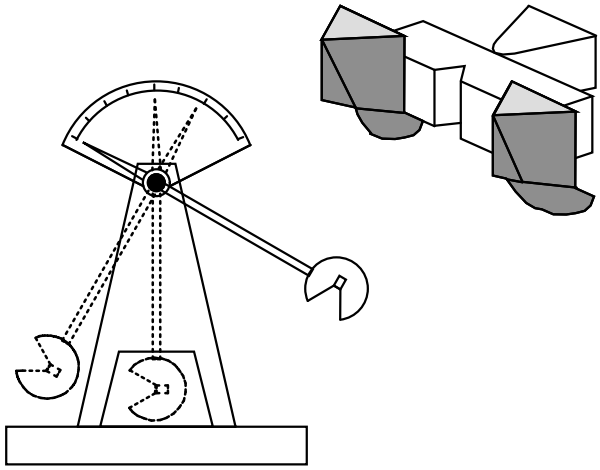

Fig. 2.6 : *Charpy V-notch test.*

The impact toughness can be determined for various specimen temperatures T. For intrinsic brittle materials like high strength steel, the dissipated energy will be low for all T. For intrinsic ductile materials like FCC-metals, C_v will be high for all T. A large number of materials show a transition from brittle to ductile fracture with increasing temperature. The transition trajectory is characterized by three temperatures :

NDT : Nil Ductility Temperature
FATT : Fracture Appearance Transition Temperature (T_t)
FTP : Fracture Transition Plastic

As a rule of thumb we have for BCC alloys $T_t = 0.1$ à $0.2T_m$ and for ceramics $T_t = 0.5$ à $0.7T_m$, where T_m is the melting temperature.

More on the Charpy test can be found in [29]. Other tests to determine the brittleness are the Izod test and Drop Weight Test.

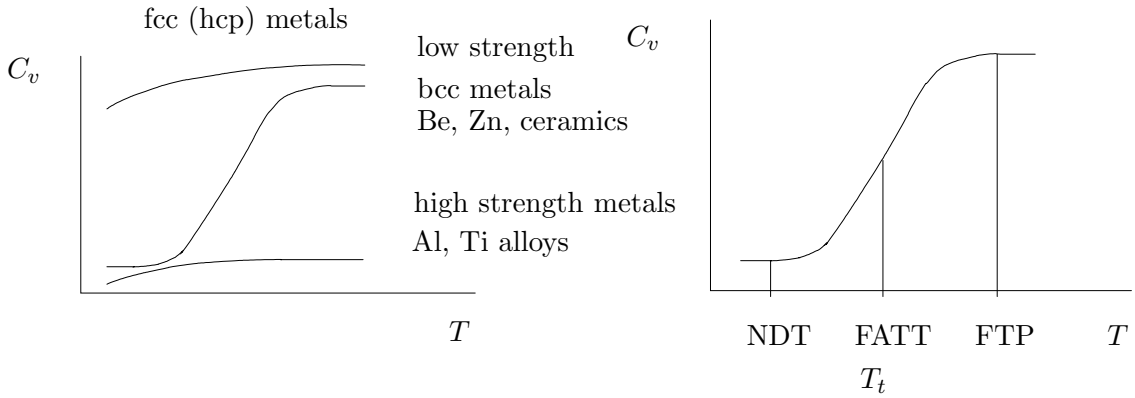

Fig. 2.7 : *C_v-values as a function of temperature T.*

2.3 Theoretical strength

Metal alloys consist of many crystals, each of which has lattice planes in a certain spatial orientation. In a first attempt to calculate the strength of such a crystalline material, one atomic plane perpendicular to the tensile load is considered. The bonding force f between two atoms in two neighboring planes depends on their distance r and can be calculated from a potential. The interaction force can be approximated by a sine function, using the equilibrium distance a_0, the half wavelength λ and the maximum force f_{max}. With this approximation, the interaction force is zero and the bond is broken, when $r = a_0 + \frac{1}{2}\lambda$.

The interaction force between all atoms in an area S of the two lattice planes can be calculated by addition. The stress σ, which is the ratio of this total force and the area S, can be expressed in the maximum stress σ_{max}, being the theoretical material strength.

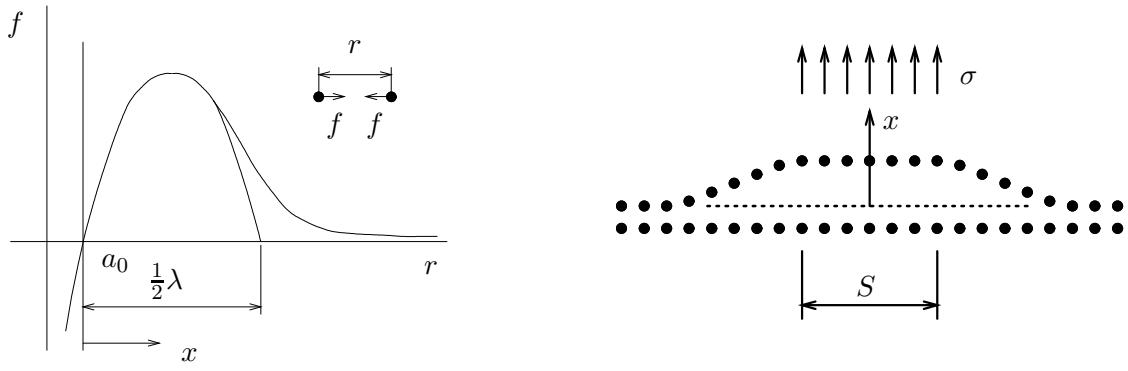

Fig. 2.8 : *Atomic bond strength between atom in a lattice.*

$$f(x) = f_{max} \sin\left(\frac{2\pi x}{\lambda}\right) \quad ; \quad x = r - a_0$$

$$\sigma(x) = \frac{1}{S}\sum f(x) = \sigma_{max}\sin\left(\frac{2\pi x}{\lambda}\right)$$

The theoretical strength σ_{max} can be determined from an energy balance. When the interaction force and thus the inter-atomic distance increases, elastic energy is stored in each bond. When the bond breaks at $x = \lambda/2$, the stored energy is released. The stored elastic energy per unit of area is U_i and can be calculated by integration.

It is assumed that all bonds in the area S snap at the same time and that all the stored energy is transformed in surface energy, which, per unit of area is $U_a = 2\gamma$, with γ the specific surface energy of the material.

From the energy balance $U_i = U_a$, the wave length of the sine function can be calculated and the stress as a function of the displacement x can be expressed in σ_{max}.

available elastic energy per surface-unity [N m^{-1}]

$$U_i = \frac{1}{S}\int_{x=0}^{x=\lambda/2}\sum f(x)\,dx = \int_{x=0}^{x=\lambda/2}\sigma_{max}\sin\left(\frac{2\pi x}{\lambda}\right)dx = \sigma_{max}\frac{\lambda}{\pi} \qquad [\mathrm{Nm}^{-1}]$$

required surface energy

$$U_a = 2\gamma \qquad [\mathrm{Nm}^{-1}]$$

energy balance at fracture

$$U_i = U_a \quad \rightarrow \quad \lambda = \frac{2\pi\gamma}{\sigma_{max}} \quad \rightarrow \quad \sigma = \sigma_{max}\sin\left(\frac{x}{\gamma}\sigma_{max}\right)$$

The argument of the sine function is assumed to be small enough to allow a linear approximation. The displacement x between the atomic planes is expressed in the linear strain ε. The macroscopic Young's modulus E of the material is introduced as the derivative of the stress w.r.t. the linear strain in the undeformed state. This leads to a relation for the theoretical strength $\sigma_{th} = \sigma_{max}$.

linearization

$$\sigma = \sigma_{max}\sin\left(\frac{x}{\gamma}\sigma_{max}\right) \approx \frac{x}{\gamma}\,\sigma_{max}^2$$

linear strain of atomic bond

$$\varepsilon = \frac{x}{a_0} \quad \rightarrow \quad x = \varepsilon a_0 \quad \rightarrow \quad \sigma = \frac{\varepsilon a_0}{\gamma}\sigma_{max}^2$$

elastic modulus

$$E = \left(\frac{d\sigma}{d\varepsilon}\right)\Big|_{x=0} = \left(\frac{d\sigma}{dx}\,a_0\right)\Big|_{x=0} = \sigma_{max}^2\,\frac{a_0}{\gamma} \quad \rightarrow \quad \sigma_{max} = \sqrt{\frac{E\gamma}{a_0}}$$

theoretical strength $\sigma_{th} = \sqrt{\frac{E\gamma}{a_0}}$

2.3.1 Discrepancy with experimental observations

The surface energy γ does not differ much for various solid materials and approximately equals 1 Jm^{-2}. (Diamond is an exception with $\gamma = 5$ Jm^{-2}.) The equilibrium distance a_0 between atoms, is also almost the same for solids (about 10^{-10} m).

The table below lists values of theoretical strength and experimental fracture stress for some materials. It is clear that there is a large discrepancy between the two values : the theoretical strength is much too high. The reason for this deviation has been discovered by Griffith in 1921.

	a_0 [m]	E [GPa]	σ_{th} [GPa]	σ_b [MPa]	σ_{th}/σ_b
glass	$3 * 10^{-10}$	60	14	170	82
steel	10^{-10}	210	45	250	180
silica fibers	10^{-10}	100	31	25000	1.3
iron whiskers	10^{-10}	295	54	13000	4.2
silicon whiskers	10^{-10}	165	41	6500	6.3
alumina whiskers	10^{-10}	495	70	15000	4.7
ausformed steel	10^{-10}	200	45	3000	15
piano wire	10^{-10}	200	45	2750	16.4

$$\sigma_{th} \gg \sigma_b$$

2.3.2 Griffith's experiments

In 1921 Griffith determined experimentally the fracture stress σ_b of glass fibers as a function of their diameter. For $d > 20$ μm the bulk strength of 170 MPa was found. However, σ_b approached the theoretical strength of 14000 MPa in the limit of zero thickness.

Griffith new of the earlier (1913) work of Inglis [32], who calculated stress concentrations at circular holes in plates, being much higher than the nominal stress. He concluded that in his glass fibers such stress concentrations probably occurred around defects and caused the discrepancy between theoretical and experimental fracture stress. He reasoned that for glass fibers with smaller diameters, there was less volume and less chance for a defect to exist in the specimen. In the limit of zero volume there would be no defect and the theoretical strength would be found experimentally. Griffith published his work in 1921 and his paper [28] can be seen as the birth of Fracture Mechanics. It was shown in 1976 by Parratt, March en Gordon, that surface defects instead of volume defects were the cause for the limiting strength.

The ingenious insight that strength was highly influenced by defects has lead to the shift of attention to the behavior of cracks and the formulation of crack growth criteria. Fracture Mechanics was born!

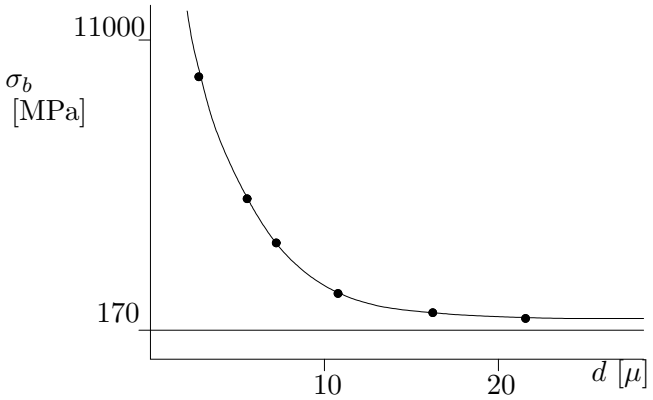

Fig. 2.9 : *Fracture strength of glass fibers in relation to their thickness.*

2.3.3 Crack loading modes

Irwin was one of the first to study the behavior of cracks. He introduced three different loading modes, which are still used today [33].

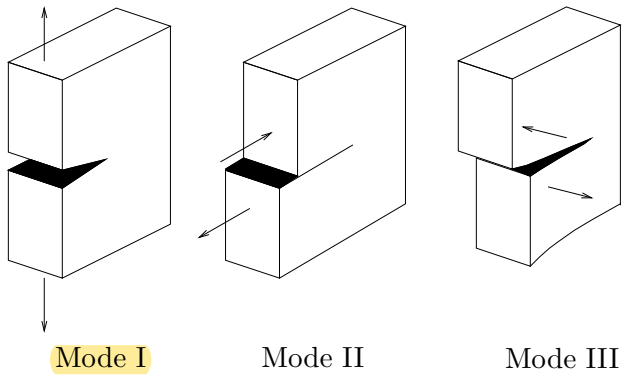

Fig. 2.10 : *Three standard loading modes of a crack.*

Mode I	=	opening mode
Mode II	=	sliding mode
Mode III	=	tearing mode

Chapter 3

Experimental techniques

To predict the behavior of a crack, it is essential to know its location, geometry and dimensions. Experiments have to be done to reveal these data.

Experimental techniques have been and are still being developed. Some of these procedures use physical phenomena to gather information about a crack. Other techniques strive towards visualization of the crack.

3.1 Surface cracks

One of the most simple techniques to reveal surface cracks is based on dye penetration into the crack due to capillary flow of the dye. Although it can be applied easily and on-site, only surface cracks can be detected.

Other simple procedures are based on the observation of the disturbance of the magnetic or electric field, caused by a crack. Magnetic fields can be visualized with magnetic particles and electric fields by the use of inertances. Only cracks at or just below the surface can be detected in this way.

Fig. 3.1 : *Dye penetration in the stiffening cone of a turbine.*
(Source: Internet site www.venti-oelde.de (2009))

3.2 Electrical resistance

A crack is a discontinuity in the material and as such diminishes the cross-sectional area. This may be associated with an increase of the electrical resistance, which can be measured for metallic materials and carbon composites.

3.3 X-ray

Direct visualization of a crack can be done using electromagnetic waves. X-rays are routinely used to control welds.

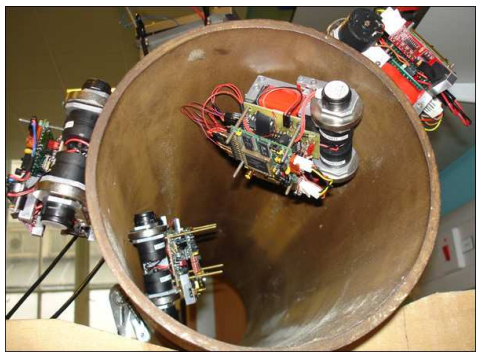

Fig. 3.2 : *X-ray robots inside and outside of a pipe searching for cracks. (Source: Internet site University of Strathclyde (2006))*

3.4 Ultrasound

Visualization is also possible with sound waves. This is based on the measurement of the distance over which a wave propagates from its source via the reflecting crack surface to a detector.

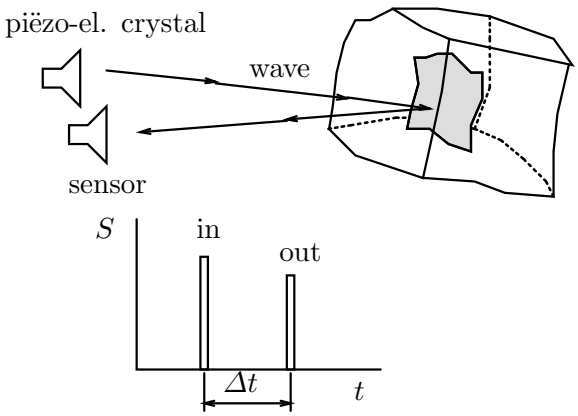

Fig. 3.3 : *Ultrasound crack detection.*

3.5 Acoustic emission

The release of energy in the material due to crack generation and propagation, results in sound waves (elastic stress waves), which can be detected at the surface. There is a correlation of their amplitude and frequency with failure phenomena inside the material. This *acoustic emission* (AE) is much used in laboratory experiments.

3.6 Adhesion tests

Many experimental techniques are used to determine adhesion strength of surface layers on a substrate. Some of them are illustrated below.

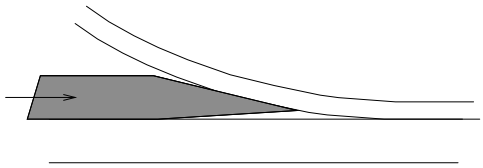

blade wedge test

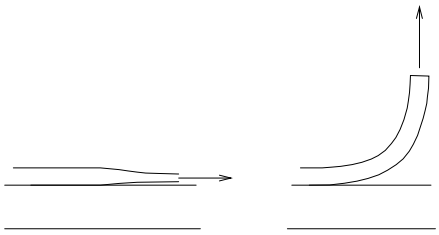

peel test (0^o and 90^o)

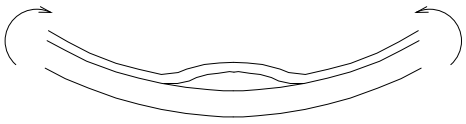

bending test

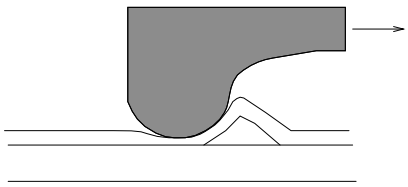

scratch test

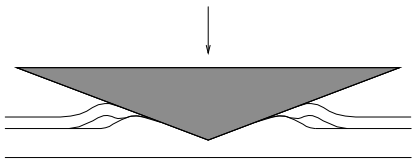

indentation test

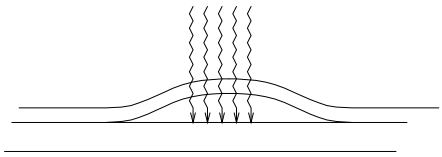

laser blister test

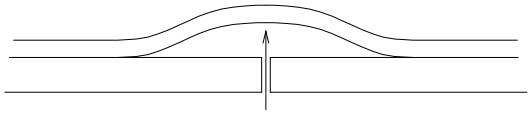

pressure blister test

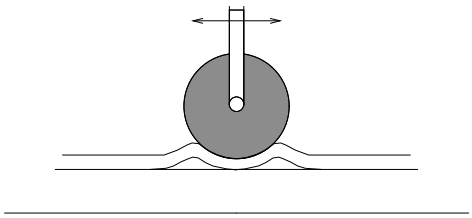

fatigue friction test

Chapter 4

Fracture energy

4.1 Energy balance

Abandoning the influence of thermal effects, the first law of thermodynamics can be formulated for a unit material volume :

> the total amount of mechanical energy that is supplied to a material volume per unit of time ($\dot{U}_e$) must be transferred into internal energy ($\dot{U}_i$), surface energy ($\dot{U}_a$), dissipated energy ($\dot{U}_d$) and kinetic energy ($\dot{U}_k$).

The internal energy is the elastically stored energy. The surface energy changes, when new free surface is generated, e.g. when a crack propagates. The kinetic energy is the result of material velocity. The dissipation may have various characteristics, but is mostly due to friction and plastic deformation. It results in temperature changes.

Instead of taking time derivatives ($\dot{}$) to indicate changes, we can also use another state variable, e.g. the crack surface area A. Assuming the crack to be through the thickness of a plate, whose thickness B is uniform and constant, we can also use the crack length a as a state variable.

The internally stored elastic energy is considered to be an energy source and therefore it is moved to the left-hand side of the energy balance equation.

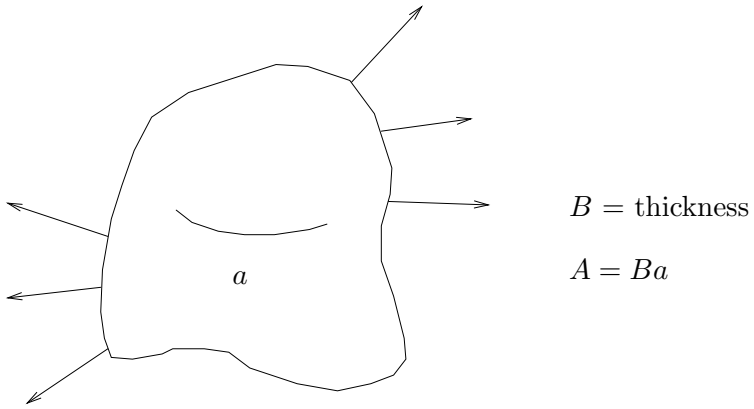

Fig. 4.1 : *Plate with a line crack of length a.*

$$\dot{U}_e = \dot{U}_i + \dot{U}_a + \dot{U}_d + \dot{U}_k \qquad [\mathrm{Js}^{-1}]$$

$$\frac{d}{dt}(\ ) = \frac{dA}{dt}\frac{d}{dA}(\ ) = \dot{A}\frac{d}{dA}(\ ) = \dot{a}\frac{d}{da}(\ )$$

$$\frac{dU_e}{da} = \frac{dU_i}{da} + \frac{dU_a}{da} + \frac{dU_d}{da} + \frac{dU_k}{da} \qquad [\mathrm{Jm}^{-1}]$$

$$\boxed{\frac{dU_e}{da} - \frac{dU_i}{da} = \frac{dU_a}{da} + \frac{dU_d}{da} + \frac{dU_k}{da}} \qquad [\mathrm{Jm}^{-1}]$$

4.2 Griffith's energy balance

It is now assumed that the available external and internal energy is transferred into surface energy. Dissipation and kinetic energy are neglected. This results in the so-called Griffith energy balance.

After division by the plate thickness B, the left-hand side of the equation is called the *energy release rate* G and the right-hand side the *crack resistance force* R, which equals 2γ, where γ is the surface energy of the material.

energy balance $\qquad \dfrac{dU_e}{da} - \dfrac{dU_i}{da} = \dfrac{dU_a}{da}$

energy release rate $\qquad G = \dfrac{1}{B}\left(\dfrac{dU_e}{da} - \dfrac{dU_i}{da}\right) \qquad [\mathrm{Jm}^{-2}]$

crack resistance force $\qquad R = \dfrac{1}{B}\left(\dfrac{dU_a}{da}\right) = 2\gamma \qquad [\mathrm{Jm}^{-2}]$

Griffith's crack criterion $\qquad \boxed{G = R = 2\gamma} \qquad [\mathrm{Jm}^{-2}]$

According to Griffith's energy balance, a crack will grow, when the energy release rate equals the crack resistance force.

This is illustrated with the following example, where a plate is loaded in tension and fixed at its edges. An edge crack of length a is introduced in the plate. Because the edges are clamped, the reaction force, due to prestraining, does not do any work, so in this case of *fixed grips* we have $dU_e = 0$. The material volume, where elastic energy is released, is indicated as the shaded area around the crack. The released elastic energy is a quadratic function of the crack length a. The surface energy, which is associated with the crack surface is $2\gamma a$.

Both surface energy U_a and internal energy U_i are plotted as a function of the crack length. The initial crack length a is indicated in the figure and it must be concluded that for crack growth da, the increment in surface energy is higher than the available (decrease of) internal energy. This crack therefore cannot growth and is stable.

When we gradually increase the crack length, the crack becomes unstable at the length a_c. In that case the crack growth criterion is just met ($G = R$). The increase of surface energy equals the decrease of the internal energy.

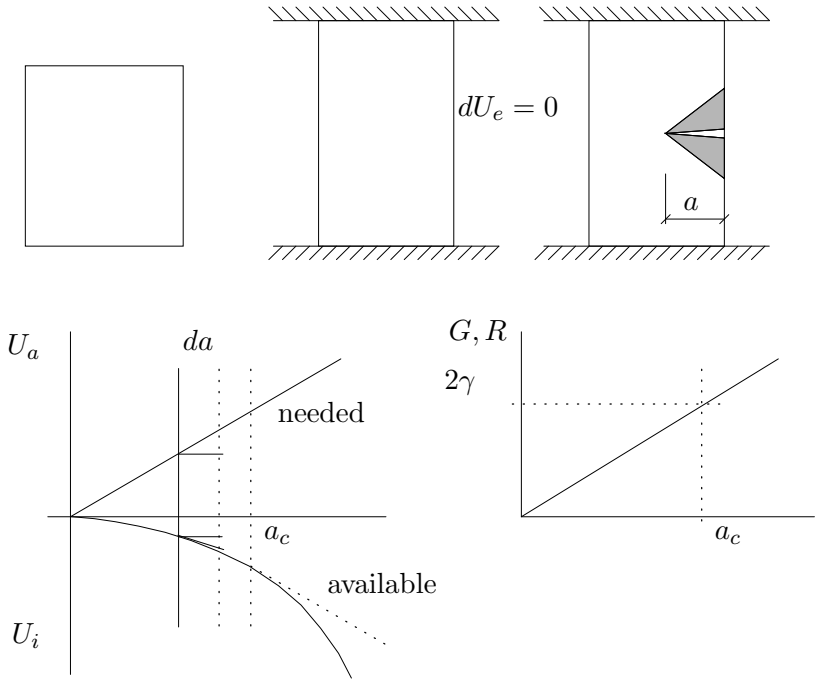

Fig. 4.2 : *Illustration of Griffith's energy balance criterion.*

$$-\frac{dU_i}{da} < \frac{dU_a}{da} \quad \rightarrow \quad \text{no crack growth}$$
$$-\frac{dU_i}{da} > \frac{dU_a}{da} \quad \rightarrow \quad \text{unstable crack growth}$$
$$-\frac{dU_i}{da} = \frac{dU_a}{da} \quad \rightarrow \quad \text{critical crack length}$$

4.3 Griffith stress

We consider a crack of length $2a$ in an "infinite" plate with uniform thickness B [m]. The crack is loaded in mode I by a nominal stress σ [Nm^{-2}], which is applied on edges at large distances from the crack.

Because the edges with the applied stress are at a far distance from the crack, their displacement will be very small when the crack length changes slightly. Therefore it is assumed that $dU_e = 0$ during crack propagation. It is further assumed that the elastic energy in the elliptical area is released, when the crack with length a is introduced. The energy release rate and the crack resistance force can now be calculated. According to Griffith's energy balance,

the applied stress σ and the crack length a are related. From this relation we can calculate the *Griffith stress* σ_{gr} and also the *critical crack length* a_c.

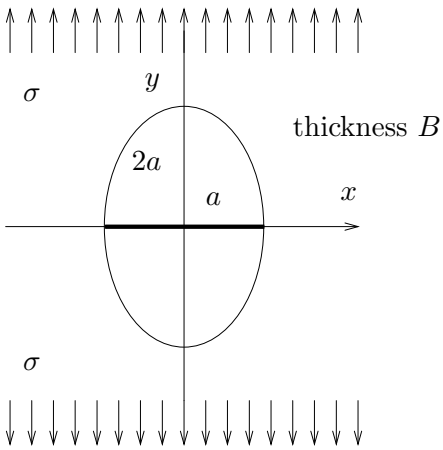

Fig. 4.3 : *Elliptical region, which is unloaded due to the central crack of length* $2a$.

$$U_i = 2\pi a^2 B\, \tfrac{1}{2}\frac{\sigma^2}{E} \qquad ; \qquad U_a = 4aB\,\gamma \qquad [\mathrm{Nm} = \mathrm{J}]$$

$$G = -\frac{1}{B}\left(\frac{dU_i}{da}\right) = \frac{1}{B}\left(\frac{dU_a}{da}\right) = R \qquad \rightarrow \qquad 2\pi a\frac{\sigma^2}{E} = 4\gamma \qquad [\mathrm{Jm}^{-2}]$$

Griffith stress $\qquad \sigma_{gr} = \sqrt{\dfrac{2\gamma E}{\pi a}}$

critical crack length $\qquad a_c = \dfrac{2\gamma E}{\pi \sigma^2}$

Because only one stress is included in the analysis, the above relations apply to a uni-axial state, which can be assumed to exist in a thin plate. For a thick plate the contraction has to be included and the Griffith stress becomes a function of Poisson's ratio.

$$\sigma_{gr} = \sqrt{\frac{2\gamma E}{(1-\nu^2)\pi a}}$$

4.3.1 Discrepancy with experimental observations

When the Griffith stress is compared to the experimental critical stress for which a crack of length a will propagate, it appears that the Griffith stress is much too small: it underestimates the strength.

The reason for this discrepancy is mainly due to the fact that in the Griffith energy balance the dissipation is neglected. This can be concluded from the comparison of the crack resistance force $R = 4\gamma$ and the measured critical energy release rate G_c. For materials which are very brittle (e.g. glass) and thus show little dissipation during crack growth, the difference

between R and G_c is not very large. For ductile materials, showing much dissipation (e.g. metal alloys), G_c can be 10^5 times R.

Griffith's energy balance can be used in practice, when the calculated energy release rate is compared to a measured critical value G_c.

energy balance	$G = \frac{1}{B}\left(\frac{dU_e}{da} - \frac{dU_i}{da}\right) = R = G_c$
critical crack length	$a_c = \frac{G_c E}{2\pi\sigma^2}$
Griffith's crack criterion	$G = G_c$

4.4 Compliance change

The energy release rate can be calculated from the change in stiffness due to the elongation of a crack. It is common practice to use the compliance C instead of the stiffness and the relation between G and the change of C will be derived for a plate with an edge crack, which is loaded by a force F in point P. When the crack length increases from a to $a + da$, two extreme situations can be considered :

- *fixed grips* : point P is not allowed to move ($u = 0$),
- *constant load* : force F is kept constant.

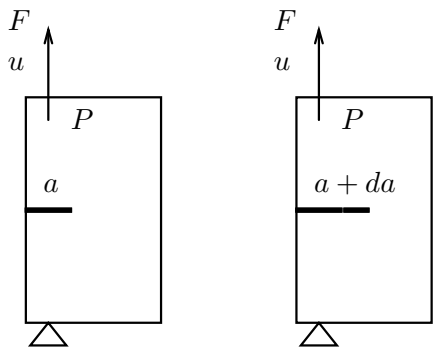

Fig. 4.4 : *Edge crack in a plate loaded by a force F.*

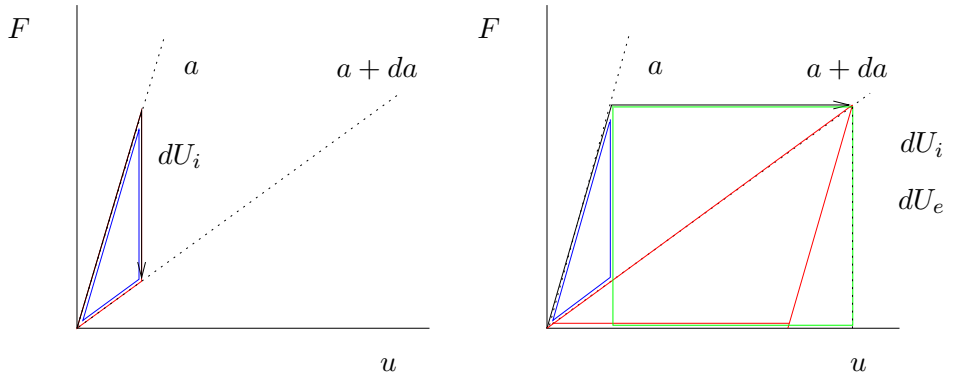

Fig. 4.5 : *Internal and external energy for fixed grips (left) and constant load (right).*

4.4.1 Fixed grips

Using the fixed grips approach, it is obvious that $dU_e = 0$. The force F will decrease ($dF < 0$) upon crack growth and the change of the internally stored elastic energy can be expressed in the displacement u and the change dF. The energy release rate can be calculated according to its definition.

fixed grips : $dU_e = 0$

$$\begin{aligned} dU_i &= U_i(a+da) - U_i(a) \qquad (<0) \\ &= \tfrac{1}{2}(F+dF)u - \tfrac{1}{2}Fu \\ &= \tfrac{1}{2}udF \end{aligned}$$

Griffith's energy balance

$$G = -\frac{1}{2B}u\frac{dF}{da} = \frac{1}{2B}\frac{u^2}{C^2}\frac{dC}{da} = \frac{1}{2B}F^2\frac{dC}{da}$$

4.4.2 Constant load

With the constant load approach, the load will supply external work, when the crack propagates and the point P moves over a distance du. Also the elastic energy will diminish and this change can be expressed in F and du. The energy release rate can be calculated according to its definition.

constant load

$$dU_e = U_e(a+da) - U_e(a) = Fdu$$

$$\begin{aligned} dU_i &= U_i(a+da) - U_i(a) \qquad (>0) \\ &= \tfrac{1}{2}F(u+du) - \tfrac{1}{2}Fu \\ &= \tfrac{1}{2}Fdu \end{aligned}$$

Griffith's energy balance

$$G = \frac{1}{2B} F \frac{du}{da} = \frac{1}{2B} F^2 \frac{dC}{da}$$

4.4.3 Experiment

It can be concluded that the energy release rate can be calculated from the change in compliance and that the result for the *fixed grip* approach is exactly the same as that for the *constant load* method.

In reality the loading of the plate may not be purely according to the extreme cases, as is shown in the figure. From such a real experiment the energy release rate can be determined from the force-displacement curve.

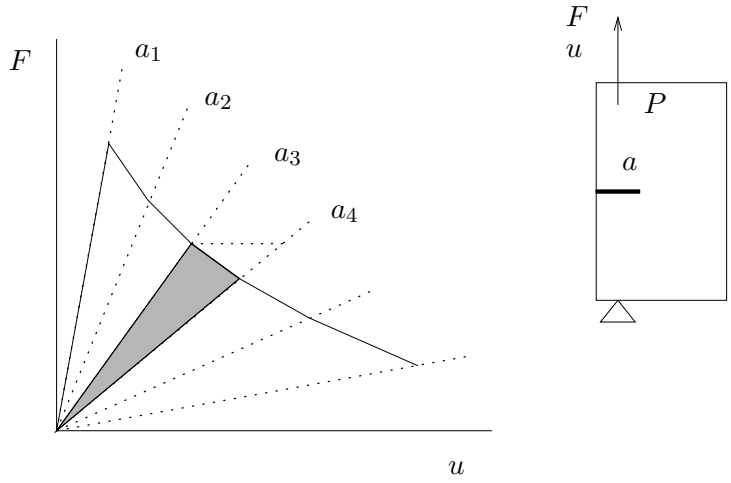

Fig. 4.6 : *Experimental force-displacement curve during crack growth.*

$$G = \frac{\text{shaded area}}{a_4 - a_3} \frac{1}{B}$$

4.4.4 Examples

As an example the energy release rate is calculated for the so-called double cantilever beam, shown in the figure.

Using linear elastic beam theory, the opening Δu of the crack can be expressed in the force F, the crack length a, beam thickness B, beam height $2h$ and Young's modulus E. The compliance is the ratio of opening and force. Differentiating the compliance w.r.t. the crack length results in the energy release rate G, which appears to be quadratic in a.

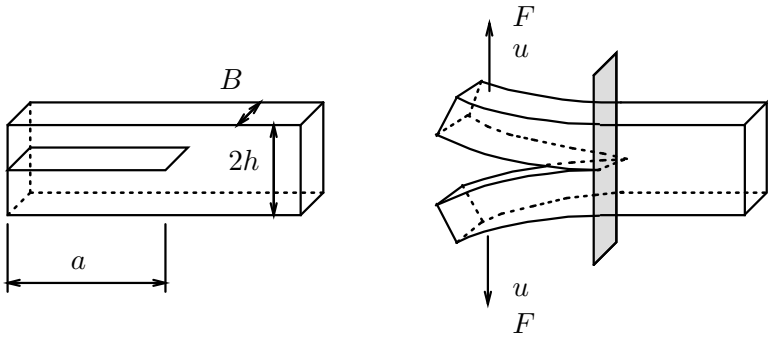

Fig. 4.7 : *Beam with a central crack loaded in Mode I.*

$$u = \frac{Fa^3}{3EI} = \frac{4Fa^3}{EBh^3} \quad \rightarrow \quad C = \frac{\Delta u}{F} = \frac{2u}{F} = \frac{8a^3}{EBh^3} \quad \rightarrow \quad \frac{dC}{da} = \frac{24a^2}{EBh^3} \quad \rightarrow$$

$$G = \frac{1}{B}\left[\tfrac{1}{2}F^2\frac{dC}{da}\right] = \frac{12F^2a^2}{EB^2h^3} \qquad [\mathrm{J\ m^{-2}}]$$

$$G_c = 2\gamma \quad \rightarrow \quad F_c = \frac{B}{a}\sqrt{\tfrac{1}{6}\gamma Eh^3}$$

The question arises for which beam geometry, the energy release rate will be constant, so no function of the crack length. It is assumed that the height of the beam is an exponential function of a. Applying again formulas from linear elastic beam theory, it can be derived for which shape G is no function of a.

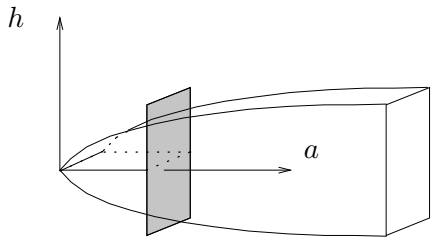

Fig. 4.8 : *Cracked beam with variable cross-section.*

$$C = \frac{\Delta u}{F} = \frac{2u}{F} = \frac{8a^3}{EBh^3} \quad \rightarrow \quad \frac{dC}{da} = \frac{24a^2}{EBh^3}$$

$$\text{choice} \quad : \quad h = h_0 a^n \quad \rightarrow$$

$$u = \frac{Fa^3}{3(1-n)EI} = \frac{4Fa^3}{(1-n)EBh^3} = \frac{4Fa^{3(1-n)}}{(1-n)EBh_0^3}$$

$$C = \frac{2u}{F} = \frac{8a^{3(1-n)}}{(1-n)EBh_0^3} \quad \rightarrow \quad \frac{dC}{da} = \frac{24a^{(2-3n)}}{EBh_0^3}$$

$$\frac{dC}{da} \quad \text{constant for} \quad n = \tfrac{2}{3} \quad \rightarrow \quad h = h_0 a^{\frac{2}{3}}$$

Chapter 5

Stress concentrations

In this chapter attention is given to stress concentrations due to holes. Throughout this chapter it is assumed that the material behavior is linear elastic and isotropic. The stress state is calculated using Airy stress functions. The first sections present a summary of the theory of linear elasticity.

5.1 Deformation and strain

The basic problem in mechanics is the prediction of the mechanical behavior of a body when it is subjected to an external load. We want to predict the deformation, the deformation rate and the stresses in the material. (Temperature is not considered here, but could also be determined, making the behavior thermomechanical.)

To set up a mathematical model, which can be used to solve the above problem, we must be able to identify the position of material points. For this purpose we use position vectors : $\vec{X}$ in the undeformed state and $\vec{x}$ in the deformed state. The displacement during deformation is obviously the difference between $\vec{x}$ and $\vec{X}$. In the mathematics of the next sections, we use the components of the vectorial (and tensorial) variables w.r.t. a coordinate system. These components are indicated by indices, which take values in the rage $\{1, 2, 3\}$ for three-dimensional deformations.

In continuum mechanics we assume that the body is perfect, i.e. that it does not contain voids, cracks or other imperfections. This implies that relevant variables, like the displacement, are a continuous function of the location within the body. In this way the difference vector between two adjacent points in undeformed and deformed state can be related.

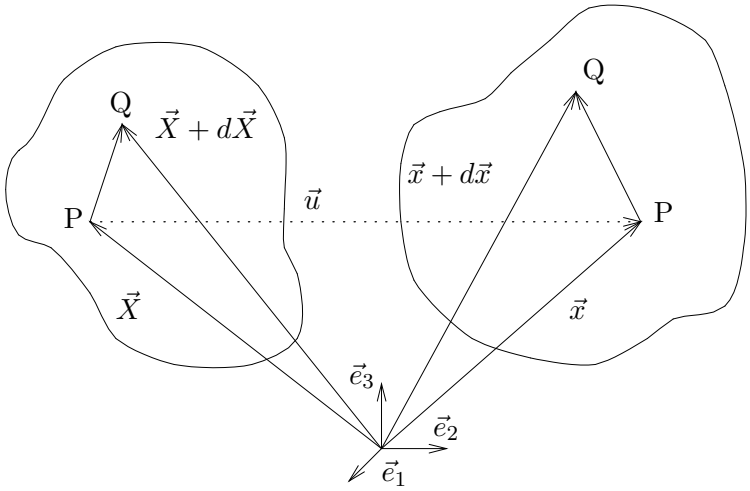

Fig. 5.1 : *Deformation of a continuum.*

$$
\begin{aligned}
x_i &= X_i + u_i(X_i) \\
x_i + dx_i &= X_i + dX_i + u_i(X_i + dX_i) = X_i + dX_i + u_i(X_i) + u_{i,j} dX_j dx_i \\
&= dX_i + u_{i,j} dX_j = (\delta_{ij} + u_{i,j}) dX_j
\end{aligned}
$$

The local deformation, i.e. the deformation of a small material volume in a material point, is described by strains. When elongations and rotations are large, the Green-Lagrange strains γ_{ij} are commonly used. For small elongations and rotations, these can be linearized to the linear strains ε_{ij}.

$$
\begin{aligned}
ds^2 = dx_i dx_i &= [(\delta_{ij} + u_{i,j}) dX_j][(\delta_{ik} + u_{i,k}) dX_k] \\
&= (\delta_{ij}\delta_{ik} + \delta_{ij} u_{i,k} + u_{i,j}\delta_{ik} + u_{i,j} u_{i,k}) dX_j dX_k \\
&= (\delta_{jk} + u_{j,k} + u_{k,j} + u_{i,j} u_{i,k}) dX_j dX_k \\
&= (\delta_{ij} + u_{i,j} + u_{j,i} + u_{k,i} u_{k,j}) dX_i dX_j \\
&= dX_i dX_i + (u_{i,j} + u_{j,i} + u_{k,i} u_{k,j}) dX_i dX_j \\
&= dS^2 + (u_{i,j} + u_{j,i} + u_{k,i} u_{k,j}) dX_i dX_j
\end{aligned}
$$

$$
\begin{aligned}
ds^2 - dS^2 &= (u_{i,j} + u_{j,i} + u_{k,i} u_{k,j}) dX_i dX_j \\
&= 2\gamma_{ij} dX_i dX_j
\end{aligned}
$$

Green-Lagrange strains $\quad \gamma_{ij} = \frac{1}{2}(u_{i,j} + u_{j,i} + u_{k,i} u_{k,j})$

linear strains $\quad \varepsilon_{ij} = \frac{1}{2}(u_{i,j} + u_{j,i})$

Because three displacement components are the basis for the definition of six strain components, the latter cannot be independent. The compatibility relations express this dependency.

$$
\begin{aligned}
2\varepsilon_{12,12} - \varepsilon_{11,22} - \varepsilon_{22,11} &= 0 \\
2\varepsilon_{23,23} - \varepsilon_{22,33} - \varepsilon_{33,22} &= 0 \\
2\varepsilon_{31,31} - \varepsilon_{33,11} - \varepsilon_{11,33} &= 0 \\
\varepsilon_{11,23} + \varepsilon_{23,11} - \varepsilon_{31,12} - \varepsilon_{12,13} &= 0 \\
\varepsilon_{22,31} + \varepsilon_{31,22} - \varepsilon_{12,23} - \varepsilon_{23,21} &= 0 \\
\varepsilon_{33,12} + \varepsilon_{12,33} - \varepsilon_{23,31} - \varepsilon_{31,32} &= 0
\end{aligned}
$$

5.2 Stress

When deformation is not completely unconstrained, it provokes stresses in the material. The stress vector $\vec{p}$ on a plane in a material point, can be calculated from the unity normal vector $\vec{n}$ on the plane and the Cauchy stress tensor. Using index notation in a coordinate system, the components of $\vec{p}$ can be related to those of $\vec{n}$ by the Cauchy stress components σ_{ij} $(i, j = 1, 2, 3)$. These stress components can be represented as the stress vectors on the sides of an infinitesimal stress cube in the material point, with its sides normal to the coordinate axes.

unity normal vector	$\vec{n} = n_i \vec{e}_i$
stress vector	$\vec{p} = p_i \vec{e}_i$
Cauchy stress components	$p_i = \sigma_{ij} n_j$

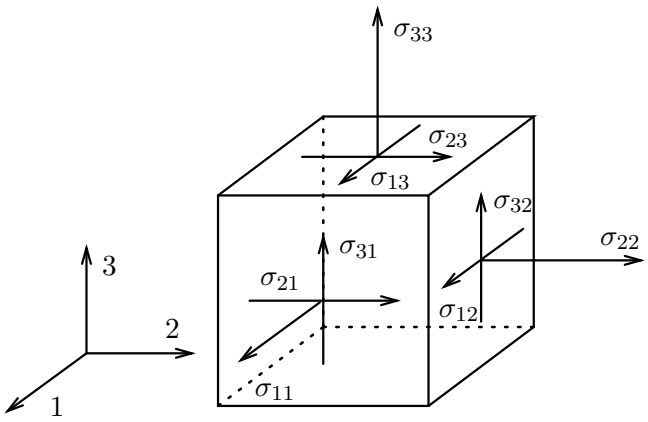

Fig. 5.2 : *Stress components on a stress cube.*

5.3 Linear elastic material behavior

For very small deformations, the mechanical behavior of a solid material is reversible and characterized by a linear relation between stress and strain components. The relation is given by the stiffness parameters C_{ijkl} $(i, j, k, l = 1, 2, 3)$ and is referred to as Hooke's law.

Due to symmetry of stress and strain components, there are no more than 21 independent

stiffness parameters. Due to material symmetry – crystal structure – the elastic behavior of most materials can be described by considerably less material parameters. For isotropic materials, two material parameters are sufficient : Young's modulus E and Poisson's ratio ν.

$$\sigma_{ij} = C_{ijkl}\varepsilon_{lk}$$

Hooke's law for isotropic materials

For isotropic materials, Hooke's law can be written in index notation, relating six strain components to six stress components and vice versa. When these components are stored in columns, Hooke's law is represented by a six-by-six matrix.

$$\sigma_{ij} = \frac{E}{1+\nu}\left(\varepsilon_{ij} + \frac{\nu}{1-2\nu}\,\delta_{ij}\varepsilon_{kk}\right) \qquad i = 1,2,3$$
$$\varepsilon_{ij} = \frac{1+\nu}{E}\left(\sigma_{ij} - \frac{\nu}{1+\nu}\,\delta_{ij}\sigma_{kk}\right) \qquad i = 1,2,3$$

$$\begin{bmatrix} \sigma_{11} \\ \sigma_{22} \\ \sigma_{33} \\ \sigma_{12} \\ \sigma_{23} \\ \sigma_{31} \end{bmatrix} = \alpha \begin{bmatrix} 1-\nu & \nu & \nu & 0 & 0 & 0 \\ \nu & 1-\nu & \nu & 0 & 0 & 0 \\ \nu & \nu & 1-\nu & 0 & 0 & 0 \\ 0 & 0 & 0 & 1-2\nu & 0 & 0 \\ 0 & 0 & 0 & 0 & 1-2\nu & 0 \\ 0 & 0 & 0 & 0 & 0 & 1-2\nu \end{bmatrix} \begin{bmatrix} \varepsilon_{11} \\ \varepsilon_{22} \\ \varepsilon_{33} \\ \varepsilon_{12} \\ \varepsilon_{23} \\ \varepsilon_{31} \end{bmatrix}$$
$$\alpha = E/[(1+\nu)(1-2\nu)]$$

$$\begin{bmatrix} \varepsilon_{11} \\ \varepsilon_{22} \\ \varepsilon_{33} \\ \varepsilon_{12} \\ \varepsilon_{23} \\ \varepsilon_{31} \end{bmatrix} = \frac{1}{E} \begin{bmatrix} 1 & -\nu & -\nu & 0 & 0 & 0 \\ -\nu & 1 & -\nu & 0 & 0 & 0 \\ -\nu & -\nu & 1 & 0 & 0 & 0 \\ 0 & 0 & 0 & 1+\nu & 0 & 0 \\ 0 & 0 & 0 & 0 & 1+\nu & 0 \\ 0 & 0 & 0 & 0 & 0 & 1+\nu \end{bmatrix} \begin{bmatrix} \sigma_{11} \\ \sigma_{22} \\ \sigma_{33} \\ \sigma_{12} \\ \sigma_{23} \\ \sigma_{31} \end{bmatrix}$$

5.4 Equilibrium equations

A material, which is subjected to external loads, will deform and the stresses in the deformed state have to satisfy the equilibrium equations in each point. The three equilibrium equations for forces are partial differential equations, which can only be solved with proper boundary conditions. The three equilibrium equations for moments indicate that the Cauchy stress components are symmetric.

We have assumed here that the acceleration of the material points can be neglected.

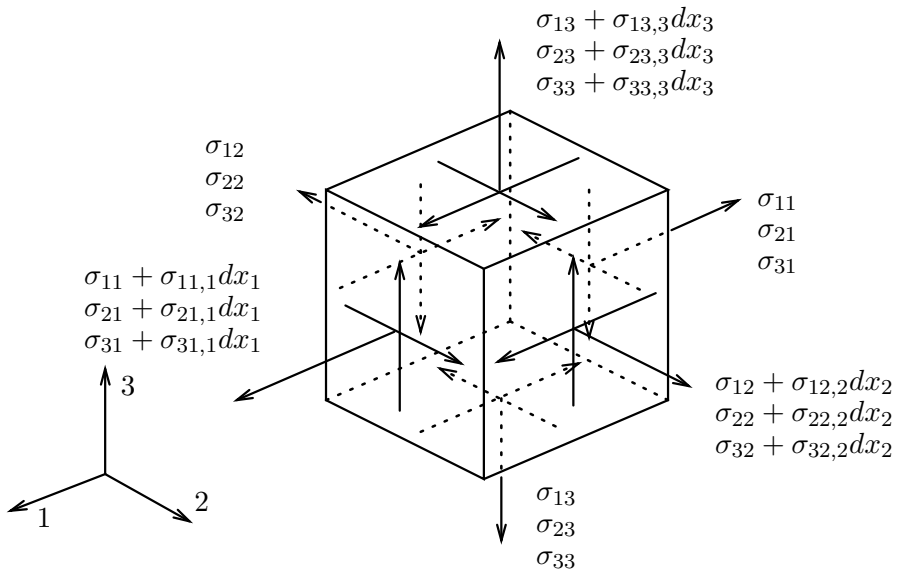

Fig. 5.3 : *Stress components on a stress cube with a volume load.*

volume load	ρq_i	
force equilibrium	$\sigma_{ij,j} + \rho q_i = 0$	$i = 1, 2, 3$
moment equilibrium	$\sigma_{ij} = \sigma_{ji}$	

5.5 Plane stress

When stresses are zero on a certain plane, which we take to be the 12-plane in this case, we have a *plane stress* state.

Only the three independent stress components in the plane have to be considered. They have to satisfy two equilibrium equations. The three strain components in the plane are related by one compatibility relation. Hooke's law for linear elastic material behavior relates the three stress components to the three strain components, with a 3×3 stiffness matrix or compliance matrix.

equilibrium ($q_i = 0$)	$\sigma_{11,1} + \sigma_{12,2} = 0$	;	$\sigma_{21,1} + \sigma_{22,2} = 0$
compatibility	$2\varepsilon_{12,12} - \varepsilon_{11,22} - \varepsilon_{22,11} = 0$		

Hooke's law

$$\sigma_{ij} = \frac{E}{1+\nu}\left(\varepsilon_{ij} + \frac{\nu}{1-\nu}\,\delta_{ij}\varepsilon_{kk}\right) \quad ; \quad \varepsilon_{ij} = \frac{1+\nu}{E}\left(\sigma_{ij} - \frac{\nu}{1+\nu}\,\delta_{ij}\sigma_{kk}\right) \qquad i = 1, 2$$

Hooke's law in matrix notation

$$\begin{bmatrix} \varepsilon_{11} \\ \varepsilon_{22} \\ \varepsilon_{12} \end{bmatrix} = \frac{1}{E} \begin{bmatrix} 1 & -\nu & 0 \\ -\nu & 1 & 0 \\ 0 & 0 & 1+\nu \end{bmatrix} \begin{bmatrix} \sigma_{11} \\ \sigma_{22} \\ \sigma_{12} \end{bmatrix}$$

$$\begin{bmatrix} \sigma_{11} \\ \sigma_{22} \\ \sigma_{12} \end{bmatrix} = \frac{E}{1-\nu^2} \begin{bmatrix} 1 & \nu & 0 \\ \nu & 1 & 0 \\ 0 & 0 & 1-\nu \end{bmatrix} \begin{bmatrix} \varepsilon_{11} \\ \varepsilon_{22} \\ \varepsilon_{12} \end{bmatrix}$$

$$\varepsilon_{33} = -\frac{\nu}{E}(\sigma_{11} + \sigma_{22}) = -\frac{\nu}{1-\nu}(\varepsilon_{11} + \varepsilon_{22})$$
$$\varepsilon_{13} = \varepsilon_{23} = 0$$

5.6 Plane strain

In the plane strain situation, the deformation of the material is such that there is no elongation and shear in and perpendicular to one direction, which we here take to be the 3-direction, perpendicular to the 12-plane.

Only three strain components remain, which have to satisfy one compatibility relation. Three stress components have to be solved from two equilibrium equations. Hooke's law can be simplified and represented with 3×3 stiffness and compliance matrices.

equilibrium ($q_i = 0$) $\qquad \sigma_{11,1} + \sigma_{12,2} = 0 \qquad ; \qquad \sigma_{21,1} + \sigma_{22,2} = 0$

compatibility $\qquad 2\varepsilon_{12,12} - \varepsilon_{11,22} - \varepsilon_{22,11} = 0$

Hooke's law

$$\varepsilon_{ij} = \frac{1+\nu}{E}(\sigma_{ij} - \nu\delta_{ij}\sigma_{kk}) \quad ; \quad \sigma_{ij} = \frac{E}{1+\nu}\left(\varepsilon_{ij} + \frac{\nu}{1-2\nu}\delta_{ij}\varepsilon_{kk}\right) \qquad i = 1, 2$$

Hooke's law in matrix notation

$$\begin{bmatrix} \sigma_{11} \\ \sigma_{22} \\ \sigma_{12} \end{bmatrix} = \frac{E}{(1+\nu)(1-2\nu)} \begin{bmatrix} 1-\nu & \nu & 0 \\ \nu & 1-\nu & 0 \\ 0 & 0 & 1-2\nu \end{bmatrix} \begin{bmatrix} \varepsilon_{11} \\ \varepsilon_{22} \\ \varepsilon_{12} \end{bmatrix}$$

$$\begin{bmatrix} \varepsilon_{11} \\ \varepsilon_{22} \\ \varepsilon_{12} \end{bmatrix} = \frac{1+\nu}{E} \begin{bmatrix} 1-\nu & -\nu & 0 \\ -\nu & 1-\nu & 0 \\ 0 & 0 & 1 \end{bmatrix} \begin{bmatrix} \sigma_{11} \\ \sigma_{22} \\ \sigma_{12} \end{bmatrix}$$

$$\sigma_{33} = \frac{E\nu}{(1+\nu)(1-2\nu)}(\varepsilon_{11} + \varepsilon_{22}) = \nu(\sigma_{11} + \sigma_{22})$$
$$\sigma_{13} = \sigma_{23} = 0$$

5.7 Displacement method

The displacement method is based on transforming the equilibrium equations to differential equations for the displacement components.

First, the stress-strain relation according to Hooke's law are substituted into the equilibrium equations, leading to two differential equations for the strain components. Next, the strain-displacement relations are substituted, resulting in the final two differential equations for the two displacement components. These equations can be solved with proper boundary conditions (BC's). Analytical solutions can only be determined for simple cases.

$$
\left.\begin{aligned}
&\sigma_{ij,j} = 0 \\
&\sigma_{ij} = \frac{E}{1+\nu}\left(\varepsilon_{ij} + \frac{\nu}{1-2\nu}\,\delta_{ij}\varepsilon_{kk}\right)
\end{aligned}\right\}
$$

$$
\left.\begin{aligned}
&\frac{E}{1+\nu}\left(\varepsilon_{ij,j} + \frac{\nu}{1-2\nu}\,\delta_{ij}\varepsilon_{kk,j}\right) = 0 \\
&\varepsilon_{ij} = \tfrac{1}{2}\left(u_{i,j} + u_{j,i}\right)
\end{aligned}\right\}
$$

$$
\left.\begin{aligned}
&\frac{E}{1+\nu}\,\tfrac{1}{2}\left(u_{i,jj} + u_{j,ij}\right) + \frac{E\nu}{(1+\nu)(1-2\nu)}\delta_{ij}u_{k,kj} = 0 \\
&\text{BC's}
\end{aligned}\right\}
$$

$$
u_i \quad \rightarrow \quad \varepsilon_{ij} \quad \rightarrow \quad \sigma_{ij}
$$

5.8 Stress function method

According to the displacement method, the equilibrium equation is transformed to a differential equation in the displacements. In the so-called stress function method, the equilibrium is transformed to a differential equation in the Airy stress function ψ.

The stress components are related to derivatives of the stress function, such that they satisfy the equilibrium equations. Using Hooke's law, the strain components are expressed in derivatives of ψ. The strain components are then substituted in the compatibility equations. Here only two-dimensional problems are considered, so only one compatibility equation is relevant.

The result is a fourth-order differential equation for the stress function ψ, which is called the *bi-harmonic equation*. It can be written in short form using the Laplace operator ∇^2.

With proper boundary conditions (4), the bi-harmonic equation can be solved (theoretically). When the stress function is known, the stresses, strains and displacements can be derived rather straightforwardly.

$$
\left.\begin{aligned}
&\psi(x_1, x_2) \quad \rightarrow \quad \sigma_{ij} = -\psi_{,ij} + \delta_{ij}\psi_{,kk} \quad \rightarrow \quad \sigma_{ij,j} = 0 \\
&\varepsilon_{ij} = \frac{1+\nu}{E}\left(\sigma_{ij} - \nu\delta_{ij}\sigma_{kk}\right)
\end{aligned}\right\}
$$

$$\left.\begin{array}{l} \varepsilon_{ij} = \dfrac{1+\nu}{E}\left\{-\psi_{,ij} + (1-\nu)\delta_{ij}\psi_{,kk}\right\} \\ 2\varepsilon_{12,12} - \varepsilon_{11,22} - \varepsilon_{22,11} = 0 \end{array}\right\}$$

$$2\psi_{,1122} + \psi_{,2222} + \psi_{,1111} = 0 \qquad \rightarrow$$

$$\left.\begin{array}{l} (\psi_{,11} + \psi_{,22})_{,11} + (\psi_{,11} + \psi_{,22})_{,22} = 0 \\ \text{Laplace operator} \quad : \quad \nabla^2 = \dfrac{\partial^2}{\partial x_1^2} + \dfrac{\partial^2}{\partial x_2^2} = (\ )_{11} + (\ )_{22} \\ \left.\begin{array}{ll} \text{bi-harmonic equation} & \nabla^2(\nabla^2\psi) = \nabla^4\psi = 0 \\ \text{BC's} & \end{array}\right\} \end{array}\right\} \rightarrow$$

$$\psi \quad \rightarrow \quad \sigma_{ij} \quad \rightarrow \quad \varepsilon_{ij} \quad \rightarrow \quad u_i$$

Cylindrical coordinates

The bi-harmonic equation has been derived and expressed in Cartesian coordinates. To get an expression in cylindrical coordinates, the base vectors of the cylindrical coordinate system are expressed in the base vectors of the Cartesian coordinate system. It is immediately clear that cylindrical base vectors are a function of the cylindrical coordinate θ.

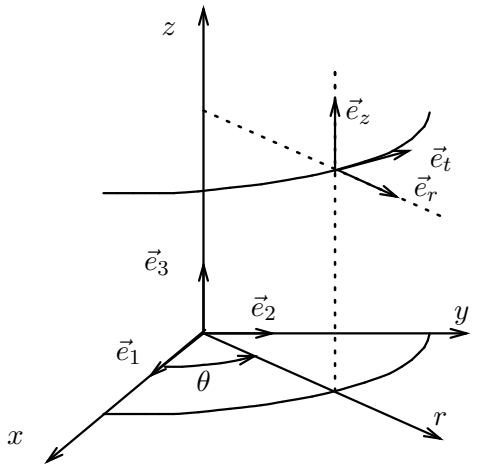

Fig. 5.4 : *Cartesian and cylindrical coordinate system.*

vector bases $\qquad \{\vec{e}_1, \vec{e}_2, \vec{e}_3\} \qquad \rightarrow \qquad \{\vec{e}_r, \vec{e}_t, \vec{e}_z\}$

$$\vec{e}_r = \vec{e}_r(\theta) = \vec{e}_1 \cos\theta + \vec{e}_2 \sin\theta$$
$$\vec{e}_t = \vec{e}_t(\theta) = -\vec{e}_1 \sin\theta + \vec{e}_2 \cos\theta$$

$$\frac{\partial}{\partial\theta}\{\vec{e}_r(\theta)\} = \vec{e}_t(\theta) \qquad ; \qquad \frac{\partial}{\partial\theta}\{\vec{e}_t(\theta)\} = -\vec{e}_r(\theta)$$

Laplace operator

The Laplace operator is a scalar operator and can be written as the inner product of the gradient operator, which is a vector operator.

gradient operator $$\vec{\nabla} = \vec{e}_r \frac{\partial}{\partial r} + \vec{e}_t \frac{1}{r}\frac{\partial}{\partial\theta} + \vec{e}_z \frac{\partial}{\partial z}$$

Laplace operator $$\nabla^2 = \vec{\nabla}\cdot\vec{\nabla} = \frac{\partial^2}{\partial r^2} + \frac{1}{r}\frac{\partial}{\partial r} + \frac{1}{r^2}\frac{\partial^2}{\partial\theta^2} + \frac{\partial^2}{\partial z^2}$$

two-dimensional $$\nabla^2 = \frac{\partial^2}{\partial r^2} + \frac{1}{r}\frac{\partial}{\partial r} + \frac{1}{r^2}\frac{\partial^2}{\partial\theta^2}$$

Bi-harmonic equation

The bi-harmonic equation can now be written in cylindrical coordinates. Also the stress components, which are derivatives of the stress function, can be written in cylindrical coordinates. The latter expression can best be derived from the expression for the stress tensor and using the expression for the gradient operator in cylindrical coordinates.

bi-harmonic equation

$$\left(\frac{\partial^2}{\partial r^2} + \frac{1}{r}\frac{\partial}{\partial r} + \frac{1}{r^2}\frac{\partial^2}{\partial\theta^2}\right)\left(\frac{\partial^2\psi}{\partial r^2} + \frac{1}{r}\frac{\partial\psi}{\partial r} + \frac{1}{r^2}\frac{\partial^2\psi}{\partial\theta^2}\right) = 0$$

stress components

$$\begin{aligned}
\sigma_{rr} &= \frac{1}{r}\frac{\partial\psi}{\partial r} + \frac{1}{r^2}\frac{\partial^2\psi}{\partial\theta^2} \\
\sigma_{tt} &= \frac{\partial^2\psi}{\partial r^2} \\
\sigma_{rt} &= \frac{1}{r^2}\frac{\partial\psi}{\partial\theta} - \frac{1}{r}\frac{\partial\psi}{\partial r\partial\theta} = -\frac{\partial}{\partial r}\left(\frac{1}{r}\frac{\partial\psi}{\partial\theta}\right)
\end{aligned}$$

5.9 Circular hole in 'infinite' plate

A circular hole with diameter $2a$ is located in a plate with uniform thickness. Dimensions of the plate are much larger than $2a$. The plate is loaded with a uniform stress σ in the global x-direction. The center of the hole is the origin of a cylindrical coordinate system. To determine the stress components as a function of r and θ, the bi-harmonic equation must be solved to determine the Airy stress function $\psi(r,\theta)$ for this problem.

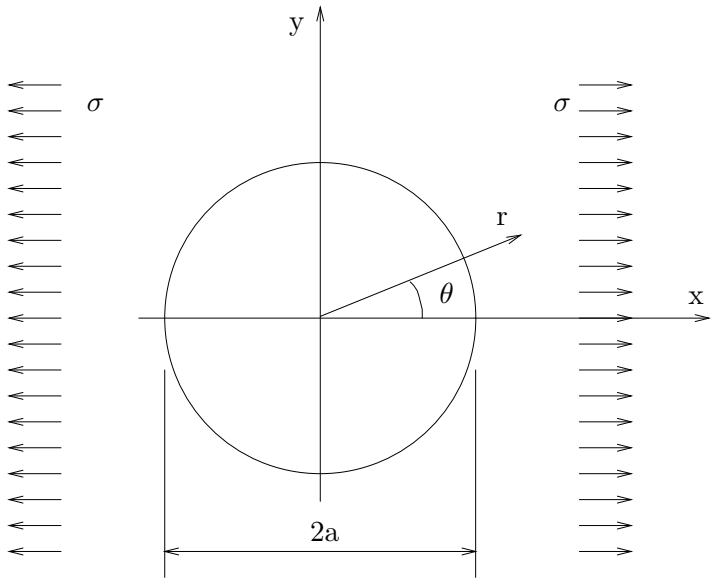

Fig. 5.5 : *A circular hole in a plate, loaded with a uniform stress σ in x-direction.*

Load transformation

At a circular cross-section at a distance $r = b \gg a$, the uniform stress σ can be decomposed in a radial stress σ_{rr} and a shear stress σ_{rt}, which can be related to σ using equilibrium.

The total load at the cross-section $r = b$ is the sum of a radial load and a load that depends on θ. For both loadcases, the stress field for $b \leq r \leq a$ will be determined, after which the combined solution follows from superposition.

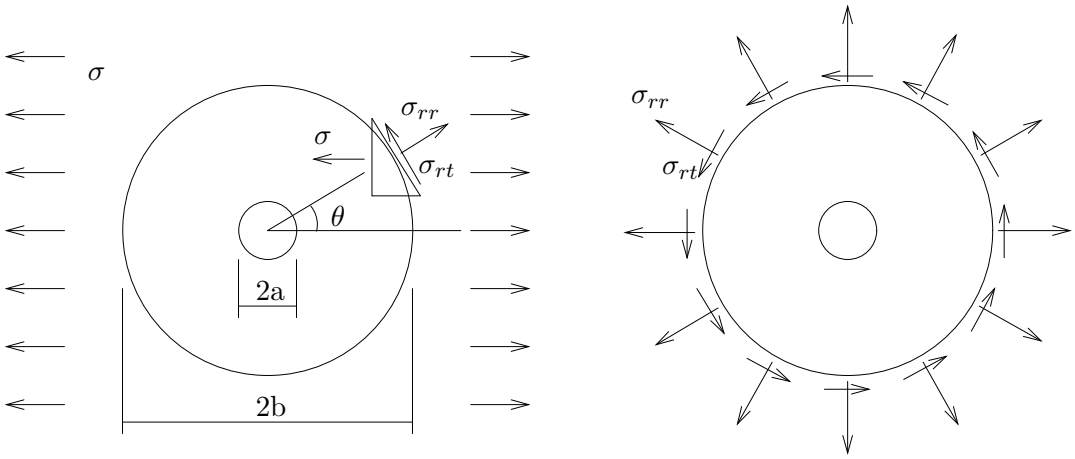

Fig. 5.6 : *Transformation of the x-load in radial and circumferential loads.*

$$\sigma_{rr}(r = b, \theta) = \tfrac{1}{2}\sigma + \tfrac{1}{2}\sigma\cos(2\theta)$$
$$\sigma_{rt}(r = b, \theta) = -\tfrac{1}{2}\sigma\sin(2\theta)$$

two load cases

$$
\begin{aligned}
I. \quad & \sigma_{rr}(r=a) = \sigma_{rt}(r=a) = 0 \\
& \sigma_{rr}(r=b) = \tfrac{1}{2}\sigma \quad ; \quad \sigma_{rt}(r=b) = 0 \\
II. \quad & \sigma_{rr}(r=a) = \sigma_{rt}(r=a) = 0 \\
& \sigma_{rr}(r=b) = \tfrac{1}{2}\sigma\cos(2\theta) \quad ; \quad \sigma_{rt}(r=b) = -\tfrac{1}{2}\sigma\sin(2\theta)
\end{aligned}
$$

Load case I

In the first loadcase, the boundary at $r = b$ is subjected to a radial load $\sigma_{rr} = \frac{1}{2}\sigma$. Because σ_{rr} is not depending on θ, the problem is axisymmetric and ψ is only a function of r. The stress components can be expressed in this function. The bi-harmonic equation is an ordinary differential equation in the variable r.

Airy function $\psi = f(r)$

stress components

$$
\begin{aligned}
\sigma_{rr} &= \frac{1}{r}\frac{\partial\psi}{\partial r} + \frac{1}{r^2}\frac{\partial^2\psi}{\partial\theta^2} = \frac{1}{r}\frac{df}{dr} \\
\sigma_{tt} &= \frac{\partial^2\psi}{\partial r^2} = \frac{d^2f}{dr^2} \\
\sigma_{rt} &= -\frac{\partial}{\partial r}\left(\frac{1}{r}\frac{\partial\psi}{\partial\theta}\right) = 0
\end{aligned}
$$

bi-harmonic equation $\left(\frac{d^2}{dr^2} + \frac{1}{r}\frac{d}{dr}\right)\left(\frac{d^2f}{dr^2} + \frac{1}{r}\frac{df}{dr}\right) = 0$

A general solution for the differential equation has four integration constants. These have to be determined from the boundary conditions for this loadcase. However, the boundary conditions for σ_{rt} cannot be used as this stress component is zero everywhere. Instead the compatibility equation is used, which relates the strain components ε_{rr} and ε_{tt}. Also $b \gg a$ is used in the calculation.

general solution $\psi(r) = A\ln r + Br^2\ln r + Cr^2 + D$

stresses $\sigma_{rr} = \frac{A}{r^2} + B(1 + 2\ln r) + 2C \quad ; \quad \sigma_{tt} = -\frac{A}{r^2} + B(3 + 2\ln r) + 2C$

strains (from Hooke's law for plane stress)

$$
\begin{aligned}
\varepsilon_{rr} &= \frac{1}{E}\left[\frac{A}{r^2}(1+\nu) + B\{(1-3\nu) + 2(1-\nu)\ln r\} + 2C(1-\nu)\right] \\
\varepsilon_{tt} &= \frac{1}{E}\frac{1}{r}\left[-\frac{A}{r}(1+\nu) + B\{(3-\nu)r + 2(1-\nu)r\ln r\} + 2C(1-\nu)r\right]
\end{aligned}
$$

compatibility $\varepsilon_{rr} = \dfrac{du}{dr} = \dfrac{d(r\,\varepsilon_{tt})}{dr} \quad \rightarrow \quad B = 0$

2 BC's and $b \gg a \quad \rightarrow \quad A$ and $C \quad \rightarrow$

$$\sigma_{rr} = \tfrac{1}{2}\sigma(1 - \frac{a^2}{r^2}) \quad ; \quad \sigma_{tt} = \tfrac{1}{2}\sigma(1 + \frac{a^2}{r^2}) \quad ; \quad \sigma_{rt} = 0$$

Load case II

The second loadcase is again defined by the stress components at $r = a$ and $r = b$. At the boundary $r = b$ the stresses are harmonic functions of the coordinate θ. Confronting the general expressions for stresses σ_{rr} and σ_{rt} with these prescribed values at $r = b$, indicates that the Airy function $\psi(r, \theta)$ must be written as the product of a function $g(r)$ and $\cos(2\theta)$. (The term $\cos(2\theta)$ remains after two subsequent differentiations w.r.t. θ.) Substitution in the bi-harmonic equation results in a differential equation for $g(r)$ and expressions for the stress components.

Airy function $\psi(r, \theta) = g(r)\cos(2\theta)$

stress components

$$\sigma_{rr} = \frac{1}{r}\frac{\partial\psi}{\partial r} + \frac{1}{r^2}\frac{\partial^2\psi}{\partial\theta^2} \quad ; \quad \sigma_{tt} = \frac{\partial^2\psi}{\partial r^2}$$
$$\sigma_{rt} = \frac{1}{r^2}\frac{\partial\psi}{\partial\theta} - \frac{1}{r}\frac{\partial\psi}{\partial r\partial\theta} = -\frac{\partial}{\partial r}\left(\frac{1}{r}\frac{\partial\psi}{\partial\theta}\right)$$

bi-harmonic equation

$$\left(\frac{\partial^2}{\partial r^2} + \frac{1}{r}\frac{\partial}{\partial r} + \frac{1}{r^2}\frac{\partial^2}{\partial\theta^2}\right)\left\{\left(\frac{d^2g}{dr^2} + \frac{1}{r}\frac{dg}{dr} - \frac{4}{r^2}g\right)\cos(2\theta)\right\} = 0 \quad \rightarrow$$
$$\left(\frac{d^2}{dr^2} + \frac{1}{r}\frac{d}{dr} - \frac{4}{r^2}\right)\left(\frac{d^2g}{dr^2} + \frac{1}{r}\frac{dg}{dr} - \frac{4}{r^2}g\right)\cos(2\theta) = 0$$

A general solution for the differential equation has four integration constants. These have to be determined from the boundary conditions for this loadcase. Using $b \gg a$, the stress components σ_{rr}, σ_{tt} and σ_{rt} can be determined as a function of r and θ.

general solution $g = Ar^2 + Br^4 + C\dfrac{1}{r^2} + D \quad \rightarrow$

$$\psi = \left(Ar^2 + Br^4 + C\frac{1}{r^2} + D\right)\cos(2\theta)$$

stresses $\sigma_{rr} = -\left(2A + \dfrac{6C}{r^4} + \dfrac{4D}{r^2}\right)\cos(2\theta)$

$$\sigma_{tt} = \left(2A + 12Br^2 + \frac{6C}{r^4}\right)\cos(2\theta)$$
$$\sigma_{rt} = \left(2A + 6Br^2 - \frac{6C}{r^4} - \frac{2D}{r^2}\right)\sin(2\theta)$$

4 BC's and $b \gg a$ $\rightarrow$ A,B,C and D $\rightarrow$

$$\sigma_{rr} = \tfrac{1}{2}\sigma\left(1 + \frac{3a^4}{r^4} - \frac{4a^2}{r^2}\right)\cos(2\theta)$$
$$\sigma_{tt} = -\tfrac{1}{2}\sigma\left(1 + \frac{3a^4}{r^4}\right)\cos(2\theta)$$
$$\sigma_{rt} = -\tfrac{1}{2}\sigma\left(1 - \frac{3a^4}{r^4} + \frac{2a^2}{r^2}\right)\sin(2\theta)$$

Stresses for total load

The stress components σ_{rr}, σ_{tt} and σ_{rt} resulting from the total load at $r = b \gg a$, are the sum of the solutions for the separate loadcases.

$$\sigma_{rr} = \frac{\sigma}{2}\left[\left(1 - \frac{a^2}{r^2}\right) + \left(1 + \frac{3a^4}{r^4} - \frac{4a^2}{r^2}\right)\cos(2\theta)\right]$$
$$\sigma_{tt} = \frac{\sigma}{2}\left[\left(1 + \frac{a^2}{r^2}\right) - \left(1 + \frac{3a^4}{r^4}\right)\cos(2\theta)\right]$$
$$\sigma_{rt} = -\frac{\sigma}{2}\left[1 - \frac{3a^4}{r^4} + \frac{2a^2}{r^2}\right]\sin(2\theta)$$

Special points

At the inner hole boundary ($r = a$), the stress σ_{tt} is maximum for $\theta = \frac{\pi}{2}$ and the stress concentration is 3, which means that it is three times the applied stress σ. The *stress concentration factor* (SCF) K_t is a ratio of the maximum stress and the applied stress and therefore it is a dimensionless number. It appears not to depend on the hole diameter.

$$\sigma_{rr}(r = a, \theta) = \sigma_{rt}(r = a, \theta) = \sigma_{rt}(r, \theta = 0) = 0$$
$$\sigma_{tt}(r = a, \theta = \tfrac{\pi}{2}) = 3\sigma$$
$$\sigma_{tt}(r = a, \theta = 0) = -\sigma$$

stress concentration factor $K_t = \dfrac{\sigma_{max}}{\sigma} = 3$ [-]

Stress gradients

When we plot the stress σ_{tt} as a function of the distance to the hole, it appears that the stress gradient is higher when the hole diameter is smaller. For a larger hole there is more volume of material with a higher than nominal stress level. The chance that there is a defect or flaw

in this volume is higher than in the specimen with the smaller hole. This makes a larger hole to be more dangerous regarding the occurrence of damage than the smaller hole.

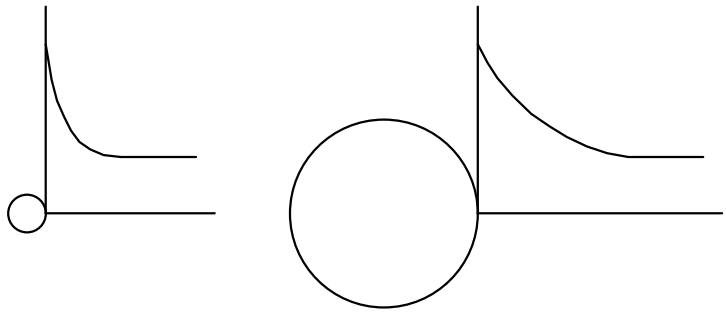

Fig. 5.7 : *Different stress gradient at holes with different radius.*

5.10 Elliptical hole

Stress components in the vicinity of an elliptical hole can be calculated also. The solution reveals that at the location of the smallest radius ρ, the stress concentration becomes infinite when the radius approaches zero, as would be the situation for a real crack.

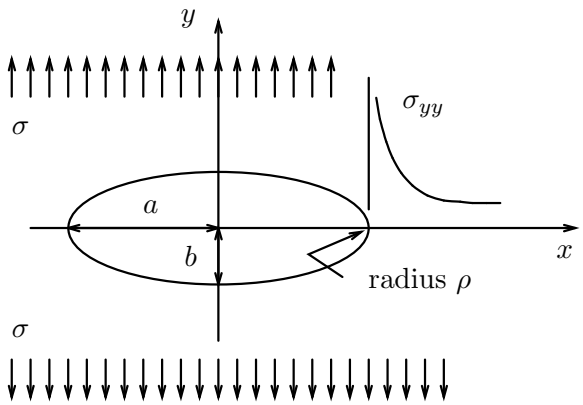

Fig. 5.8 : *Elliptical hole loaded with a uniform stress σ in y-direction.*

$$\sigma_{yy}(x=a, y=0) = \sigma\left(1+2\frac{a}{b}\right) = \sigma\left(1+2\sqrt{a/\rho}\right) \approx 2\sigma\sqrt{a/\rho}$$

stress concentration factor $K_t = 2\sqrt{a/\rho}$ [-]

Chapter 6

Crack tip stresses

When a linear crack is loaded in Mode-I, II or III, stress components at the crack tip can be calculated with the Airy stress function method. However, a real crack has zero radius ($\rho = 0$) and such a crack tip represents a singularity. Due to this singularity, complex variables and functions will enter the mathematics.

6.1 Complex plane

The crack tip is considered to be the origin of a complex coordinate system with real axis x_1 and imaginary axis x_2. The position in this complex plane can be identified by a complex number and all variables – Airy function, stresses, strains, displacements – are considered to be complex functions of this position.

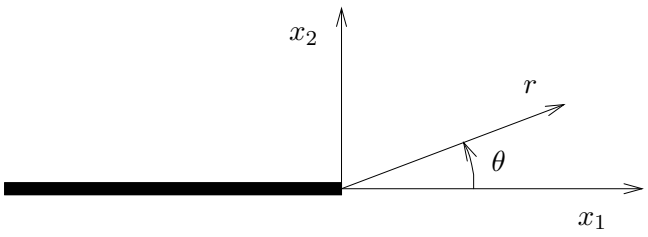

Fig. 6.1 : *Line crack with local coordinate systems originating in the crack tip.*

6.1.1 Complex variables

A complex number z has a real (x_1) and an imaginary (x_2) part, which are located on the real and imaginary axis of the complex coordinate system. The conjugate complex number $\bar{z}$ is mirrored with respect to the real axis. The real and imaginary part of z can be expressed in z and $\bar{z}$.

Introducing unity vectors $\vec{e}_r$ and $\vec{e}_i$ along the real and imaginary axis, allows the complex numbers to be represented as a vector $\vec{z}$. It is easily seen that multiplying $\vec{z}$ with the imaginary

constant i results in a counter-clockwise rotation over $\frac{\pi}{2}$ of vector $\vec{z}$. It is obvious that we can write : $\vec{e}_i = i\vec{e}_r$.

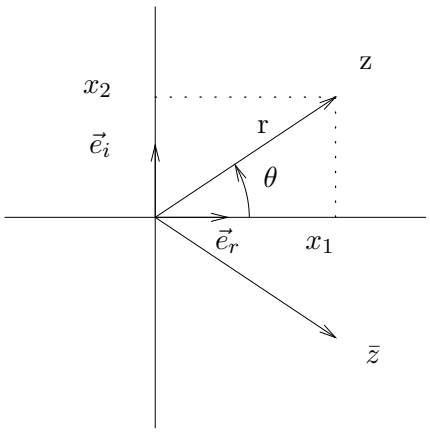

Fig. 6.2 : *Complex plane and two complex numbers.*

$$z = x_1 + ix_2 = re^{i\theta} \qquad ; \qquad \bar{z} = x_1 - ix_2 = re^{-i\theta}$$
$$x_1 = \tfrac{1}{2}(z + \bar{z}) \qquad ; \qquad x_2 = \tfrac{1}{2i}(z - \bar{z}) = -\tfrac{1}{2}i(z - \bar{z})$$
$$\vec{z} = x_1\vec{e}_r + x_2\vec{e}_i = x_1\vec{e}_r + x_2 i\vec{e}_r = (x_1 + ix_2)\vec{e}_r$$

6.1.2 Complex functions

A scalar function of a complex number z results in a complex number f. We only consider functions which can be written as the sum of a real (ϕ) and an imaginary (ζ) part. When the conjugate complex number $\bar{z}$ is substituted in the scalar function, the result is a complex number $\bar{f}$, which is conjugate to f. It can be shown (see Appendix A) that both the real and the imaginary part of f (and $\bar{f}$) satisfy the Laplace equation.

$$\left.\begin{aligned} f(z) &= \phi + i\zeta = \phi(x_1, x_2) + i\zeta(x_1, x_2) = f \\ f(\bar{z}) &= \phi(x_1, x_2) - i\zeta(x_1, x_2) = \bar{f} \end{aligned}\right\} \quad \rightarrow$$

$$\phi = \tfrac{1}{2}\{f + \bar{f}\} \qquad ; \qquad \zeta = -\tfrac{1}{2}i\{f - \bar{f}\}$$

6.1.3 Laplace operator

The bi-harmonic equation includes the Laplace operator ∇^2. In Cartesian coordinates this operator comprises second-order derivatives with respect to the Cartesian coordinates x_1 and x_2. These derivatives can be transformed to derivatives with respect to the variables z and $\bar{z}$, resulting in a Laplace operator in terms of these variables. In Appendix B a detailed derivation is presented.

complex function $g(x_1, x_2) = g(z, \bar{z})$

Laplacian $\nabla^2 g = \dfrac{\partial^2 g}{\partial x_1^2} + \dfrac{\partial^2 g}{\partial x_2^2}$

derivatives

$$\frac{\partial g}{\partial x_1} = \frac{\partial g}{\partial z}\frac{\partial z}{\partial x_1} + \frac{\partial g}{\partial \bar{z}}\frac{\partial \bar{z}}{\partial x_1} = \frac{\partial g}{\partial z} + \frac{\partial g}{\partial \bar{z}}$$

$$\frac{\partial^2 g}{\partial x_1^2} = \frac{\partial^2 g}{\partial z^2} + 2\frac{\partial g}{\partial z \partial \bar{z}} + \frac{\partial^2 g}{\partial \bar{z}^2}$$

$$\frac{\partial g}{\partial x_2} = \frac{\partial g}{\partial z}\frac{\partial z}{\partial x_2} + \frac{\partial g}{\partial \bar{z}}\frac{\partial \bar{z}}{\partial x_2} = i\frac{\partial g}{\partial z} - i\frac{\partial g}{\partial \bar{z}}$$

$$\frac{\partial^2 g}{\partial x_2^2} = -\frac{\partial^2 g}{\partial z^2} + 2\frac{\partial g}{\partial z \partial \bar{z}} - \frac{\partial^2 g}{\partial \bar{z}^2}$$

Laplacian $\nabla^2 g = \dfrac{\partial^2 g}{\partial x_1^2} + \dfrac{\partial^2 g}{\partial x_2^2} = 4\dfrac{\partial g}{\partial z \partial \bar{z}} \quad \rightarrow \quad \nabla^2 = 4\dfrac{\partial}{\partial z \partial \bar{z}}$

6.1.4 Bi-harmonic equation

The Airy stress function ψ is taken to be a function of z and $\bar{z}$ and it must be solved from the bi-harmonic equation.

Airy function $\psi(z, \bar{z})$

bi-harmonic equation $\nabla^2 \left(\nabla^2 \psi(z, \bar{z})\right) = 0$

6.2 Solution of bi-harmonic equation

According to subsection 6.1.2 (and Appendix A), the solution of a Laplace equation can be considered to be the real part of a complex function. Thus, from the bi-harmonic equation it follows that the Airy function must satisfy a Poisson equation with right-hand side the sum of a complex function and its conjugate. The general solution for ψ contains two unknown complex functions Ω and ω and there conjugates $\bar{\Omega}$ and $\bar{\omega}$.

$$\nabla^2\left(\nabla^2\psi(z,\bar{z})\right) = \nabla^2\left(\phi(z,\bar{z})\right) = 0 \quad \rightarrow \quad \phi = f + \bar{f} \quad \rightarrow$$

$$\nabla^2\psi = 4\frac{\partial\psi}{\partial z\partial\bar{z}} = \phi = f + \bar{f} \quad \rightarrow \quad \boxed{\psi = \tfrac{1}{2}\left[\bar{z}\Omega + z\bar{\Omega} + \omega + \bar{\omega}\right]}$$

6.2.1 Stresses

From the general solution for ψ the stress components σ_{11}, σ_{22} and σ_{12} can be derived and expressed in Ω, ω, $\bar{\Omega}$ and $\bar{\omega}$. Derivatives w.r.t. z and $\bar{z}$ are indicated with $(\,)'$. The detailed derivation can be found in Appendix B.

$$\sigma_{ij} = \sigma_{ij}(z,\bar{z}) = -\psi_{,ij} + \delta_{ij}\psi_{,kk} \qquad \rightarrow$$

$$\begin{aligned}
\sigma_{11} &= -\psi_{,11} + \psi_{,\gamma\gamma} = \psi_{,22} = \Omega' + \bar{\Omega}' - \tfrac{1}{2}\left\{\bar{z}\Omega'' + \omega'' + z\bar{\Omega}'' + \bar{\omega}''\right\} \\
\sigma_{22} &= -\psi_{,22} + \psi_{,\gamma\gamma} = \psi_{,11} = \Omega' + \bar{\Omega}' + \tfrac{1}{2}\left\{\bar{z}\Omega'' + \omega'' + z\bar{\Omega}'' + \bar{\omega}''\right\} \\
\sigma_{12} &= -\psi_{,12} = -\tfrac{1}{2}i\left\{\bar{z}\Omega'' + \omega'' - z\bar{\Omega}'' - \bar{\omega}''\right\}
\end{aligned}$$

6.2.2 Displacement

The displacement vector $\vec{u}$ can be written in components w.r.t. a Cartesian coordinate system $\{x_1, x_2\}$ with orthonormal base vectors $\vec{e}_1$ and $\vec{e}_2$. Considering the coordinate axes to be real and imaginary axes in a complex plane, we have $\vec{e}_1 = \vec{e}_r$ and $\vec{e}_2 = \vec{e}_i = i\vec{e}_r$. The displacement vector can thus be considered to be a vector in the direction $\vec{e}_r$, having a length u, which is a complex number. The real part is the x_1-component and the imaginary part is the x_2-component.

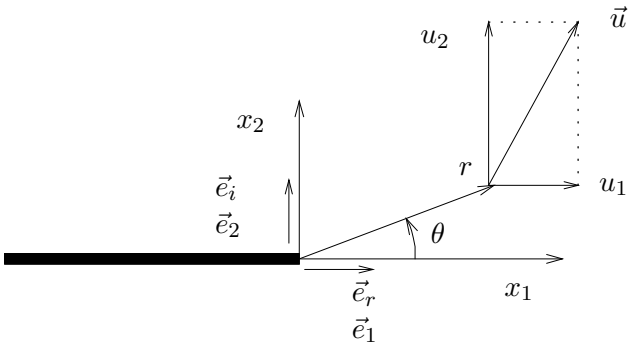

Fig. 6.3 : *Complex displacement.*

$$\begin{aligned}
&\vec{u} = u_1\vec{e}_1 + u_2\vec{e}_2 = u_1\vec{e}_r + u_2\vec{e}_i = u_1\vec{e}_r + u_2 i\vec{e}_r = (u_1 + iu_2)\vec{e}_r = u\vec{e}_r \qquad \rightarrow \\
&u = u_1 + iu_2 = u_1(x_1,x_2) + iu_2(x_1,x_2) = u(z,\bar{z}) \\
&\bar{u} = u_1 - iu_2 = \bar{u}(z,\bar{z})
\end{aligned}$$

Because the displacements u and $\bar{u}$ are a function of z and $\bar{z}$, the derivatives w.r.t. z and $\bar{z}$ can be determined. It appears that $\frac{\partial u}{\partial\bar{z}}$ and $\frac{\partial\bar{u}}{\partial z}$ can be expressed in strain components only.

$$\begin{aligned}
\frac{\partial u}{\partial \bar{z}} &= \frac{\partial u}{\partial x_1}\frac{\partial x_1}{\partial \bar{z}} + \frac{\partial u}{\partial x_2}\frac{\partial x_2}{\partial \bar{z}} = \tfrac{1}{2}\left\{\frac{\partial u}{\partial x_1} + i\frac{\partial u}{\partial x_2}\right\} \\
&= \tfrac{1}{2}\left\{\frac{\partial u_1}{\partial x_1} + i\frac{\partial u_2}{\partial x_1} + i\frac{\partial u_1}{\partial x_2} - \frac{\partial u_2}{\partial x_2}\right\} = \tfrac{1}{2}\left(\varepsilon_{11} - \varepsilon_{22} + 2i\varepsilon_{12}\right) \\
\frac{\partial u}{\partial z} &= \frac{\partial u}{\partial x_1}\frac{\partial x_1}{\partial z} + \frac{\partial u}{\partial x_2}\frac{\partial x_2}{\partial z} = \tfrac{1}{2}\left\{\frac{\partial u}{\partial x_1} - i\frac{\partial u}{\partial x_2}\right\} \\
&= \tfrac{1}{2}\left\{\frac{\partial u_1}{\partial x_1} + i\frac{\partial u_2}{\partial x_1} - i\frac{\partial u_1}{\partial x_2} + \frac{\partial u_2}{\partial x_2}\right\} = \tfrac{1}{2}\left\{\varepsilon_{11} + \varepsilon_{22} + i\left(\frac{\partial u_2}{\partial x_1} - \frac{\partial u_1}{\partial x_2}\right)\right\} \\
\frac{\partial \bar{u}}{\partial z} &= \frac{\partial \bar{u}}{\partial x_1}\frac{\partial x_1}{\partial z} + \frac{\partial \bar{u}}{\partial x_2}\frac{\partial x_2}{\partial z} = \tfrac{1}{2}\left\{\frac{\partial \bar{u}}{\partial x_1} - i\frac{\partial \bar{u}}{\partial x_2}\right\} \\
&= \tfrac{1}{2}\left\{\frac{\partial u_1}{\partial x_1} - i\frac{\partial u_2}{\partial x_1} - i\frac{\partial u_1}{\partial x_2} - \frac{\partial u_2}{\partial x_2}\right\} = \tfrac{1}{2}\left(\varepsilon_{11} - \varepsilon_{22} - 2i\varepsilon_{12}\right) \\
\frac{\partial \bar{u}}{\partial \bar{z}} &= \frac{\partial \bar{u}}{\partial x_1}\frac{\partial x_1}{\partial \bar{z}} + \frac{\partial \bar{u}}{\partial x_2}\frac{\partial x_2}{\partial \bar{z}} = \tfrac{1}{2}\left\{\frac{\partial \bar{u}}{\partial x_1} + i\frac{\partial \bar{u}}{\partial x_2}\right\} \\
&= \tfrac{1}{2}\left\{\frac{\partial u_1}{\partial x_1} - i\frac{\partial u_2}{\partial x_1} + i\frac{\partial u_1}{\partial x_2} + \frac{\partial u_2}{\partial x_2}\right\} = \tfrac{1}{2}\left\{\varepsilon_{11} + \varepsilon_{22} - i\left(\frac{\partial u_2}{\partial x_1} - \frac{\partial u_1}{\partial x_2}\right)\right\}
\end{aligned}$$

Using Hooke's law for plane strain, the derivative of u w.r.t. $\bar{z}$ can be expressed in the stress components and thus in the complex functions $\bar{\Omega}$ and $\bar{\omega}$. Integration leads to an expression for u, comprising an unknown function $M(z)$.

$$\begin{aligned}
\frac{\partial u}{\partial \bar{z}} &= \tfrac{1}{2}\,\frac{1+\nu}{E}\,\left[\sigma_{11} - \sigma_{22} + 2i\sigma_{12}\right] = -\,\frac{1+\nu}{E}\,\left[z\bar{\Omega}'' + \bar{\omega}''\right] \\
u &= -\,\frac{1+\nu}{E}\left[z\bar{\Omega}' + \bar{\omega}' + M\right]
\end{aligned}$$

Using the general solution for u and the conjugate $\bar{u}$, the derivatives of these can be determined and added. Adding the directly derived derivatives $\frac{\partial u}{\partial z}$ and $\frac{\partial \bar{u}}{\partial \bar{z}}$ leads again to an expression in strain components and through Hooke's law in the functions Ω' and $\bar{\Omega}'$. From the general solution, these derivatives can also be calculated, whereupon the integration function M can be determined.

$$\begin{aligned}
u &= -\,\frac{1+\nu}{E}\left[z\bar{\Omega}' + \bar{\omega}' + M\right] \quad \rightarrow \\
\frac{\partial u}{\partial z} &= -\frac{1+\nu}{E}\left[\bar{\Omega}' + M'\right] \\
\bar{u} &= -\,\frac{1+\nu}{E}\left[\bar{z}\Omega' + \omega' + \bar{M}\right] \quad \rightarrow \\
\frac{\partial \bar{u}}{\partial \bar{z}} &= -\frac{1+\nu}{E}\left[\Omega' + \bar{M}'\right] \\
\frac{\partial u}{\partial z} + \frac{\partial \bar{u}}{\partial \bar{z}} &= -\frac{1+\nu}{E}\left[\bar{\Omega}' + \Omega' + M' + \bar{M}'\right]
\end{aligned}$$

$$\frac{\partial u}{\partial z} + \frac{\partial \bar{u}}{\partial \bar{z}} = \varepsilon_{11} + \varepsilon_{22} = \frac{1+\nu}{E}\left[(1-2\nu)(\sigma_{11}+\sigma_{22})\right]$$
$$= \frac{(1+\nu)(1-2\nu)}{E}\, 2\, \left[\Omega' + \bar{\Omega}'\right]$$

$$M' + \bar{M}' = -(3-4\nu)\left[\bar{\Omega}' + \Omega'\right] \quad \rightarrow$$
$$M = -(3-4\nu)\Omega = -\kappa\Omega$$

$$u = -\frac{1+\nu}{E}\left[z\bar{\Omega}' + \bar{\omega}' - \kappa\Omega\right]$$

6.2.3 Choice of complex functions

Two unknown functions Ω and ω have to be determined from boundary conditions. These two functions are specified to be of a certain form, however, still containing five unknown constants : α, β, γ, δ and λ. Using these functions and their derivatives, the displacement $u(z, \bar{z})$ can be derived.

The displacement appears to be proportional to $r^{\lambda+1}$. From a physical point of view, the displacement always has to be finite. This argument requires λ to be larger than -1.

$$\left.\begin{array}{l} \Omega = (\alpha+i\beta)z^{\lambda+1} = (\alpha+i\beta)r^{\lambda+1}e^{i\theta(\lambda+1)} \\ \omega' = (\gamma+i\delta)z^{\lambda+1} = (\gamma+i\delta)r^{\lambda+1}e^{i\theta(\lambda+1)} \end{array}\right\} \quad \rightarrow$$

$$\left.\begin{array}{l} \bar{\Omega} = (\alpha-i\beta)\bar{z}^{\lambda+1} = (\alpha-i\beta)r^{\lambda+1}e^{-i\theta(\lambda+1)} \\ \bar{\Omega}' = (\alpha-i\beta)(\lambda+1)\bar{z}^{\lambda} = (\alpha-i\beta)(\lambda+1)r^{\lambda}e^{-i\theta\lambda} \\ \bar{\omega}' = (\gamma-i\delta)\bar{z}^{\lambda+1} = (\gamma-i\delta)r^{\lambda+1}e^{-i\theta(\lambda+1)} \end{array}\right\} \quad \rightarrow$$

$$u = \frac{1}{2\mu}r^{\lambda+1}\left[\kappa(\alpha+i\beta)e^{i\theta(\lambda+1)} - (\alpha-i\beta)(\lambda+1)e^{i\theta(1-\lambda)} - (\gamma-i\delta)e^{-i\theta(\lambda+1)}\right]$$

with $\qquad \mu = \dfrac{E}{2(1+\nu)}$

displacement finite $\quad \rightarrow \quad \boxed{\lambda > -1}$

6.2.4 Displacement components

The displacement u is a complex function. Its real and imaginary part, respectively, u_1 and u_2, are functions of the variables r and θ and the constants α, β, γ, δ and λ. Euler's formula is used to express u in *cosine* and *sine* functions.

$$\left.\begin{array}{l} u = \dfrac{1}{2\mu}r^{\lambda+1}\left[\kappa(\alpha+i\beta)e^{i\theta(\lambda+1)} - (\alpha-i\beta)(\lambda+1)e^{i\theta(1-\lambda)} - (\gamma-i\delta)e^{-i\theta(\lambda+1)}\right] \\ e^{i\theta} = \cos(\theta) + i\sin(\theta) \end{array}\right\}$$

$$
\begin{aligned}
u = \frac{1}{2\mu} r^{\lambda+1} & \\
& \Big[\quad \Big\{ \quad \kappa\alpha\cos(\theta(\lambda+1)) - \kappa\beta\sin(\theta(\lambda+1)) - \\
& \qquad \alpha(\lambda+1)\cos(\theta(1-\lambda)) - \beta(\lambda+1)\sin(\theta(1-\lambda)) - \\
& \qquad \gamma\cos(\theta(\lambda+1)) + \delta\sin(\theta(\lambda+1)) \quad \Big\} + \\
& \qquad i \quad \Big\{ \quad \kappa\alpha\sin(\theta(\lambda+1)) + \kappa\beta\cos(\theta(\lambda+1)) - \\
& \qquad \alpha(\lambda+1)\sin(\theta(1-\lambda)) + \beta(\lambda+1)\cos(\theta(1-\lambda)) + \\
& \qquad \gamma\sin(\theta(\lambda+1)) + \delta\cos(\theta(\lambda+1)) \quad \Big\} \quad \Big] \\
= u_1 + iu_2 &
\end{aligned}
$$

6.3 Mode I

For a crack loaded in Mode I, symmetry of the normal displacement and boundary conditions for crack face stresses, allow the determination of the integration constants.

6.3.1 Displacement

For Mode I loading of the crack, the displacement must be symmetric w.r.t. the x_1-axis, which is the crack direction. To meet this requirement, the constants β and δ have to be zero. This can be concluded when studying the displacement components and using $\sin(-\theta) = -\sin(\theta)$ and $\cos(-\theta) = \cos(\theta)$. In the functions Ω and ω' three unknown constants remain.

$$
\left.\begin{aligned} u_1(\theta > 0) &= u_1(\theta < 0) \\ u_2(\theta > 0) &= -u_2(\theta < 0) \end{aligned}\right\} \quad \rightarrow \quad \boxed{\beta = \delta = 0} \quad \longrightarrow
$$

$$
\Omega = \alpha z^{\lambda+1} = \alpha r^{\lambda+1} e^{i(\lambda+1)\theta} \qquad ; \qquad \omega' = \gamma z^{\lambda+1} = \gamma r^{\lambda+1} e^{i(\lambda+1)\theta}
$$

6.3.2 Stress components

The stress components σ_{11}, σ_{22} and σ_{12} can be expressed in the variables r and θ and the constants α, γ and λ.

$$
\begin{aligned}
\sigma_{11} &= (\lambda+1)\left[\alpha z^{\lambda} + \alpha\bar{z}^{\lambda} - \tfrac{1}{2}\left\{\alpha\lambda\bar{z}z^{\lambda-1} + \gamma z^{\lambda} + \alpha\lambda z\bar{z}^{\lambda-1} + \gamma\bar{z}^{\lambda}\right\}\right] \\
\sigma_{22} &= (\lambda+1)\left[\alpha z^{\lambda} + \alpha\bar{z}^{\lambda} + \tfrac{1}{2}\left\{\alpha\lambda\bar{z}z^{\lambda-1} + \gamma z^{\lambda} + \alpha\lambda z\bar{z}^{\lambda-1} + \gamma\bar{z}^{\lambda}\right\}\right] \\
\sigma_{12} &= -\tfrac{1}{2}i(\lambda+1)\left[\alpha\lambda\bar{z}z^{\lambda-1} + \gamma z^{\lambda} - \alpha\lambda z\bar{z}^{\lambda-1} - \gamma\bar{z}^{\lambda}\right] \\
&\qquad \text{with} \quad z = re^{i\theta} \quad ; \quad \bar{z} = re^{-i\theta} \quad \rightarrow \\
\sigma_{11} &= (\lambda+1)r^{\lambda}\left[\alpha e^{i\lambda\theta} + \alpha e^{-i\lambda\theta} - \right. \\
&\qquad \left. \tfrac{1}{2}\left\{\alpha\lambda e^{i(\lambda-2)\theta} + \gamma e^{i\lambda\theta} + \alpha\lambda e^{-i(\lambda-2)\theta} + \gamma e^{-i\lambda\theta}\right\}\right]
\end{aligned}
$$

$$\sigma_{22} = (\lambda+1)r^{\lambda}\Big[\alpha e^{i\lambda\theta} + \alpha e^{-i\lambda\theta} + \tfrac{1}{2}\Big\{\alpha\lambda e^{i(\lambda-2)\theta} + \gamma e^{i\lambda\theta} + \alpha\lambda e^{-i(\lambda-2)\theta} + \gamma e^{-i\lambda\theta}\Big\}\Big]$$
$$\sigma_{12} = -\tfrac{1}{2}i(\lambda+1)r^{\lambda}\Big[\alpha\lambda e^{i(\lambda-2)\theta} + \gamma e^{i\lambda\theta} - \alpha\lambda e^{-i(\lambda-2)\theta} - \gamma e^{-i\lambda\theta}\Big]$$

$$\text{with} \quad e^{i\theta} + e^{-i\theta} = 2\cos(\theta) \quad ; \quad e^{i\theta} - e^{-i\theta} = 2i\sin(\theta) \quad \rightarrow$$

$$\sigma_{11} = 2(\lambda+1)r^{\lambda}\left[\alpha\cos(\lambda\theta) + \tfrac{1}{2}\left\{\alpha\lambda\cos((\lambda-2)\theta) + \gamma\cos(\lambda\theta)\right\}\right]$$
$$\sigma_{22} = 2(\lambda+1)r^{\lambda}\left[\alpha\cos(\lambda\theta) - \tfrac{1}{2}\left\{\alpha\lambda\cos((\lambda-2)\theta) + \gamma\cos(\lambda\theta)\right\}\right]$$
$$\sigma_{12} = (\lambda+1)r^{\lambda}\left[\alpha\lambda\sin((\lambda-2)\theta) + \gamma\sin(\lambda\theta)\right]$$

The boundary condition stating that the crack surface is stress-free, results in two equations for the unknown constants α and γ. For a non-trivial solution the equations need to be dependent. This confines the values of λ to be a series of discrete numbers. For each value of λ we find a ratio between α and γ.

$$\sigma_{22}(\theta = \pm\pi) = \sigma_{12}(\theta = \pm\pi) = 0 \quad \longrightarrow$$

$$\begin{bmatrix} (\lambda-2)\cos(\lambda\pi) & \cos(\lambda\pi) \\ \lambda\sin(\lambda\pi) & \sin(\lambda\pi) \end{bmatrix} \begin{bmatrix} \alpha \\ \gamma \end{bmatrix} = \begin{bmatrix} 0 \\ 0 \end{bmatrix} \quad \rightarrow$$
$$det \begin{bmatrix} (\lambda-2)\cos(\lambda\pi) & \cos(\lambda\pi) \\ \lambda\sin(\lambda\pi) & \sin(\lambda\pi) \end{bmatrix} = -\sin(2\lambda\pi) = 0 \rightarrow 2\pi\lambda = n\pi \rightarrow$$
$$\lambda = -\tfrac{1}{2}, \frac{n}{2}, \qquad \text{with} \quad n = 0, 1, 2, ..$$

The stress field is a series of terms, one for each value of λ in the range $[-\frac{1}{2}, 0, \frac{1}{2}, 1, \cdots]$. The first terms are presented here. Only one unknown constant (γ) remains in these solution.

$$\lambda = -\tfrac{1}{2} \quad \rightarrow \quad \alpha = 2\gamma \qquad ; \qquad \lambda = 0 \quad \rightarrow \quad \alpha = \tfrac{1}{2}\gamma$$
$$\lambda = \tfrac{1}{2} \quad \rightarrow \quad \alpha = -2\gamma \qquad ; \qquad \lambda = 1 \quad \rightarrow \quad \alpha = \gamma$$

$$\sigma_{11} = 2\gamma r^{-\frac{1}{2}}\cos(\tfrac{1}{2}\theta)\left[1 - \sin(\tfrac{3}{2}\theta)\sin(\tfrac{1}{2}\theta)\right] + \cdots$$
$$\sigma_{22} = 2\gamma r^{-\frac{1}{2}}\cos(\tfrac{1}{2}\theta)\left[1 + \sin(\tfrac{3}{2}\theta)\sin(\tfrac{1}{2}\theta)\right] + \cdots$$
$$\sigma_{12} = 2\gamma r^{-\frac{1}{2}}\left[\cos(\tfrac{1}{2}\theta)\cos(\tfrac{3}{2}\theta)\sin(\tfrac{1}{2}\theta)\right] + \cdots$$

6.3.3 Stress intensity factor

The first term in the series is the dominant term close to the crack tip. This term represents the singularity of the stress field, because it will become infinite, when approaching the crack tip. A new parameter is introduced in the stress field, the so-called *Stress Intensity Factor*, SIF or K_I. It is defined as the limit value of the 22-component of the crack tip stress.

$$\boxed{K_I = \lim_{r \longrightarrow 0} \left(\sqrt{2\pi r}\ \sigma_{22}|_{\theta=0} \right) = 2\gamma\sqrt{2\pi}} \qquad [\ \mathrm{m}^{\frac{1}{2}}\ \mathrm{N}\ \mathrm{m}^{-2}\ ]$$

6.3.4 Crack tip solution

The stress components are determined for Mode I loading of a straight crack. The SIF K_I is the only unknown constant in this solution. It can be calculated when more boundary conditions are available in a situation where geometry and load are specified in more detail.

The displacement components are also known and for $\lambda = -\frac{1}{2}$ they are proportional to $\sqrt{r}$. For plane stress and plane strain they differ because of the different versions of Hooke's law.

$$\begin{aligned}
\sigma_{11} &= \frac{K_I}{\sqrt{2\pi r}} \left[\cos(\tfrac{1}{2}\theta) \left\{ 1 - \sin(\tfrac{1}{2}\theta) \sin(\tfrac{3}{2}\theta) \right\} \right] \\
\sigma_{22} &= \frac{K_I}{\sqrt{2\pi r}} \left[\cos(\tfrac{1}{2}\theta) \left\{ 1 + \sin(\tfrac{1}{2}\theta) \sin(\tfrac{3}{2}\theta) \right\} \right] \\
\sigma_{12} &= \frac{K_I}{\sqrt{2\pi r}} \left[\cos(\tfrac{1}{2}\theta) \sin(\tfrac{1}{2}\theta) \cos(\tfrac{3}{2}\theta) \right] \\
u_1 &= \frac{K_I}{2\mu} \sqrt{\frac{r}{2\pi}} \left[\cos(\tfrac{1}{2}\theta) \left\{ \kappa - 1 + 2\sin^2(\tfrac{1}{2}\theta) \right\} \right] \\
u_2 &= \frac{K_I}{2\mu} \sqrt{\frac{r}{2\pi}} \left[\sin(\tfrac{1}{2}\theta) \left\{ \kappa + 1 - 2\cos^2(\tfrac{1}{2}\theta) \right\} \right]
\end{aligned}$$

The second term in the stress field, for $\lambda = 0$ and $\alpha = \frac{1}{2}\gamma$, results in only a non-zero term for σ_{11} : $\sigma_{11} = 2\gamma$. This stress term is called the T-stress. It is not allowed to replace γ with $K_I/(2\sqrt{2\pi})$, as this relation only holds for the limit value of σ_{22} when taking $r \rightarrow 0$.

According to Leevers and Radon [43] the T-stress can however be expressed in K_I with the addition of a so-called *bi-axially parameter* B, which can be determined numerically for specific cases.

$$\lambda = 0 \quad \rightarrow \quad \alpha = \tfrac{1}{2}\gamma \quad \rightarrow$$
$$\sigma_{11} = 2\gamma = \frac{K_I}{\sqrt{2\pi}} \sqrt{\frac{2}{a}}\, B = \frac{K_I}{\sqrt{\pi a}}\, B \qquad ; \qquad \sigma_{22} = 0 \qquad ; \qquad \sigma_{12} = 0$$

6.4 Mode II

For a crack loaded in Mode II, anti-symmetry of the tangential displacement component and boundary conditions for the crack face stresses, allow the determination of the integration constants.

6.4.1 Displacement

For Mode II loading of the crack, the displacement must be anti-symmetric w.r.t. the x_1-axis, which is the crack direction. To meet this requirement, the constants α and γ have to be zero. This can be concluded from the displacement components, using $\sin(-\theta) = -\sin(\theta)$ and $\cos(-\theta) = \cos(\theta)$. In the functions Ω and ω' three unknown constants remain.

$$\left.\begin{array}{l} u_1(\theta > 0) = -u_1(\theta < 0) \\ u_2(\theta > 0) = u_2(\theta < 0) \end{array}\right\} \quad \rightarrow \quad \boxed{\alpha = \gamma = 0} \quad \longrightarrow$$

$$\Omega = i\beta z^{\lambda+1} = i\beta r^{\lambda+1} e^{i(\lambda+1)\theta} \quad ; \quad \omega' = i\delta z^{\lambda+1} = i\delta r^{\lambda+1} e^{i(\lambda+1)\theta}$$

6.4.2 Stress intensity factor

The stress intensity factor K_{II} is now defined as the limit value of the 12-component of the crack tip stress.

$$\boxed{K_{II} = \lim_{r \longrightarrow 0} \left(\sqrt{2\pi r}\ \sigma_{12}|_{\theta=0} \right)} \qquad [\ \mathrm{m}^{\frac{1}{2}}\ \mathrm{N\ m}^{-2}\ ]$$

6.4.3 Crack tip solution

The stress components are determined for Mode II loading of a straight crack. The SIF K_{II} is the only unknown constant in this solution. It can be calculated when more boundary conditions are available in a situation where geometry and load are specified in more detail.

The displacement components are also known and for $\lambda = -\frac{1}{2}$ they are proportional to $\sqrt{r}$. For plane stress and plane strain they differ because of the different versions of Hooke's law.

$$\sigma_{11} = \frac{K_{II}}{\sqrt{2\pi r}} \left[-\sin(\tfrac{1}{2}\theta) \left\{ 2 + \cos(\tfrac{1}{2}\theta)\cos(\tfrac{3}{2}\theta) \right\} \right]$$

$$\sigma_{22} = \frac{K_{II}}{\sqrt{2\pi r}} \left[\sin(\tfrac{1}{2}\theta)\cos(\tfrac{1}{2}\theta)\cos(\tfrac{3}{2}\theta) \right]$$

$$\sigma_{12} = \frac{K_{II}}{\sqrt{2\pi r}} \left[\cos(\tfrac{1}{2}\theta) \left\{ 1 - \sin(\tfrac{1}{2}\theta)\sin(\tfrac{3}{2}\theta) \right\} \right]$$

$$u_1 = \frac{K_{II}}{2\mu} \sqrt{\frac{r}{2\pi}} \left[\sin(\tfrac{1}{2}\theta) \left\{ \kappa + 1 + 2\cos^2(\tfrac{1}{2}\theta) \right\} \right]$$

$$u_2 = \frac{K_{II}}{2\mu} \sqrt{\frac{r}{2\pi}} \left[-\cos(\tfrac{1}{2}\theta) \left\{ \kappa - 1 - 2\sin^2(\tfrac{1}{2}\theta) \right\} \right]$$

6.5 Mode III

When a crack is loaded in Mode III, only the out-of-plane displacement u_3 is relevant

6.5.1 Laplace equation

The two relevant strain components ε_{31} and ε_{32} are substituted in Hooke's law, resulting in two stress components σ_{31} and σ_{32}. These are substituted in the equilibrium equation, leading to a Laplace equation for u_3.

$$\left.\begin{array}{l} \varepsilon_{31} = \frac{1}{2}u_{3,1} \qquad ; \qquad \varepsilon_{32} = \frac{1}{2}u_{3,2} \\ \text{Hooke's law} \end{array}\right\} \quad \rightarrow$$

$$\left.\begin{array}{l} \sigma_{31} = 2\mu\varepsilon_{31} = \mu u_{3,1} \qquad ; \qquad \sigma_{32} = 2\mu\varepsilon_{32} = \mu u_{3,2} \\ \text{equilibrium} \end{array}\right\} \quad \rightarrow$$

$$\sigma_{31,1} + \sigma_{32,2} = \mu u_{3,11} + \mu u_{3,22} = 0 \quad \rightarrow \quad \nabla^2 u_3 = 0$$

6.5.2 Displacement

The general solution of the Laplace equation is written as the sum of a complex function f and its conjugate $\bar{f}$. Choosing a specific function f with three yet unknown constants A, B and λ, it can again be argumented that the exponent λ must be larger than -1, because displacements must remain finite.

general solution $\qquad u_3 = f + \bar{f}$

specific choice $\qquad f = (A + iB)z^{\lambda+1} \quad \rightarrow \quad \bar{f} = (A - iB)\bar{z}^{\lambda+1}$

6.5.3 Stress components

Stress components σ_{31} and σ_{32} can now be expressed in the variables r and θ and the constants A, B and λ. The boundary condition that the crack surface is stress-free, results in two equations for the unknown constants A and B. For a non-trivial solution the equations need to be dependent. This confines the values of λ to be a series of discrete numbers. For each value of λ we find a ratio between A and B.

$$\begin{aligned} \sigma_{31} &= 2(\lambda+1)r^{\lambda}\{A\cos(\lambda\theta) - B\sin(\lambda\theta)\} \\ \sigma_{32} &= -2(\lambda+1)r^{\lambda}\{A\sin(\lambda\theta) + B\cos(\lambda\theta)\} \end{aligned}$$

$$\sigma_{32}(\theta = \pm\pi) = 0 \quad \rightarrow$$

$$\begin{bmatrix} \sin(\lambda\pi) & \cos(\lambda\pi) \\ \sin(\lambda\pi) & -\cos(\lambda\pi) \end{bmatrix} \begin{bmatrix} A \\ B \end{bmatrix} = \begin{bmatrix} 0 \\ 0 \end{bmatrix} \quad \rightarrow$$

$$\det \begin{bmatrix} \sin(\lambda\pi) & \cos(\lambda\pi) \\ \sin(\lambda\pi) & -\cos(\lambda\pi) \end{bmatrix} = -\sin(2\pi\lambda) = 0 \quad \rightarrow \quad 2\pi\lambda = n\pi \quad \rightarrow$$

$$\lambda = -\tfrac{1}{2}, \frac{n}{2}, .. \qquad \text{with} \qquad n = 0, 1, 2, ..$$

crack tip solution $\quad \lambda = -\frac{1}{2} \quad \rightarrow \quad A = 0 \quad \rightarrow$

$$\sigma_{31} = Br^{-\frac{1}{2}}\{\sin(\tfrac{1}{2}\theta)\} \qquad ; \qquad \sigma_{32} = -Br^{-\frac{1}{2}}\{\cos(\tfrac{1}{2}\theta)\}$$

6.5.4 Stress intensity factor

The first term in the series is the crack tip solution. It determines the singularity of the stress field. The only unknown constant B is replaced by the *Stress Intensity Factor* K_{III}.

$$\boxed{K_{III} = \lim_{r \longrightarrow 0} \left(\sqrt{2\pi r}\ \sigma_{32}|_{\theta=0} \right)}$$

6.5.5 Crack tip solution

The SIF K_{III} is the only unknown constant in the stress tip solution. It can be determined when more boundary conditions are available.

$$\sigma_{31} = \frac{K_{III}}{\sqrt{2\pi r}} \left[-\sin(\tfrac{1}{2}\theta) \right] \qquad ; \qquad \sigma_{32} = \frac{K_{III}}{\sqrt{2\pi r}} \left[\cos(\tfrac{1}{2}\theta) \right]$$

$$u_3 = \frac{2K_{III}}{\mu} \sqrt{\frac{r}{2\pi}} \left[\sin(\tfrac{1}{2}\theta) \right]$$

6.6 Crack tip stress (mode I, II, III)

For the three modes of loading, the solution of the bi-harmonic equation results in a series expansion both for the displacement components and the stress components. Each discrete value of the variable λ results in a term of the solution. The dependency of the distance r to the crack tip is $r^{\lambda+1}$ for the displacements and r^{λ} for the stresses. The first term is by far the largest in the vicinity of the crack tip, which is the reason that for the crack tip solution only the first term is considered. The solution is derived for a general crack in a large plate and is summarized below.

For other crack geometries and loadings, equivalent solutions can be derived, which only differ in the value of the stress intensity factor K. This K solely determines the amplitude of the stresses at the crack tip. The dependency of geometry is generally indicated with the geometry factor β.

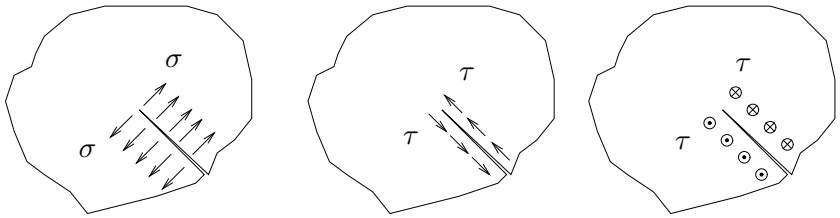

Mode I Mode II Mode III

Fig. 6.4 : *Edge crack under Mode I, II and III loading.*

$$\sigma_{ij} = \frac{K_I}{\sqrt{2\pi r}} f_{Iij}(\theta) \quad ; \quad \sigma_{ij} = \frac{K_{II}}{\sqrt{2\pi r}} f_{IIij}(\theta) \quad ; \quad \sigma_{ij} = \frac{K_{III}}{\sqrt{2\pi r}} f_{IIIij}(\theta)$$

$$K_I = \beta_I \, \sigma\sqrt{\pi a} \quad ; \quad K_{II} = \beta_{II} \, \tau\sqrt{\pi a} \quad ; \quad K_{III} = \beta_{III} \, \tau\sqrt{\pi a}$$

6.6.1 K-zone

The question may arise at what distance to the crack tip, displacement and stresses are still described accurately by the first term of the total solution. There is no clear answer to this question. The K-zone, where the first term, whose value is determined by the stress intensity factor K, is the only important one, depends on geometry and loading, as is illustrated in the figure.

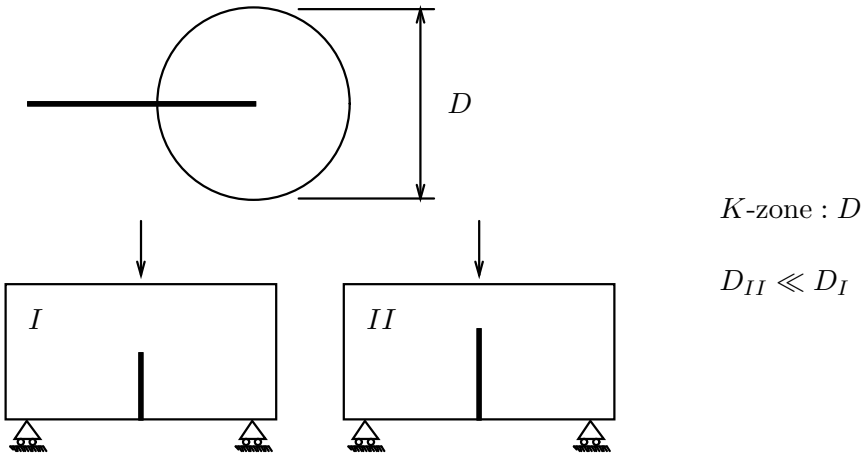

Fig. 6.5 : *K-zone at the crack tip in a three-point bending test.*

6.7 SIF for specified cases

The SIF can be determined when boundary conditions are specified in more detail. Solutions for many cases can be found in literature. Some examples for distributed loading are presented.

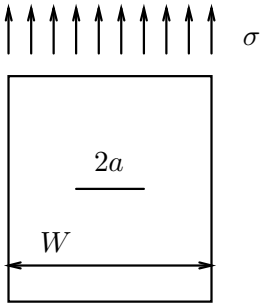

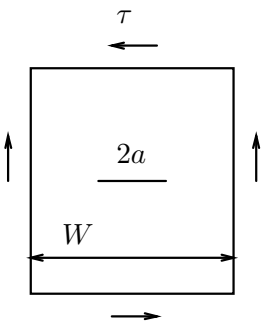

$$K_I = \sigma\sqrt{\pi a}\left(\sec\frac{\pi a}{W}\right)^{1/2}$$

$$K_{II} = \tau\sqrt{\pi a} \qquad \text{small } \frac{a}{W}$$

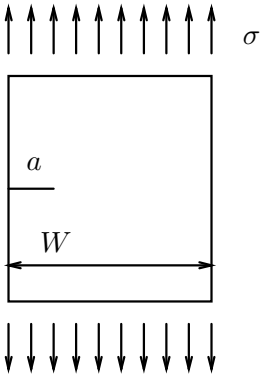

$$K_I = \sigma\sqrt{a}\left[\,1.12\sqrt{\pi} - 0.41\frac{a}{W} + 18.7\left(\frac{a}{W}\right)^2 - 38.48\left(\frac{a}{W}\right)^3 + 53.85\left(\frac{a}{W}\right)^4\,\right]$$

$$\approx 1.12\sigma\sqrt{\pi a} \qquad \text{small } \frac{a}{W}$$

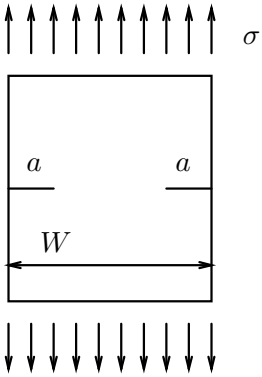

$$K_I = \sigma\sqrt{a}\left[\,1.12\sqrt{\pi} + 0.76\frac{a}{W} - 8.48\left(\frac{a}{W}\right)^2 + 27.36\left(\frac{a}{W}\right)^3\,\right]$$

$$\approx 1.12\sigma\sqrt{\pi a}$$

For point loads and a crack loaded by internal pressure, SIF's are also known from literature.

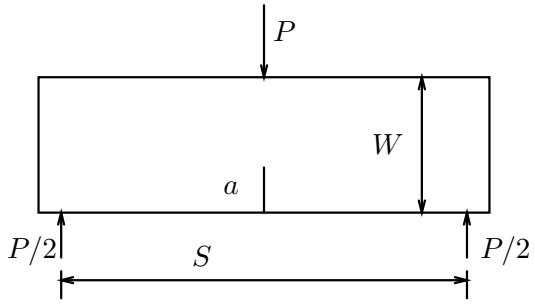

$$K_I = \frac{PS}{BW^{3/2}}\left[2.9\left(\frac{a}{W}\right)^{\frac{1}{2}} - 4.6\left(\frac{a}{W}\right)^{\frac{3}{2}} + 21.8\left(\frac{a}{W}\right)^{\frac{5}{2}} - 37.6\left(\frac{a}{W}\right)^{\frac{7}{2}} + 37.7\left(\frac{a}{W}\right)^{\frac{9}{2}}\right]$$

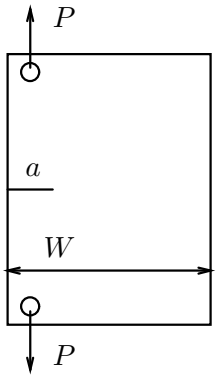

$$K_I = \frac{P}{BW^{1/2}}\left[29.6\left(\frac{a}{W}\right)^{\frac{1}{2}} - 185.5\left(\frac{a}{W}\right)^{\frac{3}{2}} + 655.7\left(\frac{a}{W}\right)^{\frac{5}{2}} - 1017\left(\frac{a}{W}\right)^{\frac{7}{2}} + 638.9\left(\frac{a}{W}\right)^{\frac{9}{2}}\right]$$

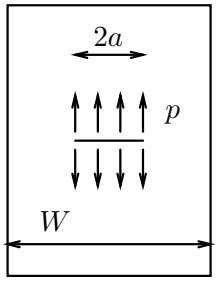

$$K_I = p\sqrt{\pi a}$$

p per unit thickness

6.8 K-based crack growth criteria

A crack will grow when the crack tip stress exceeds a certain critical value. The stress intensity factor determines the "amplitude" of the crack tip stress for a certain geometry and loading case. We may thus conclude that a crack will grow when K reaches a critical value. This implies that a crack growth criterion can be formulated, where the stress intensity factor for a certain situation is compared to this critical value. The value of the stress intensity factor has to be calculated. The critical value has to be known from experimental measurements. It is called the *Fracture Toughness* and denoted as K_c.

$$K_I = K_{Ic} \quad ; \quad K_{II} = K_{IIc} \quad ; \quad K_{III} = K_{IIIc}$$

6.9 Relation $G - K$

The global crack growth criterion was formulated in terms of the energy release rate G and derived from an energy balance. The local stress growth criterion was formulated in terms of the stress intensity factor K and derived from crack tip stresses. It may not be surprising that there is a relation between G and K, which will be derived in this section.

We consider a crack in an "infinite plate" and focus attention on normal stresses and openings in the crack plane. First we consider a crack of half length a and then a crack of half length $a + \Delta a$. To close the latter back to length a again, we know which stress is needed and which opening has to be eliminated. Multiplying normal load and closing displacement,

results in the work needed to accomplish this. This work equals the energy which has been released during opening, the energy release rate G.

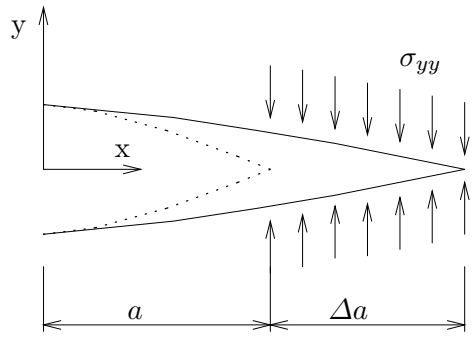

Fig. 6.6 : *Central crack opened from length a to length $a + \Delta a$.*

crack length a $\quad \sigma_{yy}(\theta = 0, r = x - a) = \dfrac{\sigma\sqrt{a}}{\sqrt{2(x-a)}} \quad ; \quad u_y = 0$

crack length $a + \Delta a$ $\quad \sigma_{yy}(\theta = \pi, r = a + \Delta a - x) = 0$

$$u_y = \frac{(1+\nu)(\kappa+1)}{E} \, \frac{\sigma\sqrt{a+\Delta a}}{\sqrt{2}} \, \sqrt{a + \Delta a - x}$$

accumulation of elastic energy

$$\Delta U = 2B \int_a^{a+\Delta a} \tfrac{1}{2}\sigma_{yy} \, dx \; u_y = B \int_a^{a+\Delta a} \sigma_{yy} u_y \, dx = B \, f(\Delta a) \, \Delta a \qquad \rightarrow$$

energy release rate

$$G = \frac{1}{B} \lim_{\Delta a \rightarrow 0} \left(\frac{\Delta U}{\Delta a} \right) = \lim_{\Delta a \rightarrow 0} f(\Delta a) = \frac{(1+\nu)(\kappa+1)}{4E} \, \sigma^2 a \pi = \frac{(1+\nu)(\kappa+1)}{4E} \, K_I^2$$

plane stress $\qquad G = \dfrac{K_I^2}{E}$

plane strain $\qquad G = (1 - \nu^2)\dfrac{K_I^2}{E}$

A relation between G and K is also available for multi-mode loading and can be derived by superposition.

$$G = \frac{1}{E} \left(c_1 K_I^2 + c_2 K_{II}^2 + c_3 K_{III}^2 \right)$$

plane stress $$G = \frac{1}{E}(K_I^2 + K_{II}^2)$$

plane strain $$G = \frac{(1-\nu^2)}{E}(K_I^2 + K_{II}^2) + \frac{(1+\nu)}{E}K_{III}^2$$

6.10 The critical SIF value

In the local crack growth criterion, the actual value K of the stress intensity factor is compared to a critical value K_c. This has to be measured according to an elaborate experimental procedure and is then considered to be a material constant. The actual procedure can be found in literature [25] and is normalized.

When K_{Ic} would be measured using a large plate with a central crack of length $2a$, the critical value would appear to be dependent on the plate thickness. This can be explained later – we have to consider the plastic crack tip zone for this –. It appears that the critical thickness B_c, from which a constant value for K_{Ic} results, is very large. This means that such an experimental setup would be unfeasible and therefore other experiments are designed and normalized.

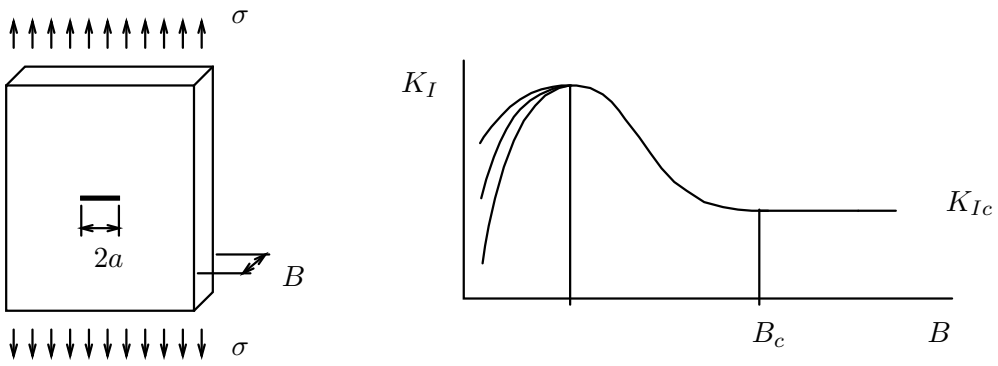

Fig. 6.7 : *Central crack in a plate, loaded with Mode I stress σ (left). Dependence of critical K-value on the plate thickness B (right).*

$$K_{Ic} = \sigma_c\sqrt{\pi a} \qquad ; \qquad B_c = 2.5\left(\frac{K_{Ic}}{\sigma_y}\right)^2$$

6.10.1 K_{Ic} values

The table lists values for the fracture toughness K_{Ic} for various materials. They are taken from [25].

Material	σ_v [MPa]	K_{Ic} [MPa$\sqrt{\text{m}}$]
steel, 300 maraging	1669	93.4
steel, 350 maraging	2241	38.5
steel, D6AC	1496	66.0
steel, AISI 4340	1827	47.3
steel, A533B reactor	345	197.8
steel, carbon	241	219.8
Al 2014-T4	448	28.6
Al 2024-T3	393	34.1
Al 7075-T651	545	29.7
Al 7079-T651	469	33.0
Ti 6Al-4V	1103	38.5
Ti 6Al-6V-2Sn	1083	37.4
Ti 4Al-4Mo-2Sn-0.5Si	945	70.3

Chapter 7

Multi-mode crack loading

In practical situations, a crack is mostly subjected to a combined Mode I and Mode II loading. In the figure the load is visualized as an edge load on a square material volume element with edges parallel and perpendicular to the crack. A tensile load parallel to the crack can be added because it has no influence on the crack tip stress. Each random load can be transformed to this loading situation by proper transformation of the edge loads. The crack tip stresses can be determined as the superposition of the stress components due to separate Mode I and Mode II loadings.

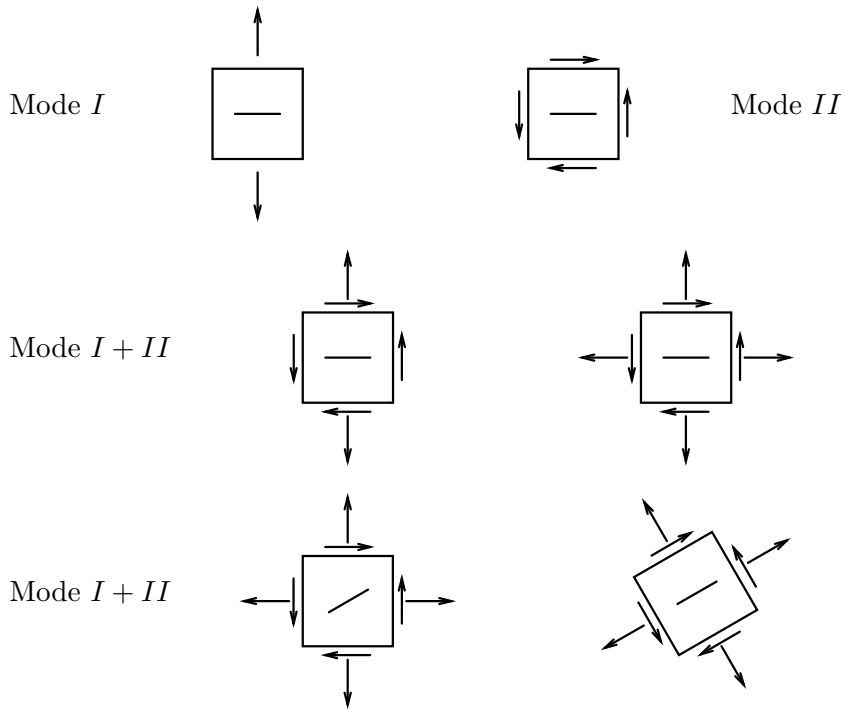

Fig. 7.1 : *Central crack loaded in Mode I, Mode II and a combination of Mode I and II.*

7.1 Stress component transformation

We consider a plane with unity normal vector $\vec{n}$ and stress vector $\vec{p}$. Components of $\vec{n}$ and $\vec{p}$ with respect to the base $\{\vec{e}_1, \vec{e}_2\}$ are stored in columns $\underset{\sim}{n}$ and $\underset{\sim}{p}$. Another base $\{\vec{e}_1^*, \vec{e}_2^*\}$ is rotated anti-clockwise over an angle θ w.r.t. $\{\vec{e}_1, \vec{e}_2\}$. Components of $\vec{n}$ and $\vec{p}$ w.r.t. this base are stored in columns $\underset{\sim}{n}^*$ and $\underset{\sim}{p}^*$. Using the relation between $\{\vec{e}_1^*, \vec{e}_2^*\}$ and $\{\vec{e}_1, \vec{e}_2\}$, a transformation matrix $\underline{T}$ can be determined which relates the columns $\underset{\sim}{n}^*$ to $\underset{\sim}{n}$, and $\underset{\sim}{p}^*$ to $\underset{\sim}{p}$.

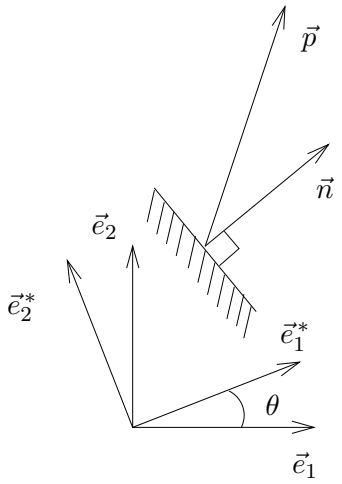

Fig. 7.2 : *Material plane with unit normal vector and stress vector.*

$$\vec{e}_1^* = \cos(\theta)\vec{e}_1 + \sin(\theta)\vec{e}_2 = c\vec{e}_1 + s\vec{e}_2$$
$$\vec{e}_2^* = -\sin(\theta)\vec{e}_1 + \cos(\theta)\vec{e}_2 = -s\vec{e}_1 + c\vec{e}_2$$

$$\vec{p} = p_1\vec{e}_1 + p_2\vec{e}_2 = p_1^*\vec{e}_1^* + p_2^*\vec{e}_2^* \quad \rightarrow$$
$$\begin{bmatrix} p_1 \\ p_2 \end{bmatrix} = \begin{bmatrix} c & -s \\ s & c \end{bmatrix} \begin{bmatrix} p_1^* \\ p_2^* \end{bmatrix} \quad \rightarrow \quad \begin{bmatrix} p_1^* \\ p_2^* \end{bmatrix} = \begin{bmatrix} c & s \\ -s & c \end{bmatrix} \begin{bmatrix} p_1 \\ p_2 \end{bmatrix} \quad \rightarrow$$
$$\underset{\sim}{p} = \underline{T}\,\underset{\sim}{p}^* \quad \rightarrow \quad \underset{\sim}{p}^* = \underline{T}^T\underset{\sim}{p} \qquad \text{idem} \quad : \quad \underset{\sim}{n}^* = \underline{T}^T\underset{\sim}{n}$$

With respect to the basis $\{\vec{e}_1, \vec{e}_2\}$, the stress vector components $\underset{\sim}{p}$ can be calculated from the Cauchy stress matrix $\underline{\sigma}$ and the components $\underset{\sim}{n}$ of the normal vector. Using the transformation matrix $\underline{T}$, the matrix $\underline{\sigma}^*$ w.r.t. the basis $\{\vec{e}_1^*, \vec{e}_2^*\}$ can be calculated from $\underline{\sigma}$.

$$\underset{\sim}{p} = \underline{\sigma}\,\underset{\sim}{n} \quad \rightarrow$$
$$\underline{T}\,\underset{\sim}{p}^* = \underline{\sigma}\,\underline{T}\,\underset{\sim}{n}^* \quad \rightarrow \quad \underset{\sim}{p}^* = \underline{T}^T\underline{\sigma}\,\underline{T}\,\underset{\sim}{n}^* = \underline{\sigma}^*\underset{\sim}{n}^* \quad \rightarrow$$
$$\underline{\sigma}^* = \underline{T}^T\underline{\sigma}\,\underline{T} \quad \rightarrow \quad \underline{\sigma} = \underline{T}\,\underline{\sigma}^*\underline{T}^T$$

$$\begin{bmatrix} \sigma_{11}^* & \sigma_{12}^* \\ \sigma_{21}^* & \sigma_{22}^* \end{bmatrix} = \begin{bmatrix} c & s \\ -s & c \end{bmatrix} \begin{bmatrix} \sigma_{11} & \sigma_{12} \\ \sigma_{21} & \sigma_{22} \end{bmatrix} \begin{bmatrix} c & -s \\ s & c \end{bmatrix}$$
$$= \begin{bmatrix} c & s \\ -s & c \end{bmatrix} \begin{bmatrix} c\sigma_{11} + s\sigma_{12} & -s\sigma_{11} + c\sigma_{12} \\ c\sigma_{21} + s\sigma_{22} & -s\sigma_{21} + c\sigma_{22} \end{bmatrix}$$

$$= \begin{bmatrix} c^2\sigma_{11} + 2cs\sigma_{12} + s^2\sigma_{22} & \\ & -cs\sigma_{11} + (c^2 - s^2)\sigma_{12} + cs\sigma_{22} \\ -cs\sigma_{11} + (c^2 - s^2)\sigma_{12} + cs\sigma_{22} & \\ & s^2\sigma_{11} - 2cs\sigma_{12} + c^2\sigma_{22} \end{bmatrix}$$

Stress component transformation can also be used to determine stress components in a cylindrical coordinate system. These will be needed later in crack growth direction criteria. With the figure below, it is easily understood that cylindrical stress components can be derived from Cartesian components by transformation of the stress matrix.

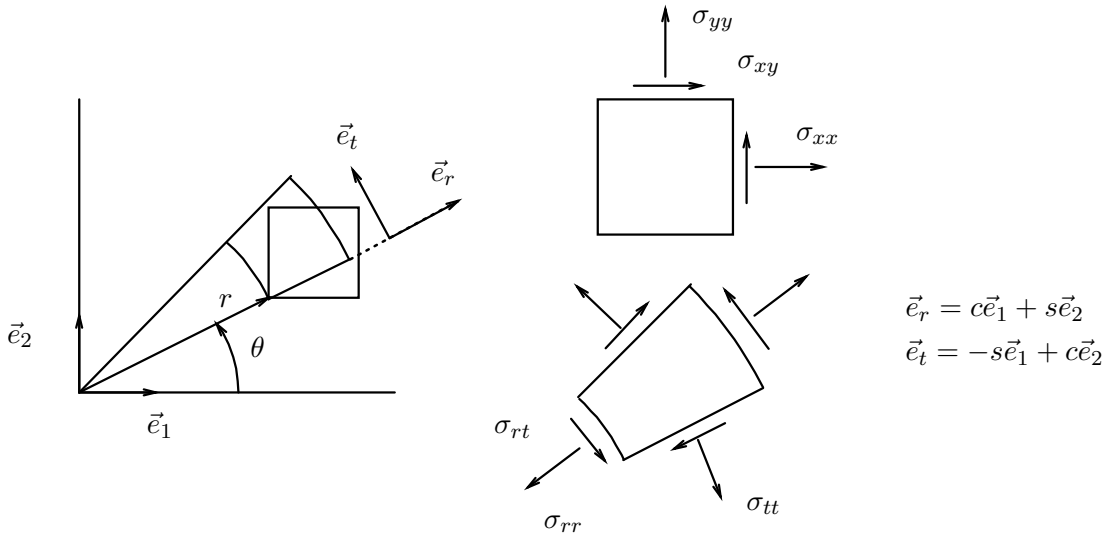

Fig. 7.3 : *Cartesian and cylindrical stress 'cubes' at the crack tip.*

$$\begin{bmatrix} \sigma_{rr} & \sigma_{rt} \\ \sigma_{tr} & \sigma_{tt} \end{bmatrix} = \begin{bmatrix} c & s \\ -s & c \end{bmatrix} \begin{bmatrix} \sigma_{xx} & \sigma_{xy} \\ \sigma_{xy} & \sigma_{yy} \end{bmatrix} \begin{bmatrix} c & -s \\ s & c \end{bmatrix}$$

$$= \begin{bmatrix} c^2\sigma_{xx} + 2cs\sigma_{xy} + s^2\sigma_{yy} & \\ & -cs\sigma_{xx} + (c^2 - s^2)\sigma_{xy} + cs\sigma_{yy} \\ -cs\sigma_{xx} + (c^2 - s^2)\sigma_{xy} + cs\sigma_{yy} & \\ & s^2\sigma_{xx} - 2cs\sigma_{xy} + c^2\sigma_{yy} \end{bmatrix}$$

The Cartesian crack tip stresses have been derived before and are summarized below.

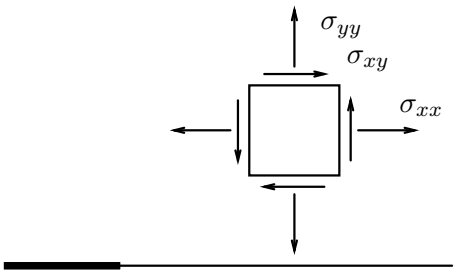

$$\sigma_{xx} = \frac{K_I}{\sqrt{2\pi r}} f_{Ixx}(\theta) + \frac{K_{II}}{\sqrt{2\pi r}} f_{IIxx}(\theta)$$
$$\sigma_{yy} = \frac{K_I}{\sqrt{2\pi r}} f_{Iyy}(\theta) + \frac{K_{II}}{\sqrt{2\pi r}} f_{IIyy}(\theta)$$
$$\sigma_{xy} = \frac{K_I}{\sqrt{2\pi r}} f_{Ixy}(\theta) + \frac{K_{II}}{\sqrt{2\pi r}} f_{IIxy}(\theta)$$

Fig. 7.4 : *Cartesian stress cube at the crack tip.*

$$f_{Ixx}(\theta) = \cos(\frac{\theta}{2}) \left[1 - \sin(\frac{\theta}{2}) \sin(\frac{3\theta}{2})\right] \qquad f_{IIxx}(\theta) = -\sin(\frac{\theta}{2}) \left[2 + \cos(\frac{\theta}{2}) \cos(\frac{3\theta}{2})\right]$$
$$f_{Iyy}(\theta) = \cos(\frac{\theta}{2}) \left[1 + \sin(\frac{\theta}{2}) \sin(\frac{3\theta}{2})\right] \qquad f_{IIyy}(\theta) = \sin(\frac{\theta}{2}) \cos(\frac{\theta}{2}) \cos(\frac{3\theta}{2})$$
$$f_{Ixy}(\theta) = \sin(\frac{\theta}{2}) \cos(\frac{\theta}{2}) \cos(\frac{3\theta}{2}) \qquad f_{IIxy}(\theta) = \cos(\frac{\theta}{2}) \left[1 - \sin(\frac{\theta}{2}) \sin(\frac{3\theta}{2})\right]$$

Substitution in the transformation relation, results in cylindrical crack tip stresses. The functions f_{rr}, f_{tt} and f_{rt} can be derived, using some trigonometry.

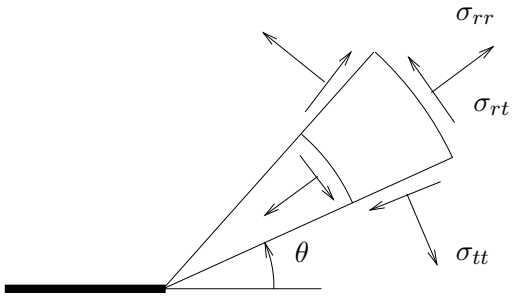

$$\sigma_{rr} = \frac{K_I}{\sqrt{2\pi r}} f_{Irr}(\theta) + \frac{K_{II}}{\sqrt{2\pi r}} f_{IIrr}(\theta)$$
$$\sigma_{tt} = \frac{K_I}{\sqrt{2\pi r}} f_{Itt}(\theta) + \frac{K_{II}}{\sqrt{2\pi r}} f_{IItt}(\theta)$$
$$\sigma_{rt} = \frac{K_I}{\sqrt{2\pi r}} f_{Irt}(\theta) + \frac{K_{II}}{\sqrt{2\pi r}} f_{IIrt}(\theta)$$

Fig. 7.5 : *Cylindrical stress 'cube' at the crack tip.*

$$f_{Irr}(\theta) = \left[\frac{5}{4} \cos(\frac{\theta}{2}) - \frac{1}{4} \cos(\frac{3\theta}{2})\right] \qquad f_{IIrr}(\theta) = \left[-\frac{5}{4} \sin(\frac{\theta}{2}) + \frac{3}{4} \sin(\frac{3\theta}{2})\right]$$
$$f_{Itt}(\theta) = \left[\frac{3}{4} \cos(\frac{\theta}{2}) + \frac{1}{4} \cos(\frac{3\theta}{2})\right] \qquad f_{IItt}(\theta) = \left[-\frac{3}{4} \sin(\frac{\theta}{2}) - \frac{3}{4} \sin(\frac{3\theta}{2})\right]$$
$$f_{Irt}(\theta) = \left[\frac{1}{4} \sin(\frac{\theta}{2}) + \frac{1}{4} \sin(\frac{3\theta}{2})\right] \qquad f_{IIrt}(\theta) = \left[\frac{1}{4} \cos(\frac{\theta}{2}) + \frac{3}{4} \cos(\frac{3\theta}{2})\right]$$

7.2 Multi-mode load

For a crack with angle θ w.r.t. the edge of the material volume element with edge loads represented by $\underline{\sigma}$, the Mode I and Mode II loading is represented by the edge loads $\underline{\sigma}^*$ on a rotated material volume element. The crack tip stresses of the combined loading are determined by superposition. The load parallel to the crack (σ^*_{11}) is assumed to have no influence on the crack tip stress state. Note that in the next cases the load is indicated by σ_{ij} and the crack tip stresses by s_{ij}.

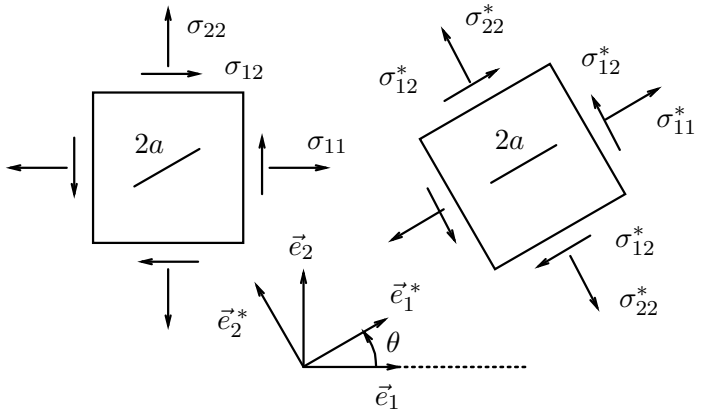

Fig. 7.6 : *Transformation of multi-mode load into Mode I and II loads.*

$$\begin{bmatrix} \sigma^*_{11} & \sigma^*_{12} \\ \sigma^*_{21} & \sigma^*_{22} \end{bmatrix} = \begin{bmatrix} c^2\sigma_{11} + 2cs\sigma_{12} + s^2\sigma_{22} & \\ & -cs\sigma_{11} + (c^2 - s^2)\sigma_{12} + cs\sigma_{22} \\ -cs\sigma_{11} + (c^2 - s^2)\sigma_{12} + cs\sigma_{22} & \\ & s^2\sigma_{11} - 2cs\sigma_{12} + c^2\sigma_{22} \end{bmatrix}$$

crack tip stresses $\quad s_{ij} = \dfrac{K_I}{\sqrt{2\pi r}} f_{Iij}(\theta) + \dfrac{K_{II}}{\sqrt{2\pi r}} f_{IIij}(\theta)$

with $\quad K_I = \beta\ \sigma^*_{22}\sqrt{\pi a} \quad ; \quad K_{II} = \gamma\ \sigma^*_{12}\sqrt{\pi a}$

Example multi-mode load

As an example we consider the bi-axial load on a crack which orientation has an angle θ with the horizontal direction.

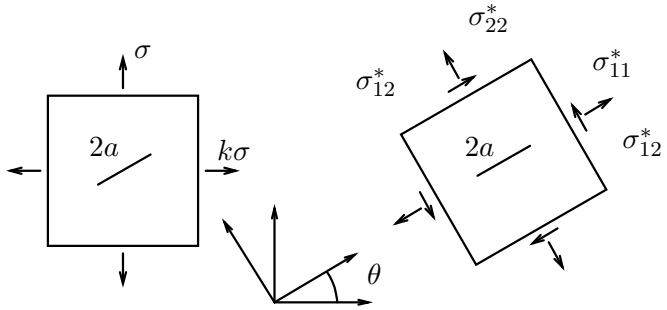

Fig. 7.7 : *Transformation of multi-mode load into Mode I and II loads.*

$$\sigma^*_{11} = c^2\sigma_{11} + 2cs\sigma_{12} + s^2\sigma_{22} = c^2k\sigma + s^2\sigma$$
$$\sigma^*_{22} = s^2\sigma_{11} - 2cs\sigma_{12} + c^2\sigma_{22} = s^2k\sigma + c^2\sigma$$
$$\sigma^*_{12} = -cs\sigma_{11} + (c^2 - s^2)\sigma_{12} + cs\sigma_{22} = cs(1-k)\sigma$$

crack tip stresses $$s_{ij} = \frac{K_I}{\sqrt{2\pi r}} f_{Iij}(\theta) + \frac{K_{II}}{\sqrt{2\pi r}} f_{IIij}(\theta)$$

$$K_I = \beta_I\ \sigma^*_{22}\sqrt{\pi a} = \beta_I\ (s^2k + c^2)\sigma\sqrt{\pi a}$$
$$K_{II} = \beta_{II}\ \sigma^*_{12}\sqrt{\pi a} = \beta_{II}\ cs(1-k)\sigma\sqrt{\pi a}$$

Example multi-mode load

The results from the example above, can be used directly in the situation of a crack through the whole thickness of the wall of a thin-walled tube. The crack has an angle θ w.r.t. the axial direction.

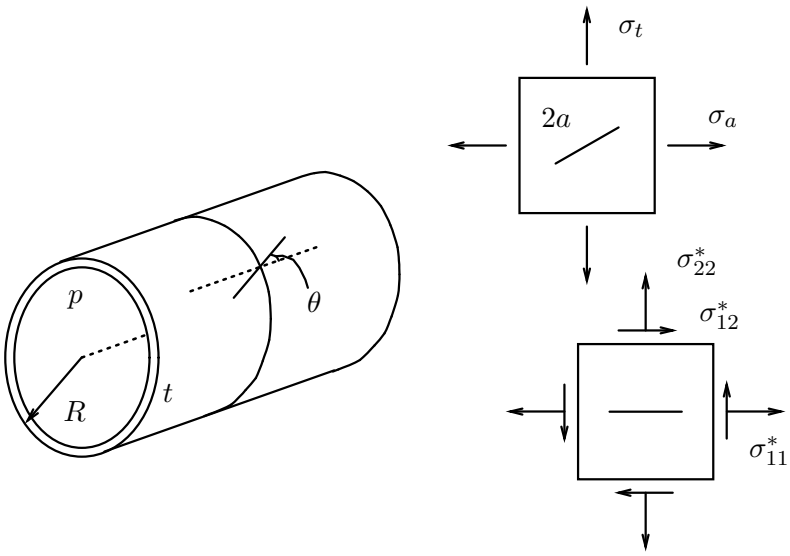

Fig. 7.8 : *Crack in tube wall at an angle θ with the tube axis.*

$$\sigma_t = \frac{pR}{t} = \sigma \quad ; \quad \sigma_a = \frac{pR}{2t} = \tfrac{1}{2}\sigma \quad \rightarrow \quad k = \frac{1}{2}$$
$$\sigma^*_{22} = s^2\,\tfrac{1}{2}\,\sigma + c^2\sigma \quad ; \quad \sigma^*_{12} = cs(1-\tfrac{1}{2})\sigma = \tfrac{1}{2}\,cs\,\sigma$$
$$K_I = \sigma^*_{22}\sqrt{\pi a} = (\tfrac{1}{2}s^2 + c^2)\sigma\sqrt{\pi a} = (\tfrac{1}{2}s^2 + c^2)\frac{pR}{t}\sqrt{\pi a}$$
$$K_{II} = \sigma^*_{12}\sqrt{\pi a} = \tfrac{1}{2}\,cs\,\sigma = \tfrac{1}{2}\,cs\,\frac{pR}{t}\sqrt{\pi a}$$

7.3 Crack growth direction

Crack growth criteria are used to check whether a crack will grow at a given external load. When the crack is loaded only in mode I, it will be expected that the crack tip will move in the crack plane. However, in multi-mode loading, the crack growth direction is not so easy to predict.

Two crack growth direction criteria will be described in the following :

- maximum tangential stress (MTS) criterion,
- strain energy density (SED) criterion.

For special loading cases it will be possible to calculate the crack growth direction by analytical means. More general cases are explored with numerical techniques.

For both criteria, we have to use stress and displacement components in a cylindrical coordinate system.

7.3.1 Maximum tangential stress criterion

The first crack growth direction criterion to be discussed here is the *maximum tangential stress* criterion, which was suggested and published by Erdogan and Sih in 1963 [18]. The hypothesis is that a crack tip will move in the direction of the point where the highest value of the tangential stress component is found. This can be expressed mathematically by first and second derivatives of the tangential stress component w.r.t. the angle θ.

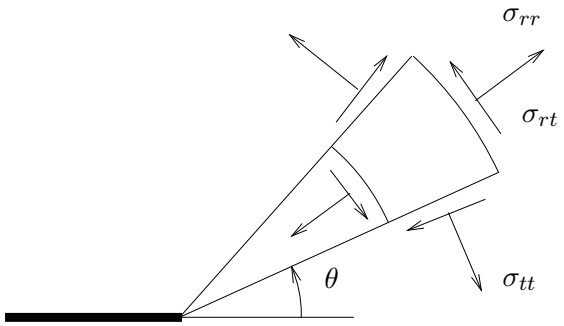

Fig. 7.9 : *Cylindrical stress components at the crack tip.*

Hypothesis : crack growth towards local maximum of σ_{tt}

$$\frac{\partial \sigma_{tt}}{\partial \theta} = 0 \qquad \text{and} \qquad \frac{\partial^2 \sigma_{tt}}{\partial \theta^2} < 0 \qquad \rightarrow \qquad \theta_c$$

$$\sigma_{tt}(\theta = \theta_c) = \sigma_{tt}(\theta = 0) = \frac{K_{Ic}}{\sqrt{2\pi r}} \quad \rightarrow \quad \text{crack growth}$$

Because the function $\sigma_{tt}(\theta)$ is known, the relations can be elaborated.

$$\frac{\partial \sigma_{tt}}{\partial \theta} = 0 \quad \rightarrow$$
$$\tfrac{3}{2}\frac{K_I}{\sqrt{2\pi r}}\left[-\tfrac{1}{4}\sin(\tfrac{\theta}{2}) - \tfrac{1}{4}\sin(\tfrac{3\theta}{2})\right] + \tfrac{3}{2}\frac{K_{II}}{\sqrt{2\pi r}}\left[-\tfrac{1}{4}\cos(\tfrac{\theta}{2}) - \tfrac{3}{4}\cos(\tfrac{3\theta}{2})\right] = 0 \quad \rightarrow$$
$$K_I \sin(\theta) + K_{II}\{3\cos(\theta) - 1\} = 0$$

$$\frac{\partial^2 \sigma_{tt}}{\partial \theta^2} < 0 \quad \rightarrow$$
$$\tfrac{3}{4}\frac{K_I}{\sqrt{2\pi r}}\left[-\tfrac{1}{4}\cos(\tfrac{\theta}{2}) - \tfrac{3}{4}\cos(\tfrac{3\theta}{2})\right] + \tfrac{3}{4}\frac{K_{II}}{\sqrt{2\pi r}}\left[\tfrac{1}{4}\sin(\tfrac{\theta}{2}) + \tfrac{9}{4}\sin(\tfrac{3\theta}{2})\right] < 0$$

$$\sigma_{tt}(\theta = \theta_c) = \frac{K_{Ic}}{\sqrt{2\pi r}} \quad \rightarrow$$
$$\tfrac{1}{4}\frac{K_I}{K_{Ic}}\left[3\cos(\tfrac{\theta_c}{2}) + \cos(\tfrac{3\theta_c}{2})\right] + \tfrac{1}{4}\frac{K_{II}}{K_{Ic}}\left[-3\sin(\tfrac{\theta_c}{2}) - 3\sin(\tfrac{3\theta_c}{2})\right] = 1$$

Mode I load

For mode I loading of the crack, it is expected that the crack tip will advance in the plane of the crack. Indeed this obviously results from solving the relations for θ.

$$\frac{\partial \sigma_{tt}}{\partial \theta} = K_I \sin(\theta) = 0 \qquad \rightarrow \qquad \theta_c = 0$$
$$\left.\frac{\partial^2 \sigma_{tt}}{\partial \theta^2}\right|_{\theta_c} < 0$$
$$\sigma_{tt}(\theta_c) = \frac{K_{Ic}}{\sqrt{2\pi r}} \qquad \rightarrow \qquad K_I = K_{Ic}$$

Mode II load

For pure mode II loading of the crack, the crack growth direction has to be determined from the relations for θ. The requirement that the first derivative of $\sigma_{tt}(\theta)$ is zero, leads to an equation, which results in two candidate values for θ_c. Only for the negative value $\theta_c = -70.6^o$, the second requirement is satisfied, so that we can conclude that the crack tip will move in that direction. The critical value of the mode II stress intensity factor can be expressed in the critical value of the mode I SIF.

$$\frac{\partial \sigma_{tt}}{\partial \theta} = K_{II}(3\cos(\theta_c) - 1) = 0 \qquad \rightarrow \qquad \theta_c = \pm \arccos(\tfrac{1}{3}) = \pm 70.6^o$$
$$\left.\frac{\partial^2 \sigma_{tt}}{\partial \theta^2}\right|_{\theta_c} < 0 \qquad \rightarrow \qquad \theta_c = -70.6^o$$
$$\sigma_{tt}(\theta_c) = \frac{K_{Ic}}{\sqrt{2\pi r}} \qquad \rightarrow \qquad K_{IIc} = \sqrt{\tfrac{3}{4}} K_{Ic}$$

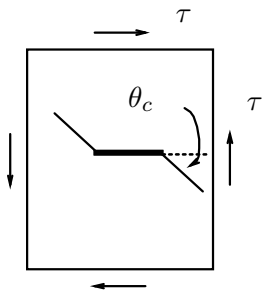

Fig. 7.10 : *Crack growth direction for Mode II loading.*

Multi-mode load

Determining the crack growth direction for multi-mode loading is only possible using numerical calculations. The relations which have to be satisfied for crack growth in a certain direction are written is terms of the parameter $\frac{K_I}{K_{Ic}}$.

$$K_I[-\sin(\tfrac{\theta}{2}) - \sin(\tfrac{3\theta}{2})] + K_{II}[-\cos(\tfrac{\theta}{2}) - 3\cos(\tfrac{3\theta}{2})] = 0$$
$$K_I[-\cos(\tfrac{\theta}{2}) - 3\cos(\tfrac{3\theta}{2})] + K_{II}[\sin(\tfrac{\theta}{2}) + 9\sin(\tfrac{3\theta}{2})] < 0$$
$$K_I[3\cos(\tfrac{\theta}{2}) + \cos(\tfrac{3\theta}{2})] + K_{II}[-3\sin(\tfrac{\theta}{2}) - 3\sin(\tfrac{3\theta}{2})] = 4K_{Ic}$$

$$\left.\begin{array}{l} -K_I f_1 - K_{II} f_2 = 0 \\ -K_I f_2 + K_{II} f_3 < 0 \\ K_I f_4 - 3K_{II} f_1 = 4K_{Ic} \end{array}\right\} \quad \rightarrow \quad \left.\begin{array}{l} -\left(\dfrac{K_I}{K_{Ic}}\right) f_1 - \left(\dfrac{K_{II}}{K_{Ic}}\right) f_2 = 0 \\ -\left(\dfrac{K_I}{K_{Ic}}\right) f_2 + \left(\dfrac{K_{II}}{K_{Ic}}\right) f_3 < 0 \\ \left(\dfrac{K_I}{K_{Ic}}\right) f_4 - 3\left(\dfrac{K_{II}}{K_{Ic}}\right) f_1 = 4 \end{array}\right\}$$

For a range of values $0 \leq \frac{K_I}{K_{Ic}} \leq 1$ a range of values for the crack growth direction angle $0 \leq \theta \leq 90^o$ is evaluated to decide if the relations are satisfied. In the first one $\frac{K_{II}}{K_{Ic}}$ is plotted as a function of $\frac{K_I}{K_{Ic}}$ and it can be used to determine which combination leads to crack growth. From the second plot the crack growth angle θ_c can then be determined.

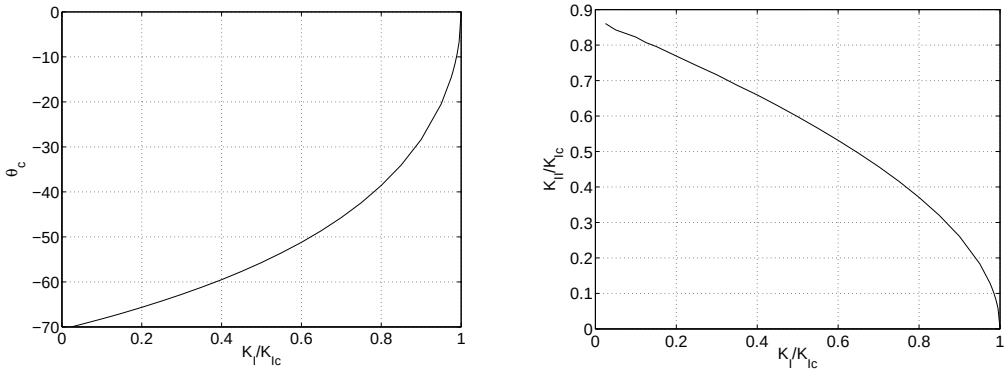

Fig. 7.11 : *Crack growth direction and Mode ratio for multi-mode loading.*

7.3.2 Strain energy density (SED) criterion

The strain energy density U_i is the stored elastic energy per unit of volume. For linear elastic material behavior this specific energy is easily calculated in the crack tip region and appears to be inverse proportional to the distance to the crack tip. The *strain energy density factor* S is now defined as the product rU_i, as such being independent of r.

The *strain energy density* criterion is proposed and published by Sih in 1973 [62] and states that at crack growth, the crack tip will move toward the point where S is minimum.

$$\begin{aligned} U_i &= \text{ Strain Energy Density (Function) } = \int_0^{\varepsilon_{ij}} \sigma_{ij}\, d\varepsilon_{ij} \\ S &= \text{ Strain Energy Density Factor } = rU_i = S(K_I, K_{II}, \theta) \end{aligned}$$

Hypothesis : crack growth towards local minimum of SED

$$\frac{\partial S}{\partial \theta} = 0 \qquad \text{and} \qquad \frac{\partial^2 S}{\partial \theta^2} > 0 \qquad \rightarrow \qquad \theta_c$$

$$S(\theta = \theta_c) = S(\theta = 0, \text{pl.strain}) = S_c \qquad \rightarrow \qquad \text{crack growth}$$

For the case of linear elastic material behavior, the strain energy density function can be expressed in the stress components and the material parameters E and ν. At the crack tip these stress components are known functions of r, θ, K_I and K_{II}. The strain energy density factor is than also known and dependent on θ. K_I and K_{II}.

The requirements for the crack growth direction result in two relations, from which θ_c can be determined.

$$U_i = \frac{1}{2E}(\sigma_{xx}^2 + \sigma_{yy}^2 + \sigma_{zz}^2) - \frac{\nu}{E}(\sigma_{xx}\sigma_{yy} + \sigma_{yy}\sigma_{zz} + \sigma_{zz}\sigma_{xx}) + \frac{1}{2G}(\sigma_{xy}^2 + \sigma_{yz}^2 + \sigma_{zx}^2)$$

$$\begin{aligned} \sigma_{xx} &= \frac{K_I}{\sqrt{2\pi r}} \cos(\tfrac{\theta}{2}) \left[1 - \sin(\tfrac{\theta}{2}) \sin(\tfrac{3\theta}{2})\right] - \frac{K_{II}}{\sqrt{2\pi r}} \sin(\tfrac{\theta}{2}) \left[2 + \cos(\tfrac{\theta}{2}) \cos(\tfrac{3\theta}{2})\right] \\ \sigma_{yy} &= \frac{K_I}{\sqrt{2\pi r}} \cos(\tfrac{\theta}{2}) \left[1 + \sin(\tfrac{\theta}{2}) \sin(\tfrac{3\theta}{2})\right] + \frac{K_{II}}{\sqrt{2\pi r}} \sin(\tfrac{\theta}{2}) \cos(\tfrac{\theta}{2}) \cos(\tfrac{3\theta}{2}) \\ \sigma_{xy} &= \frac{K_I}{\sqrt{2\pi r}} \sin(\tfrac{\theta}{2}) \cos(\tfrac{\theta}{2}) \cos(\tfrac{3\theta}{2}) + \frac{K_{II}}{\sqrt{2\pi r}} \cos(\tfrac{\theta}{2}) \left[1 - \sin(\tfrac{\theta}{2}) \sin(\tfrac{3\theta}{2})\right] \end{aligned}$$

$$\begin{aligned} S = rU_i = S(K_I, K_{II}, \theta) &= a_{11}k_I^2 + 2a_{12}k_I k_{II} + a_{22}k_{II}^2 \\ \text{with} \qquad a_{11} &= \tfrac{1}{16G}(1 + \cos(\theta))(\kappa - \cos(\theta)) \\ a_{12} &= \tfrac{1}{16G} \sin(\theta)\{2\cos(\theta) - (\kappa - 1)\} \\ a_{22} &= \tfrac{1}{16G}\{(\kappa + 1)(1 - \cos(\theta)) + (1 + \cos(\theta))(3\cos(\theta) - 1)\} \\ k_i &= K_i/\sqrt{\pi} \end{aligned}$$

Mode I load

For Mode I loading we have $K_{II} = 0$ and $K_I = \sigma\sqrt{\pi a}$. The first requirement results in two possible values of θ_c. The second requirement is only satisfied for $\theta_c = 0$, because $1 \leq \kappa \leq 3$. The obvious crack growth direction is $\theta_c = 0$. Crack growth will take place if the value of $S(\theta_c)$ equals the critical value S_c, which is the value for plane strain.

$$
\begin{aligned}
&S = a_{11}k_I^2 = \frac{\sigma^2 a}{16G}\{1+\cos(\theta)\}\{\kappa-\cos(\theta)\} \\
&\frac{\partial S}{\partial \theta} = \sin(\theta)\{2\cos(\theta)-(\kappa-1)\} = 0 \quad \rightarrow \\
&\qquad\qquad \theta_c = 0 \qquad \text{or} \qquad \arccos\left(\tfrac{1}{2}(\kappa-1)\right) \\
&\frac{\partial^2 S}{\partial \theta^2} = 2\cos(2\theta) - (\kappa-1)\cos(\theta) > 0 \qquad \rightarrow \qquad \theta_c = 0 \\
&S(\theta_c) = \frac{\sigma^2 a}{16G}\ \{2\}\{\kappa-1\} = \frac{\sigma^2 a}{8G}\ (\kappa-1) \\
&S_c = S(\theta_c, \text{pl.strain}) = \frac{(1+\nu)(1-2\nu)}{2\pi E}\ K_{Ic}^2
\end{aligned}
$$

Mode II load

For Mode II loading we have $K_I = 0$ and $K_{II} = \tau\sqrt{\pi a}$. The two requirements lead to two possible crack growth directions. The result differs for plane stress and plane strain. For $\nu = 0$, leading to $\kappa = 3$, the direction from SED is the same as the one from MTS. Crack growth will occur if the minimum S-value equals the critical value S_c, which was determined in pure Mode I loading. From this value the critical shear stress can be derived.

$$
\begin{aligned}
&S = a_{22}k_{II}^2 = \frac{\tau^2 a}{16G}\left[(\kappa+1)\{1-\cos(\theta)\} + \{1+\cos(\theta)\}\{3\cos(\theta)-1\}\right] \\
&\left.\begin{aligned}
&\frac{\partial S}{\partial \theta} = \sin(\theta)\left[-6\cos(\theta)+(\kappa-1)\right] = 0 \\
&\frac{\partial^2 S}{\partial \theta^2} = 6 - \cos^2(\theta) + (\kappa-1)\cos(\theta) > 0
\end{aligned}\right\} \quad \rightarrow \\
&\qquad\qquad \theta_c = \pm\arccos\left(\tfrac{1}{6}(\kappa-1)\right) \\
&S(\theta_c) = \frac{\tau^2 a}{16G}\{\tfrac{1}{12}(-\kappa^2+14\kappa-1)\} \\
&S(\theta_c) = S_c \quad \rightarrow \quad \tau_c = \frac{1}{\sqrt{a}}\sqrt{\frac{192GS_c}{-\kappa^2+14\kappa-1}}
\end{aligned}
$$

Multi-mode load; plane strain

It is again not possible to determine the crack growth direction for a general multi-mode loading. Numerically it can be done, however.

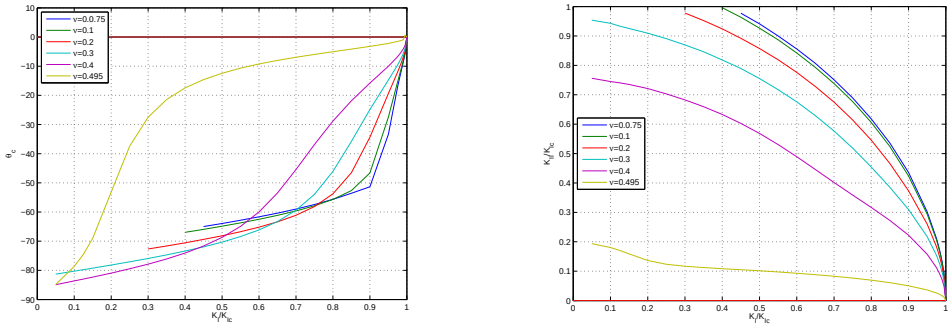

Fig. 7.12 : *Crack growth direction and Mode ratio for multi-mode loading.*

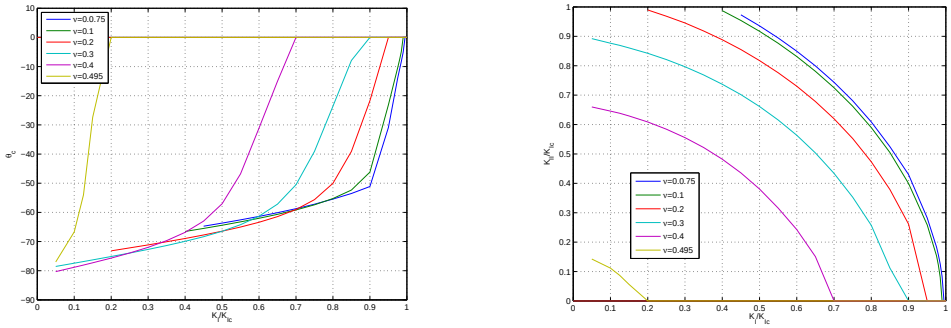

Fig. 7.13 : *Crack growth direction and Mode ratio for multi-mode loading.*

The figure below shows a crack oriented at an angle β w.r.t. the tensile load σ. For this situation the scaled stress intensity factors k_I and k_{II} can be calculated, from which follows the expression for S as a function of β and θ. The requirements according to the SED criterion can be used to test a sequence of θ_c values for a sequence of β values and a plot can be made. The figure shows the result for plane strain.

$$k_I = \sigma\sqrt{a}\sin^2(\beta) \qquad ; \qquad k_{II} = \sigma\sqrt{a}\sin(\beta)\cos(\beta)$$

$$S = \sigma^2 a \sin^2(\beta)\left\{a_{11}\sin^2(\beta) + 2a_{12}\sin(\beta)\cos(\beta) + a_{22}\cos^2(\beta)\right\}$$

$$\frac{\partial S}{\partial \theta} = (\kappa - 1)\sin(\theta_c - 2\beta) - 2\sin\{2(\theta_c - \beta)\} - \sin(2\theta_c) = 0$$
$$\frac{\partial^2 S}{\partial \theta^2} = (\kappa - 1)\cos(\theta_c - 2\beta) - 4\cos\{2(\theta_c - \beta)\} - 2\cos(2\theta_c) > 0$$

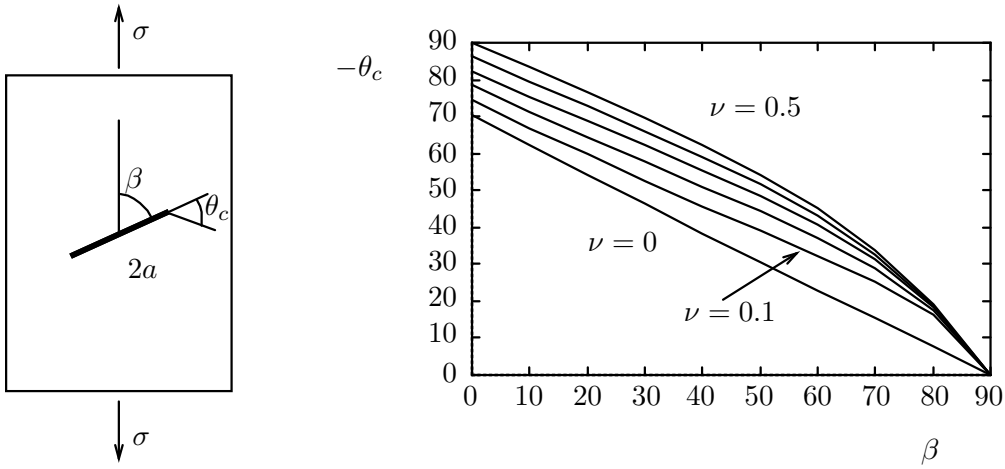

Fig. 7.14 : *Crack growth directions for multi-mode loading.*

Chapter 8

Dynamic fracture mechanics

When a crack is subjected to impact loading, the crack tip stresses and strains can only be calculated by taking into account dynamic effects like material acceleration and solving the equations of motion. This is the subject of *Dynamic Fracture Mechanics* (DFM) and understandably involves rather sophisticated mathematics.

Another subject, studied in DFM, is the behavior of a crack, which grows at high rate under (quasi)static loading after reaching its critical length. In this chapter an approximate value for the crack tip speed is derived, using the global energy balance, taking into account the kinetic energy term. This approach is referred to as the *kinetic approach*. In DFM a so-called *static approach* is also used to study the behavior of cracks, subjected to thermal shock loading.

8.1 Crack growth rate

To calculate the crack tip speed or crack growth rate, the general energy balance is used as a starting point. It is elaborated for a crack with length $2a$ in an infinitely large plate with uniform and constant thickness B. The crack is subjected to a Mode I load σ, resulting from an external load applied at edges far away from the crack. This implies that $dU_e = 0$ when the crack length changes. It is assumed that the presence of the crack has led to a complete release of elastic energy U_i in the elliptical area, indicated in the figure. Dissipation is assumed to be zero, so all available energy is going to be transformed into surface energy U_a and kinetic energy U_k.

$$\frac{dU_e}{da} - \frac{dU_i}{da} = \frac{dU_a}{da} + \frac{dU_d}{da} + \frac{dU_k}{da}$$

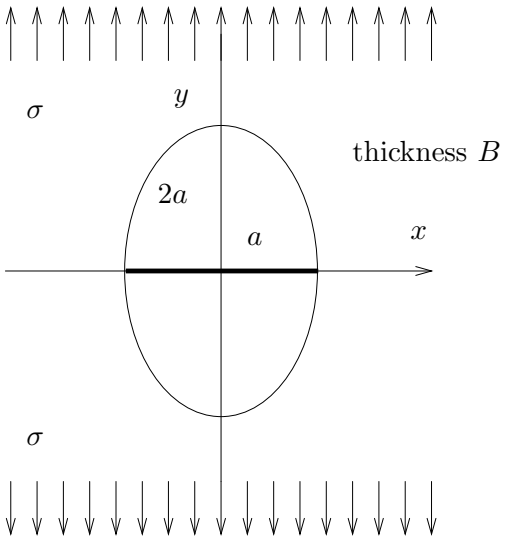

$$\frac{dU_e}{da} = 0 \qquad ; \quad \frac{dU_d}{da} = 0$$

$$U_a = 4aB\gamma \qquad \rightarrow \quad \frac{dU_a}{da} = 4\gamma B$$

$$U_i = 2\pi a^2 B \tfrac{1}{2}\frac{\sigma^2}{E} \quad \rightarrow \quad -\frac{dU_i}{da} = \frac{2\pi a B \sigma^2}{E}$$

Fig. 8.1 : *Central crack in large plate with unloaded elliptical area.*

Kinetic energy

The total kinetic energy of the plate is the integral over its volume of the specific kinetic energy $\frac{1}{2}\rho(\dot{u}_x^2 + \dot{u}_y^2)$, where ρ is the material density and $\dot{u}_x$ and $\dot{u}_y$ the material velocity components.

When the crack opens, the material velocity perpendicular to the crack faces ($\dot{u}_y$) is much higher than the velocity in the crack plane ($\dot{u}_x$). To allow further derivations, it is assumed that the crack tip speed s is independent of the (half) crack length a.

The displacement u_y of the crack face ($\theta = \pi$) is available from the analytical solution for a static crack, here assumed to be in a state of plane stress. The kinetic energy change at crack growth can now be calculated by integration. However, the integral cannot be calculated analytically. Its value is indicated as $ak(a)$ and will be considered later.

$$\left.\begin{array}{ll} U_k = \frac{1}{2}\rho B \displaystyle\int_\Omega (\dot{u}_x^2 + \dot{u}_y^2)\, dxdy & \\ \text{material velocity} & \dot{u}_x \ll \dot{u}_y = \dfrac{du_y}{dt} = \dfrac{du_y}{da}\,\dfrac{da}{dt} = \dfrac{du_y}{da}\, s \end{array}\right\}$$

$$\left.\begin{array}{ll} U_k = \frac{1}{2}\rho s^2 B \displaystyle\int_\Omega \left(\frac{du_y}{da}\right)^2 dxdy & \\ \text{assumption} & \dfrac{ds}{da} = 0 \end{array}\right\}$$

$$\left.\begin{aligned} &\frac{dU_k}{da} = \tfrac{1}{2}\rho s^2 B \int_\Omega \frac{d}{da}\left(\frac{du_y}{da}\right)^2 dxdy \\ &u_y = 2\sqrt{2}\frac{\sigma}{E}\sqrt{a^2-ax} \qquad \rightarrow \qquad \frac{du_y}{da} = \sqrt{2}\,\frac{\sigma}{E}\,\frac{2a-x}{\sqrt{a^2-ax}} \end{aligned}\right\}$$

$$\frac{dU_k}{da} = \rho s^2 B\left(\frac{\sigma}{E}\right)^2 a \int_\Omega \frac{1}{a^3}\,\frac{x^2(x-2a)}{(a-x)^2}\,dxdy = \rho s^2 B\left(\frac{\sigma}{E}\right)^2 a\,k(a)$$

Substitution of all results in the energy balance leads to an expression for the crack tip speed s where the critical crack length a_c and the sound speed c can be introduced.

The earlier assumption that s is independent of a does not appear to hold, so the result must be an approximation. More approximation is involved in the calculation of $k(a)$, which is done numerically. Roberts and Wells did this in 1954 [57] and came up with $k = 43.51$.

As can be seen from the expression for s, the crack will grow at high speed, so that the actual (half) crack length a will be much larger than the critical crack length a_c. This leads to the final approximation for the crack tip speed.

$$\left.\begin{aligned} &\frac{2\pi a\sigma^2}{E} = 4\gamma + \rho s^2\left(\frac{\sigma}{E}\right)^2 ak \qquad \rightarrow \\ &s = \left(\frac{E}{\rho}\right)^{\frac{1}{2}}\left(\frac{2\pi}{k}\right)^{\frac{1}{2}}\left(1-\frac{2\gamma E}{\pi a\sigma^2}\right)^{\frac{1}{2}} \\ &\sqrt{\frac{2\pi}{k}} \approx 0.38 \qquad ; \qquad a_c = \frac{2\gamma E}{\pi\sigma^2} \qquad ; \qquad c = \sqrt{\frac{E}{\rho}} \end{aligned}\right\}$$

$$\left.\begin{aligned} &s = 0.38\,c\left(1-\frac{a_c}{a}\right)^{\frac{1}{2}} \\ &a \gg a_c \end{aligned}\right\} \qquad \rightarrow \qquad \boxed{s \approx 0.38\ c}$$

For some materials the table lists values for Young's modulus E, density ρ and calculated sound speed c. The measured crack tip speed s is also listed. The ratio s/c takes values between 0.2 and 0.4, so the approximation 0.38 is well within this range. Mostly the experimental ratio is found to be smaller, due to the dissipation during crack growth.

	steel	copper	aluminum	glass	rubber
E [GPa]	210	120	70	70	20
ρ [kg/m^2]	7800	8900	2700	2500	900
ν	0.29	0.34	0.34	0.25	0.5
c [m/sec]	5190	3670	5090	5300	46
s [m/sec]	1500			2000	
s/c	0.29			0.38	

$$\boxed{0.2 < \frac{s}{c} < 0.4}$$

8.2 Elastic wave speeds

In the derivation of the crack tip speed s, the sound speed c was introduced, which is the speed of a wave front with elastic elongational strain, also indicated as C_0. In DFM more sophisticated analyzes of crack growth rate use other deformation modes, e.g. dilatation (volume change) and shear, with wave front speeds C_1 and C_2, respectively. Frequently used is the Rayleigh velocity C_R of wave fronts traveling at the surface of a material.

$$\begin{array}{lcll} C_0 & = & \text{elongational wave speed} & = \sqrt{\dfrac{E}{\rho}} \\ C_1 & = & \text{dilatational wave speed} & = \sqrt{\dfrac{\kappa+1}{\kappa-1}}\sqrt{\dfrac{\mu}{\rho}} \\ C_2 & = & \text{shear wave speed} & = \sqrt{\dfrac{\mu}{\rho}} \\ C_R & = & \text{Rayleigh velocity} & = 0.54\,C_0 \quad \acute{a} \quad 0.62\,C_0 \end{array}$$

Corrections

More elaborate derivations of the crack tip speed have been published. Dulancy & Brace (1960) derived an expression without assuming s to be independent of a. Freund (1972) related s to the Rayleigh velocity C_R.

Dulancy & Brace (1960)	$s = 0.38\,C_0\left(1 - \dfrac{a_c}{a}\right)$
Freund (1972)	$s = C_R\left(1 - \dfrac{a_c}{a}\right)$

8.3 Crack tip stress

When a crack tip moves at high speed through a material, the elastic stresses σ_{Dij} at the crack tip can be calculated [71]. The first term in this stress field appears to be proportional to $K_D/\sqrt{2\pi r}$, with r the distance to the crack tip and K_D the *Dynamic Stress Intensity Factor*. The stress components are, just as in the static case, a function of the angle θ w.r.t. the crack plane. In this dynamic case, however, they also depend on material parameters and the crack tip speed.

$$\sigma_{Dij} = \frac{K_D}{\sqrt{2\pi r}}\, f_{ij}(\theta, r, s, E, \nu)$$

8.3.1 Crack branching

Cylindrical stress components for Mode I loading can be derived by transformation as has been done for the static loading case. The ratio of the tangential stress $\sigma_{IDtt}(\theta)$ and the tangential stress in the crack plane ($\theta = 0$), can be calculated as a function of θ. The graphical representation shows different curves for various values of the crack tip speed s. For $s/C_R \approx 0.87$ the curve has a maximum value at $\theta \approx \pi/4$. According to the *Maximum Tangential Stress* criterion, the crack will move out of the crack plane. This crack branching will occur repeatedly, when the crack runs through the material, and will soon lead to complete material failure.

$$\sigma_{Dij} = \frac{K_{ID}}{\sqrt{2\pi r}}\, f_{ij}(\theta, r, s, E, \nu)$$

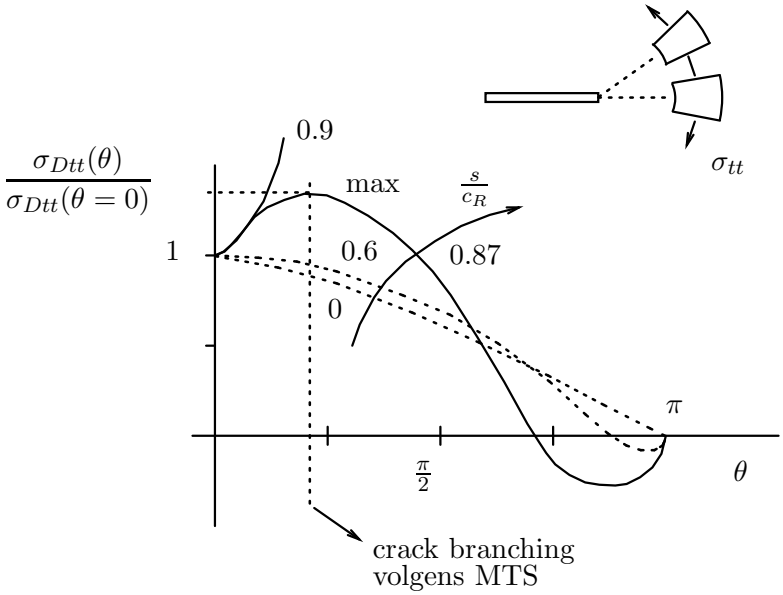

Fig. 8.2 : *Tangential stress ratio as a function of crack growth direction, illustrating crack branching.*

8.3.2 Fast fracture and crack arrest

A crack, which runs through a material, can reach a location, where it is subjected to different loading conditions, which may result in crack arrest. This will occur when K_D is below a critical value K_A, being the minimal value of a measured *Dynamic Fracture Toughness* K_{Dc}, which is a function of crack tip speed s and temperature T.

$$K_D \geq K_{Dc}(s,T) \qquad \rightarrow \quad \text{crack growth}$$

$$K_D < \min_{0<s<C_R} K_{Dc}(s,T) = K_A \qquad \rightarrow \quad \text{crack arrest}$$

8.4 Experiments

In DFM experiments are done to measure crack tip speeds, using instrumented DCB specimens, sometimes in combination with high speed photography (typically 10^6 frames/sec).

To determine the temperature dependent K_{Dc}, the Robertson Crack Arrest Temperature (CAT) test is done, where a crack is forced to run from a low temperature region into a higher temperature region.

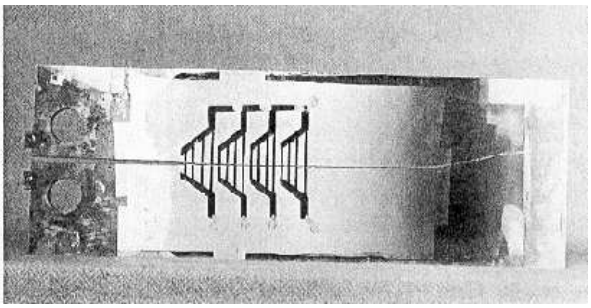

Fig. 8.3 : *Instrumented DCB specimen to measure crack propagation speed [39].*

Chapter 9

Plastic crack tip zone

The elastic crack tip stresses reach an infinite value, when the distance to the crack tip decreases to zero. In reality the material will yield before the crack tip is reached and the elastic solution is no longer valid.

In this chapter the region at the crack tip where yielding occurs is determined. The influence of this plastic crack tip zone on the crack behavior is explained. Post-yield hardening is not considered, so the material behaves ideal plastic.

In three-dimensional cases, the occurrence of yielding is tested by means of a yield criterion. Here, we employ the Von Mises and the Tresca criteria. Both are formulated in terms of principal stresses σ_1, σ_2 and σ_3, where the first two are in the plane of the plate and σ_3 is in the normal direction. For plane stress cases $\sigma_3 = 0$ and for plane strain situations Hooke's law gives $\sigma_3 = \nu(\sigma_1 + \sigma_2)$, with ν as Poisson's ratio.

9.1 Von Mises and Tresca yield criteria

Von Mises yield criterion is based on the hypothesis that yielding occurs when the specific distorsional elastic energy W^d reaches a critical value W_c^d. The critical value is determined from a tensile test and expressed in the yield stress σ_y. The Von Mises yield criterion can be expressed in the principal stresses.

Tresca yield criterion is based on the hypothesis that yielding occurs when the maximum shear stress τ_{max} reaches a critical value τ_{max_c}. This critical value is again determined in a tensile test and related to the yield stress σ_y. The Tresca yield criterion can be expressed in the difference of the maximum and the minimum principal stresses.

Von Mises

$$W^d = W_c^d$$
$$(\sigma_1 - \sigma_2)^2 + (\sigma_2 - \sigma_3)^2 + (\sigma_3 - \sigma_1)^2 = 2\sigma_y^2$$

Tresca

$$\tau_{max} = \tau_{max_c}$$
$$\sigma_{max} - \sigma_{min} = \sigma_y$$

9.2 Principal stresses at the crack tip

For both the Von Mises and the Tresca yield criterion, the principal stresses have to be used. They are the eigenvalues of the Cauchy stress matrix and for the plane stress case they can be calculated analytically. For plane strain the third principal stress is not zero but related to the first two principal stresses.

$$\text{plane stress state} \qquad \sigma_{zz} = \sigma_{zx} = \sigma_{zy} = 0$$

$$\underline{\sigma} = \begin{bmatrix} \sigma_{xx} & \sigma_{xy} & 0 \\ \sigma_{xy} & \sigma_{yy} & 0 \\ 0 & 0 & 0 \end{bmatrix} \qquad \rightarrow \qquad \det(\underline{\sigma} - \sigma \underline{I}) = 0 \qquad \rightarrow$$

$$\sigma \left[\sigma^2 - \sigma(\sigma_{xx} + \sigma_{yy}) + (\sigma_{xx}\sigma_{yy} - \sigma_{xy}^2)\right] = 0 \qquad \rightarrow$$

$$\sigma_1 = \tfrac{1}{2}(\sigma_{xx} + \sigma_{yy}) + \left\{\tfrac{1}{4}(\sigma_{xx} - \sigma_{yy})^2 + \sigma_{xy}^2\right\}^{1/2}$$
$$\sigma_2 = \tfrac{1}{2}(\sigma_{xx} + \sigma_{yy}) - \left\{\tfrac{1}{4}(\sigma_{xx} - \sigma_{yy})^2 + \sigma_{xy}^2\right\}^{1/2}$$
$$\sigma_3 = 0$$

$$\text{plane strain state} \qquad \sigma_3 = \nu(\sigma_1 + \sigma_2)$$

Elastic crack tip stress components for Mode I are used to derive the principal crack tip stresses. The first principal stress is always the largest. For plane stress the third principal stress is zero and the smallest. For plane strain the smallest value may be the second principal stress, because the value of the third principal stress depends on Poisson's ratio.

$$\text{crack tip stresses} \qquad \sigma_{ij} = \frac{K_I}{\sqrt{2\pi r}} f_{Iij}(\theta)$$

$$\sigma_{1(+),2(-)} = \frac{K_I}{\sqrt{2\pi r}} \left[\cos(\tfrac{\theta}{2}) \pm \sqrt{\tfrac{1}{4}\left\{-2\cos(\tfrac{\theta}{2})\sin(\tfrac{\theta}{2})\sin(\tfrac{3\theta}{2})\right\}^2 + \left\{\sin(\tfrac{\theta}{2})\cos(\tfrac{\theta}{2})\cos(\tfrac{3\theta}{2})\right\}^2}\right]$$

$$\sigma_1 = \frac{K_I}{\sqrt{2\pi r}} \cos(\tfrac{\theta}{2})\{1 + \sin(\tfrac{\theta}{2})\} \qquad ; \qquad \sigma_2 = \frac{K_I}{\sqrt{2\pi r}} \cos(\tfrac{\theta}{2})\{1 - \sin(\tfrac{\theta}{2})\}$$

$$\sigma_3 = 0 \qquad \text{or} \qquad \sigma_3 = \frac{2\nu K_I}{\sqrt{2\pi r}} \cos(\tfrac{\theta}{2})$$

plane stress	$\sigma_1 > \sigma_2 > \sigma_3$		
plane strain	$\sigma_1 > \sigma_2 > \sigma_3$	or	$\sigma_1 > \sigma_3 > \sigma_2$

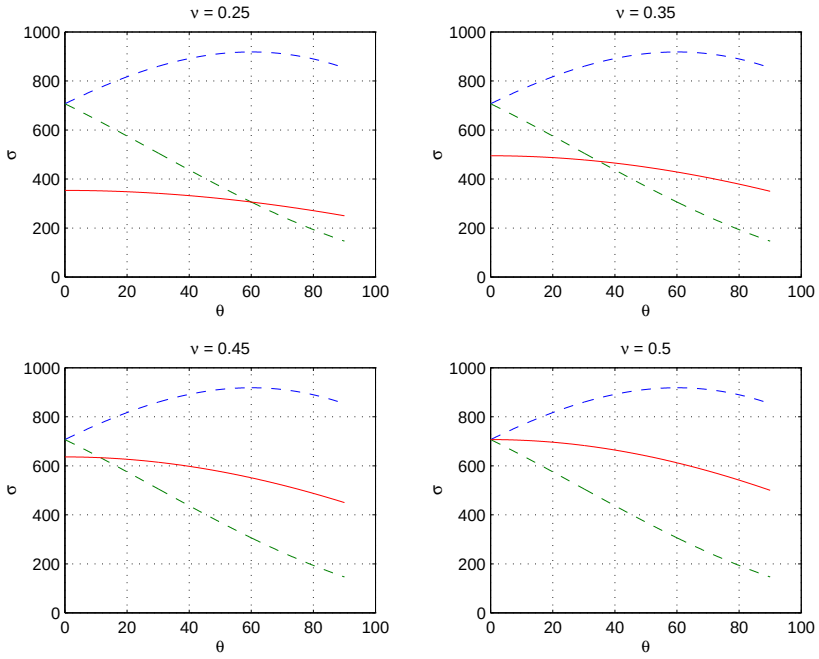

Fig. 9.1 : *Principal stresses for plane strain as a function of the direction angle. The third principal stress depends on Poisson's ratio.*

9.3 Von Mises plastic zone

In the Von Mises yield criterion all principal stresses are used. For plane stress and plane strain the distance r_y of the elastic/plastic boundary is easily calculated. The derivation uses the next trigonometric relations :

$$\cos(\theta) = \cos^2(\tfrac{\theta}{2}) - \sin^2(\tfrac{\theta}{2}) = 2\cos^2(\tfrac{\theta}{2}) - 1 \quad \rightarrow \quad \cos^2(\tfrac{\theta}{2}) = \tfrac{1}{2}\{1 + \cos(\theta)\}$$
$$\cos^2(\tfrac{\theta}{2})\sin^2(\tfrac{\theta}{2}) = \tfrac{1}{4}\sin^2(\theta)$$

Von Mises yield criterion

$$(\sigma_1 - \sigma_2)^2 + (\sigma_2 - \sigma_3)^2 + (\sigma_3 - \sigma_1)^2 = 2\sigma_y^2$$

plane stress $\sigma_3 = 0$

$$(\sigma_1 - \sigma_2)^2 + \sigma_2^2 + \sigma_1^2 = 2\sigma_y^2$$
$$\frac{K_I^2}{2\pi r_y}\cos^2(\tfrac{\theta}{2})\left[6\sin^2(\tfrac{\theta}{2}) + 2\right] = 2\sigma_y^2$$
$$r_y = \frac{K_I^2}{2\pi\sigma_y^2}\cos^2(\tfrac{\theta}{2})\left[1 + 3\sin^2(\tfrac{\theta}{2})\right] = \frac{K_I^2}{4\pi\sigma_y^2}\left[1 + \cos(\theta) + \tfrac{3}{2}\sin^2(\theta)\right]$$

plane strain $\sigma_3 = \nu(\sigma_1 + \sigma_2)$

$$(\nu^2 - \nu + 1)(\sigma_1^2 + \sigma_2^2) + (2\nu^2 - 2\nu - 1)\sigma_1\sigma_2 = \sigma_y^2$$
$$\frac{K_I^2}{2\pi r_y}\cos^2(\tfrac{\theta}{2})\left[6\sin^2(\tfrac{\theta}{2}) + 2(1-2\nu)^2\right] = 2\sigma_y^2$$
$$r_y = \frac{K_I^2}{4\pi\sigma_y^2}\left[(1-2\nu)^2\left\{1+\cos(\theta)\right\} + \tfrac{3}{2}\sin^2(\theta)\right]$$

The elastic/plastic boundaries can be plotted in an xy-coordinate system with the crack tip in the origin and the crack along the line $-\infty < x < 0; y = 0$. It appears that the plane stress plastic zone is larger than the plane strain plastic zone.

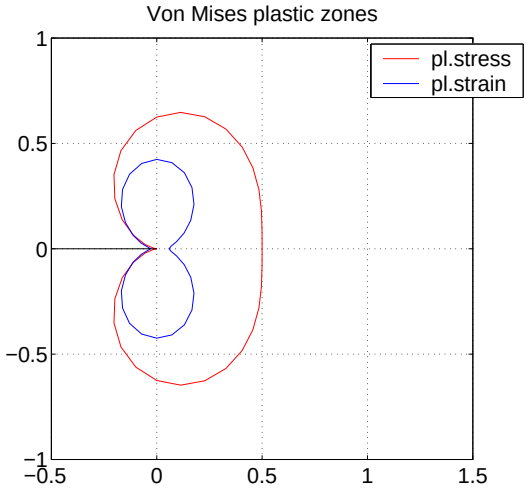

Fig. 9.2 : *Plastic zones according to the Von Mises yield criterion.*

9.4 Tresca plastic zone

Using the Tresca yield criterion implies using the maximum and minimum principal stresses. For the plane stress case $\sigma_3 = 0$ is always the minimum. For the plane strain case, however, the minimal principal stress can be σ_3 or σ_2, depending on the coordinate angle θ and on Poisson's ratio ν. For plane strain two different elastic/plastic boundaries can be calculated.

$$\sigma_{max} - \sigma_{min} = \sigma_y$$

plane stress

$$\{\sigma_{max}, \sigma_{min}\} = \{\sigma_1, \sigma_3\}$$

$$\frac{K_I}{\sqrt{2\pi r_y}}\left[\cos(\tfrac{\theta}{2}) + \left|\cos(\tfrac{\theta}{2})\sin(\tfrac{\theta}{2})\right|\right] = \sigma_y$$
$$r_y = \frac{K_I^2}{2\pi\sigma_y^2}\left[\cos(\tfrac{\theta}{2}) + \left|\cos(\tfrac{\theta}{2})\sin(\tfrac{\theta}{2})\right|\right]^2$$

plane strain I $\sigma_1 > \sigma_2 > \sigma_3 \quad \rightarrow \quad \{\sigma_{max}, \sigma_{min}\} = \{\sigma_1, \sigma_3\}$

$$r_y = \frac{K_I^2}{2\pi\sigma_y^2}\left[(1-2\nu)\cos(\tfrac{\theta}{2}) + \left|\cos(\tfrac{\theta}{2})\sin(\tfrac{\theta}{2})\right|\right]^2$$

plane strain II $\sigma_1 > \sigma_3 > \sigma_2 \quad \rightarrow \quad \{\sigma_{max}, \sigma_{min}\} = \{\sigma_1, \sigma_2\}$

$$r_y = \frac{K_I^2}{2\pi\sigma_y^2}\sin^2(\theta)$$

Plotting the elastic-plastic boundary reveals again that the largest plastic zone occurs for the plane stress case. For the plane strain situation, the plastic region is defined by two curves, one for $\sigma_1 > \sigma_2 > \sigma_3$ (smallest) and one for $\sigma_1 > \sigma_3 > \sigma_2$ (largest).

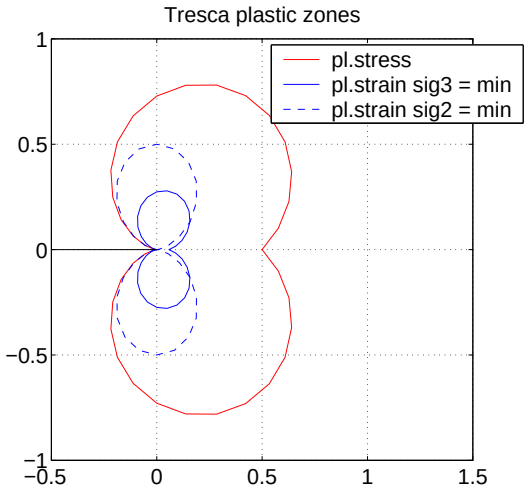

Fig. 9.3 : *Plastic zones according to the Tresca yield criterion.*

9.5 Influence of the plate thickness

The plastic crack tip zone is considerably different for a crack in a thin and a thick plate. In a thin plate the material can contract freely perpendicular to the plate (3-direction), when an in-plane load is applied. Over the whole plate thickness a plane stress state exists with $\sigma_3 = 0$. The plane stress plastic crack tip zone develops over the whole plate thickness.

For the thick plate, only the surface layers are free to contract in normal direction and are thus in a plane stress state. The crack tip material at greater depth from the surface is prohibited to contract by the surrounding material, which is at a much lower stress and has no intention at all to contract. The inner crack tip material is thus in a state of plane strain. In the surface layers we find plane stress plastic zones and in the deeper bulk material the plastic crack tip zone is smaller as it is associated with plane strain. A typical *dog-bone*

plastic zone develops at the crack tip.

In a thin plate the relative volume of yielding material is much larger than in the thick plate. This explains that measured K_{Ic} values are higher when determined with thin test specimens. For thicker specimens, the value is lower and becomes independent of the thickness, when this is larger than a threshold value B_c, which is empirically related to K_{Ic} and σ_y.

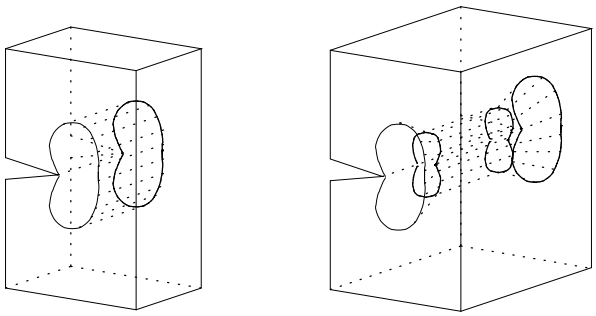

Fig. 9.4 : *Plastic crack tip zone for a thin and a thick plate.*

$$B_c > \frac{25}{3\pi}\left(\frac{K_{Ic}}{\sigma_y}\right)^2 > 2.5\left(\frac{K_{Ic}}{\sigma_y}\right)^2$$

9.6 Shear planes

Plastic deformation takes place by sliding of crystallographic planes induced by shear stresses. The planes with the maximum shear stresses can be found at an angle of 45^o between the planes with the maximum and minimum principal stresses, which are perpendicular. Employing an etching procedure, the shear planes can be visualized in some cutting planes.

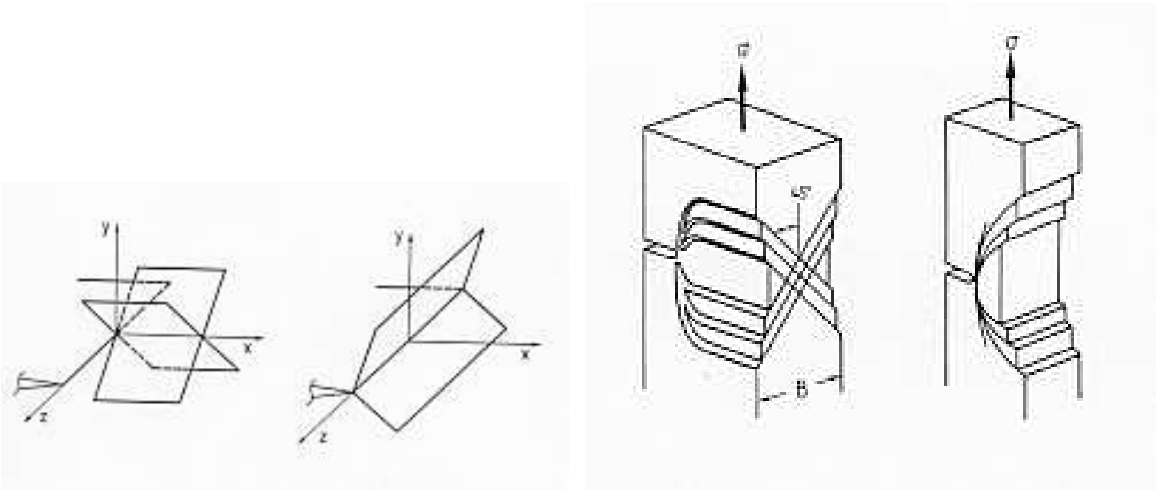

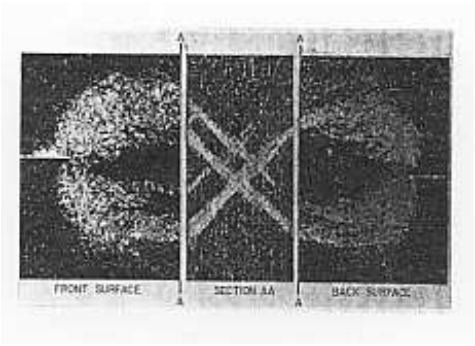

Fig. 9.5 : *Shear planes at the crack tip: plane stress (left), plane strain (right) [39, 25, 30].*

9.7 Plastic zone in the crack plane

Considering the plastic zone in the crack plane ($\theta = 0$) for plane stress state, it becomes clear that the requirement of σ_{yy} to be not larger than the yield stress σ_y, results in loss of equilibrium. The total internal force in y-direction is decreased, while the external force remains the same.

9.7.1 Irwin plastic zone correction

In 1958 Irwin [35] has devised a solution to this inconsistency, based on the enlargement of the plastic zone, such that the total y-force again equals the force associated with the elastic solution (= shaded area in the figure).

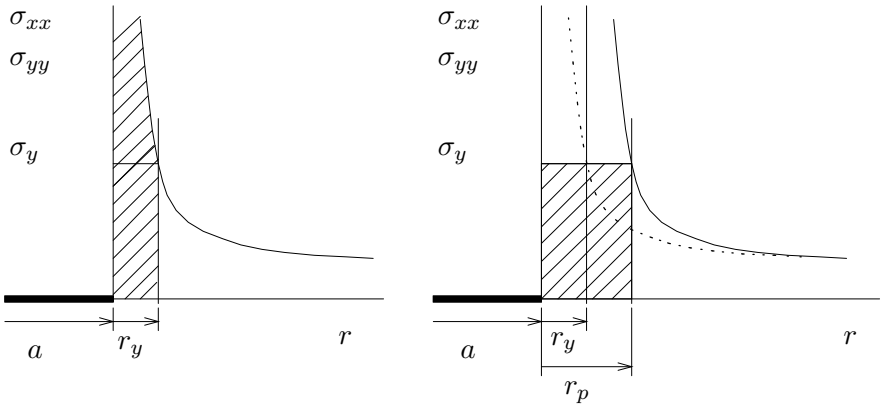

Fig. 9.6 : *Irwin correction of plastic zone in the crack plane.*

$$\theta = 0 \qquad \rightarrow \qquad \sigma_{xx} = \sigma_{yy} = \frac{K_I}{\sqrt{2\pi r}}$$

$$\text{yield} \qquad \sigma_{xx} = \sigma_{yy} = \sigma_y \qquad \rightarrow \qquad r_y = \frac{1}{2\pi}\left(\frac{K_I}{\sigma_y}\right)^2$$

$$\sigma_y r_p = \int_0^{r_y} \sigma_{yy}(r)\, dr = \frac{K_I}{\sqrt{2\pi}} \int_0^{r_y} r^{-\frac{1}{2}}\, dr = \frac{2K_I}{\sqrt{2\pi}} \sqrt{r_y} \quad \rightarrow$$

$$r_p = \frac{2K_I}{\sqrt{2\pi}} \frac{\sqrt{r_y}}{\sigma_y} \qquad \rightarrow \qquad r_p = \frac{1}{\pi} \left(\frac{K_I}{\sigma_y} \right)^2 = 2\, r_y$$

9.7.2 Dugdale-Barenblatt plastic zone correction

In 1960 Dugdale and Barenblatt have published a plastic zone calculation [15], based on the requirement that in the elastic region outside the plastic zone the stresses must be finite. Two load cases are considered to act on the crack with half length $a + r_p$, where r_p is the plastic zone length to be determined. The first load is the Mode I load σ. The second load is the yield stress σ_y, applied to the crack faces over the distance r_p and closing the crack to its initial half length a. The elastic stresses for $x > a + r_p$ are known to be a series of terms of which the first term is singular, so leading to infinite stress values. This first term is completely determined by the addition of the two stress intensity factors of the two load cases. The requirement that this first term is zero leads to the value of r_p.

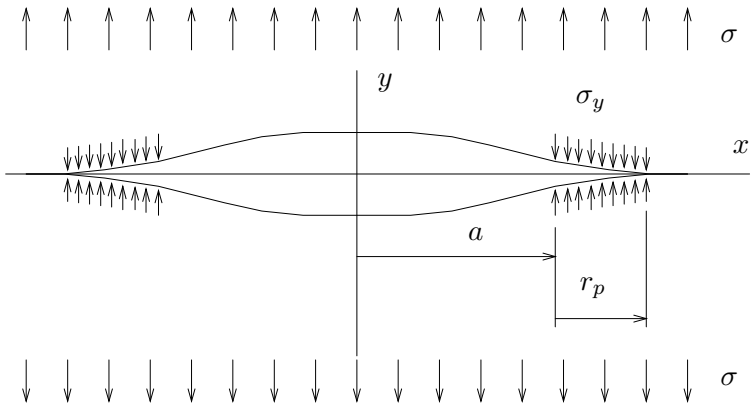

Fig. 9.7 : *Dugdale-Barenblatt correction of plastic zone in the crack plane.*

load σ $\qquad K_I(\sigma) = \sigma \sqrt{\pi(a + r_p)}$

load σ_y $\qquad K_I(\sigma_y) = 2\sigma_y \sqrt{\dfrac{a + r_p}{\pi}} \arccos\left(\dfrac{a}{a + r_p} \right)$

singular term = 0 $\qquad \rightarrow \qquad K_I(\sigma) = K_I(\sigma_y) \qquad \rightarrow$

$$\frac{a}{a + r_p} = \cos\left(\frac{\pi\sigma}{2\sigma_y} \right) \qquad \rightarrow \qquad r_p = \frac{\pi K_I^2}{8\sigma_y^2}$$

9.8 Plastic constraint factor

When the maximum principal stress is indicated as $\sigma_{max} = \sigma_1$, the other two principal stresses can be written as $\sigma_2 = n\sigma_1$ and $\sigma_3 = m\sigma_1$. The Von Mises equivalent stress can be expressed in σ_{max} and the ratios n and m. The *plastic constraint factor*, PCF, is the ratio of the maximum principal stress at yield and the yield stress. It can be used as a multiplication factor of the yield stress to take into account other principal stresses.

$$\sqrt{\tfrac{1}{2}\left\{(\sigma_1-\sigma_2)^2+(\sigma_2-\sigma_3)^2+(\sigma_3-\sigma_1)^2\right\}} = \left[\sqrt{1-n-m+n^2+m^2-mn}\,\right]\sigma_{max} = \sigma_y$$

$$\mathsf{PCF} = \frac{\sigma_{max}}{\sigma_y} = \frac{1}{\sqrt{1-n-m+n^2+m^2-mn}}$$

For a uni-axial stress state, obviously $\mathsf{PCF} = 1$, as in that case we have $m = n = 0$.

For a bi-axial plane stress state, we have $m = 0$ and PCF is a function of n only. The maximum value of PCF, and thus the maximum principal stress value, can be determined and seen in the two-dimensional Von Mises yield contour.

$$m = 0 \quad \rightarrow \quad \mathsf{PCF} = \left(1-n+n^2\right)^{-\frac{1}{2}} \quad \rightarrow$$

$$\frac{d(\mathsf{PCF})}{dn} = 0 \quad \rightarrow \quad n = \tfrac{1}{2} \quad \rightarrow \quad \mathsf{PCF}_{max} = \sqrt{\frac{4}{3}} \quad \rightarrow \quad \sigma_{max} = \sqrt{\frac{4}{3}}\,\sigma_y$$

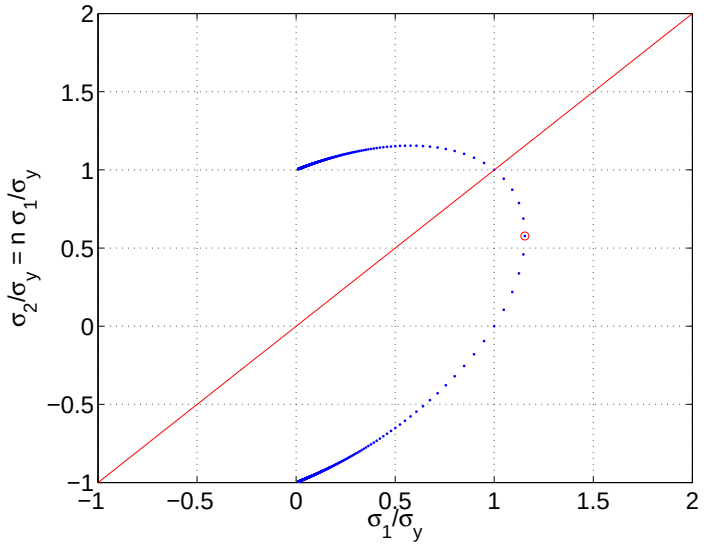

Fig. 9.8 : *Von Mises plane stress yield contour*

In the crack tip region the principal stresses are known as a function of the angle θ around and at the distance r to the crack tip. The ratio of σ_2 and σ_1, n, can be calculated. The ratio of σ_3 and σ_1, m, is zero for plane stress and a function of Poisson's ratio ν for plane strain.

plane stress $\qquad n = \left[1-\sin(\frac{\theta}{2})\right] / \left[1+\sin(\frac{\theta}{2})\right] \quad ; \quad m = 0$

plane strain $\qquad n = \left[1 - \sin(\frac{\theta}{2})\right] / \left[1 + \sin(\frac{\theta}{2})\right] \quad ; \quad m = 2\nu / \left[1 + \sin(\frac{\theta}{2})\right]$

In the plane of the crack where $\theta = 0$ we have $n = 1$, because $\sigma_1 = \sigma_2$. For plane stress we already saw that $m = 0$ and for plane strain $m = 2\nu$. The *plastic constraint factor* can then be determined as a function of Poisson's ratio ν. For $\nu = \frac{1}{3}$ its value is 3, but experiments indicate that it is smaller. Irwin [36] suggests an over the thickness averaged value $\mathsf{PCF} = \sqrt{2\sqrt{2}} = 1.68$.

plane stress $\qquad n = 1 \; ; \; m = 0 \quad \rightarrow \quad \mathsf{PCF} = 1$

plane strain $\qquad n = 1 \; ; \; m = 2\nu \quad \rightarrow \quad \mathsf{PCF} = \dfrac{1}{\sqrt{1 - 4\nu + 4\nu^2}}$

9.8.1 Plastic zones in the crack plane

For comparison, the boundary of the elastic-plastic transition is considered for $\theta = 0$, so in the plane of the crack. Poisson's ratio is $\nu = \frac{1}{3}$. The table lists the distance to the crack tip of the elastic-plastic transition. Although Irwin and Dugdale plastic zones were calculated for plane stress, the plane strain equivalent results from the application of the *plastic constraint factor* as a magnification factor for the yield stress σ_y.

criterion	state	r_y or r_p	$\dfrac{r_y \vert r_p}{(K_I/\sigma_y)^2}$
Von Mises	plane stress	$\dfrac{1}{2\pi}\left(\dfrac{K_I}{\sigma_y}\right)^2$	0.1592
Von Mises	plane strain	$\dfrac{1}{18\pi}\left(\dfrac{K_I}{\sigma_y}\right)^2$	0.0177
Tresca	plane stress	$\dfrac{1}{2\pi}\left(\dfrac{K_I}{\sigma_y}\right)^2$	0.1592
Tresca	plane strain $\sigma_1 > \sigma_2 > \sigma_3$	$\dfrac{1}{18\pi}\left(\dfrac{K_I}{\sigma_y}\right)^2$	0.0177
Tresca	plane strain $\sigma_1 > \sigma_3 > \sigma_2$	0	0
Irwin	plane stress	$\dfrac{1}{\pi}\left(\dfrac{K_I}{\sigma_y}\right)^2$	0.3183
Irwin	plane strain ($\mathsf{PCF} = 3$)	$\dfrac{1}{\pi}\left(\dfrac{K_I}{3\sigma_y}\right)^2$	0.0354
Dugdale	plane stress	$\dfrac{\pi}{8}\left(\dfrac{K_I}{\sigma_y}\right)^2$	0.3927
Dugdale	plane strain ($\mathsf{PCF} = 3$)	$\dfrac{\pi}{8}\left(\dfrac{K_I}{3\sigma_y}\right)^2$	0.0436

9.9 Small Scale Yielding

The occurrence of a plastic zone at the crack tip rises the question whether the stress intensity factor K can still be used in a crack growth criterion, as it is associated with a purely linear elastic solution. The answer is that the elastic stress solution and thus its amplitude K, can be used when the K-domain is much larger than the plastic zone. This situation is referred to as *Small Scale Yielding* (SSY).

The accuracy of the elastic stress field in SSY can be enhanced by using an effective crack length, which takes the plastic zone into account, and is calculated by adding r_y or r_p to a. Calculation of K has to be done iteratively, as the plastic zone size depends on K and vice versa.

$$a_{eff} = a + (r_y | r_p) \quad \leftrightarrow \quad K_I = \beta_I(a_{eff})\sigma\sqrt{\pi a_{eff}}$$

Chapter 10

Nonlinear Fracture Mechanics

When Small Scale Yielding cannot be assumed or when the material behavior is intrinsically nonlinear, concepts from LEFM loose their meaning. For such cases Non Linear Fracture Mechanics (NLFM) or Elasto-Plastic Fracture Mechanics provides new theories and concepts to analyze the behavior of cracks.

10.1 Crack-tip opening displacement

In LEFM the displacement of material points in the region around the crack tip can be calculated. With the crack along the x-axis, the displacement u_y in y-direction is known as a function of r (distance) and θ (angle), both for plane stress and for plane strain. The displacement of points at the upper crack surface results for $\theta = \pi$ and can be expressed in the coordinate x, by taking $r = a - x$, where a is the half crack length. The origin of this xy-coordinate system is at the crack center. The crack opening (displacement) (COD) δ is two times this displacement. It is obvious that the opening at the crack tip (CTOD), δ_t, is zero.

$$u_y = \frac{\sigma\sqrt{\pi a}}{2\mu}\sqrt{\frac{r}{2\pi}}\left[\sin(\tfrac{1}{2}\theta)\left\{\kappa + 1 - 2\cos^2(\tfrac{1}{2}\theta)\right\}\right]$$

displacement in crack plane $\quad \theta = \pi;\ r = a - x$

$$u_y = \frac{(1+\nu)(\kappa+1)}{E}\,\frac{\sigma}{2}\,\sqrt{2a(a-x)}$$

Crack Opening Displacement (COD)

$$\delta(x) = 2u_y(x) = \frac{(1+\nu)(\kappa+1)}{E}\,\sigma\sqrt{2a(a-x)}$$

Crack Tip Opening Displacement (CTOD)

$$\delta_t = \delta(x = a) = 0$$

Wells (1963) [69] suggested that this CTOD can be used in a crack growth criterion, when plasticity at the crack tip is taken into account and the actual crack length is replaced by the effective crack length.

10.1.1 CTOD by Irwin

The influence of the crack tip plastic zone can be taken into account by using an effective crack length a_{eff}, which is the actual crack length plus the length of the plastic zone in front of the crack tip. The correction of Irwin is illustrated in the figure. Be aware that r_y is used here and not the corrected plastic zone r_p.

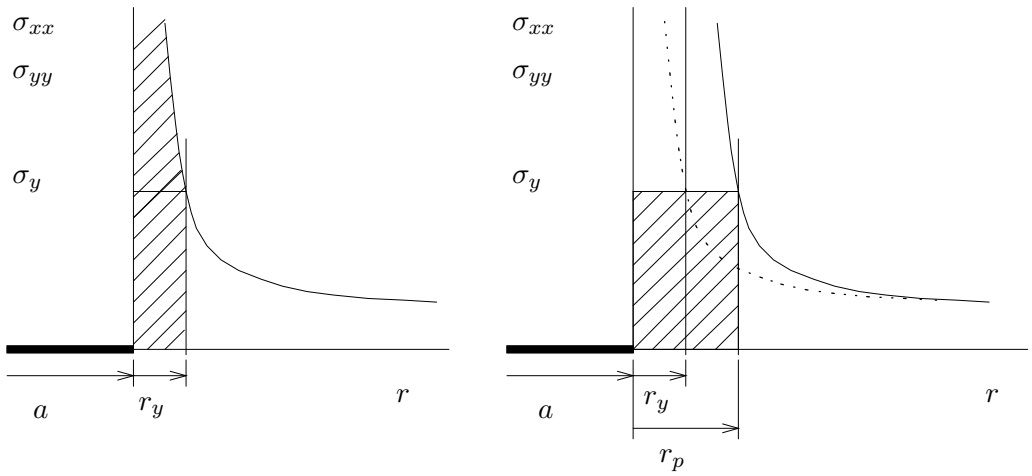

Fig. 10.1 : *Irwin plastic zone correction.*

$$a_{eff} = a + r_y = a + \frac{1}{2\pi}\left(\frac{K_I}{\sigma_y}\right)^2$$

When the effective crack length of Irwin is used, the crack tip opening can be calculated for plane stress and for plane strain.

$$\begin{aligned}\delta(x) &= \frac{(1+\nu)(\kappa+1)}{E}\,\sigma\sqrt{2a_{eff}(a_{eff}-x)} \\ &= \frac{(1+\nu)(\kappa+1)}{E}\,\sigma\sqrt{2(a+r_y)(a+r_y-x)}\end{aligned}$$

$$\begin{aligned}\delta_t = \delta(x=a) &= \frac{(1+\nu)(\kappa+1)}{E}\,\sigma\sqrt{2(a+r_y)r_y} \\ &= \frac{(1+\nu)(\kappa+1)}{E}\,\sigma\sqrt{2ar_y+2r_y^2} \\ &\approx \frac{(1+\nu)(\kappa+1)}{E}\,\sigma\sqrt{2ar_y}\end{aligned}$$

plane stress : $\delta_t = \frac{4}{\pi}\,\frac{K_I^2}{E\sigma_y} = \frac{4}{\pi}\frac{G}{\sigma_y}$

plane strain : $\delta_t = \left[\frac{1}{\sqrt{3}}\right] \frac{4(1-\nu^2)}{\pi} \frac{K_I^2}{E\sigma_y}$

10.1.2 CTOD by Dugdale

In the vision of Barenblatt-Dugdale, the length of the plastic zone follows from the requirement that the stress at the elastic-plastic boundary is not singular.

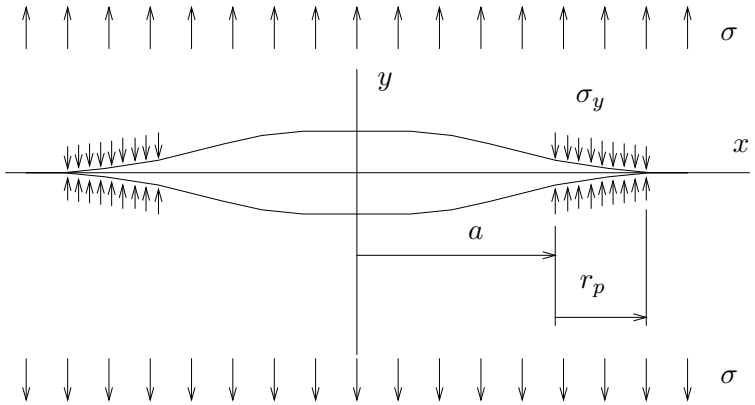

Fig. 10.2 : *Dugdale plastic zone correction.*

$$a_{eff} = a + r_p = a + \frac{\pi}{8}\left(\frac{K_I}{\sigma_y}\right)^2$$

The requirement that the singular term in the stresses at the crack tip must be zero, results in a crack tip opening which is not zero. It can be calculated for plane stress and for plane strain.

displacement from requirement "singular term = 0" : $\bar{u}_y(x)$

$$\bar{u}_y(x) = \frac{(a+r_p)\sigma_y}{\pi E}\left[\frac{x}{a+r_p}\ln\left\{\frac{\sin^2(\hat{\gamma}-\gamma)}{\sin^2(\hat{\gamma}+\gamma)}\right\} + \cos(\hat{\gamma})\ \ln\left\{\frac{\sin(\hat{\gamma})+\sin(\gamma)}{\sin(\hat{\gamma})-\sin(\gamma)}\right\}^2\right]$$

$$\gamma = \arccos\left(\frac{x}{a+r_p}\right) \quad ; \quad \hat{\gamma} = \frac{\pi}{2}\frac{\sigma}{\sigma_y}$$

Crack Tip Opening Displacement

$$\left.\begin{array}{l} \delta_t = \lim_{x\longrightarrow a} 2\bar{u}_y(x) = \dfrac{8\sigma_v a}{\pi E}\ \ln\left\{\sec\left(\dfrac{\pi}{2}\dfrac{\sigma}{\sigma_y}\right)\right\} \\ \text{series expansion} \quad \& \quad \sigma \ll \sigma_y \end{array}\right\} \rightarrow$$

plane stress : $\delta_t = \dfrac{K_I^2}{E\sigma_y} = \dfrac{G}{\sigma_y}$

plane strain : $\delta_t = \left[\dfrac{1}{2}\right] (1-\nu^2)\, \dfrac{K_I^2}{E\sigma_y}$

10.1.3 CTOD crack growth criterion

In LEFM the CTOD can be related to the energy release rate G and the stress intensity factor K_I. In NLFM the CTOD is a measure for the deformation at the crack tip, which can be compared to a critical value in a crack growth criterion. The critical value, which may depend on strain rate and/or temperature, has to be measured.

$$\boxed{\delta_t = \delta_{tc}(\dot{\varepsilon}, T)}$$

10.2 J-integral

In LEFM, crack growth can be predicted after calculation of the energy release rate G or the stress intensity factor K. In NLFM, the behavior of a crack can be described with the J-integral, which has been introduced by Rice in fracture mechanics in 1968 [55]. The J-integral is a vector, $\vec{J}$, with three components in a three-dimensional (here Cartesian) coordinate system. Its value results from an integration along a trajectory Γ. In each point of this trajectory, the specific elastic energy must be calculated from stresses and strains. Also the unit normal vector $\vec{n}$ in that point, the stress vector $\vec{t}$ and the spatial derivatives of the displacement $\vec{u}$ play a role.

What is generally called the J-integral in fracture mechanics, is the first component of the vector $\vec{J}$, so the component in x_1-direction.

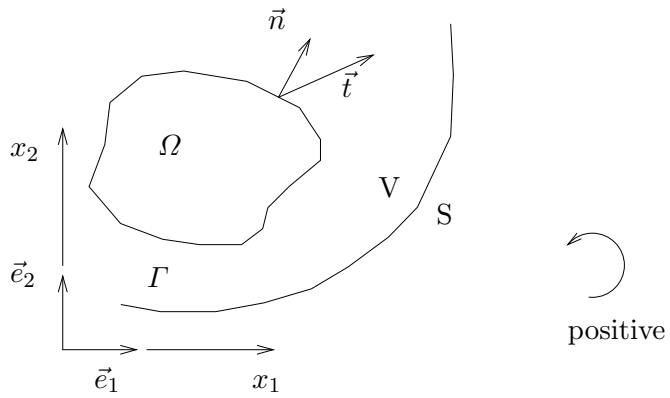

Fig. 10.3 : *Closed curve in a plane with unit normal vector and stress vector.*

$$J_k = \int_\Gamma \left(W n_k - t_i \frac{\partial u_i}{\partial x_k} \right) d\Gamma \qquad ; \qquad W = \int_0^{\varepsilon_{pq}} \sigma_{ij}\, d\varepsilon_{ij}$$

$$J = J_1 = \int_\Gamma \left(W n_1 - t_i \frac{\partial u_i}{\partial x_1} \right) d\Gamma \qquad \left[\frac{\mathrm{N}}{\mathrm{m}} \right]$$

10.2.1 Integral along closed curve

The J-integral vector is defined by integration along a path in a two-dimensional plane. When this path is closed, it can be proved that the resulting value is always zero, under the conditions that there are no singularities in the area within the closed path. The prove assumes that the material behavior is hyper-elastic and homogeneous, the material is not subjected to volume loads and the acceleration is zero. It is also necessary to use a linear strain-displacement definition, which is only allowed when deformation and rotations are small.

$$J_k = \int_\Gamma \left(W \delta_{jk} - \sigma_{ij} u_{i,k} \right) n_j \, d\Gamma$$

inside Γ no singularities $\rightarrow$ Stokes (Gauss in 3D)

$$\int_\Omega \left(\frac{dW}{d\varepsilon_{mn}} \frac{\partial \varepsilon_{mn}}{\partial x_j} \delta_{jk} - \sigma_{ij,j} u_{i,k} - \sigma_{ij} u_{i,kj} \right) d\Omega$$

homogeneous hyper-elastic $\qquad \sigma_{mn} = \dfrac{\partial W}{\partial \varepsilon_{mn}}$

linear strain $\qquad \varepsilon_{mn} = \frac{1}{2}(u_{m,n} + u_{n,m})$

equilibrium equations $\qquad \sigma_{ij,j} = 0$

$$\int_\Omega \left\{ \tfrac{1}{2} \sigma_{mn} (u_{m,nk} + u_{n,mk}) - \sigma_{ij} u_{i,kj} \right\} d\Omega =$$

$$\int_\Omega \left(\sigma_{mn} u_{m,nk} - \sigma_{ij} u_{i,kj} \right) d\Omega = 0$$

10.2.2 Path independency

A crack is now introduced along the x_1-axis. The J-integral – first component of the vector – is calculated along a closed path, which runs around the crack tip and along both crack surfaces. The integral can be written as a summation of four parts. Obviously the calculated value is zero.

It is assumed that the crack faces are not loaded ($t_i = 0_i$). On the crack faces, the unit normal vector is pointing in x_2-direction, so its first component n_1 is zero. This result of the integration along the crack faces is zero, and the J-integral is the sum of two terms

representing an integration along two lines Γ_A and Γ_B around the crack tip. When we take the vector $\vec{n}$ on both Γ_A as Γ_B always directed outwardly from the enclosed area containing the crack tip, the integral over Γ_B will reverse its sign. With this sign convention, it appears that the value of both integrals has to be equal. This important result means that the integral over a non-closed path around the crack tip, starting at one crack face and ending at the other, always has the same value and so the J-integral is path independent.

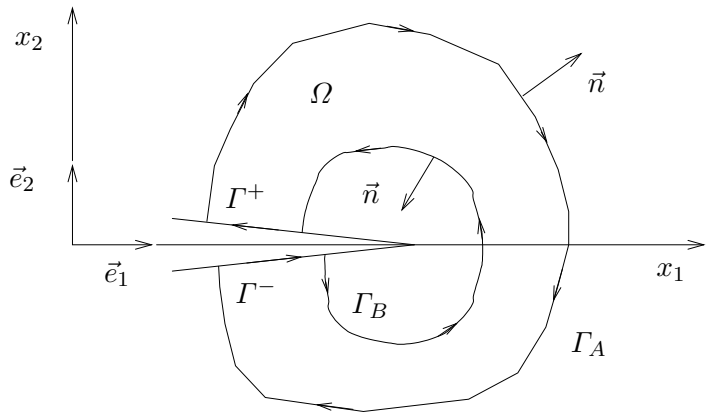

Fig. 10.4 : *Closed curve including crack surfaces.*

$$\int_{\Gamma_A} f_k\,d\Gamma + \int_{\Gamma_B} f_k\,d\Gamma + \int_{\Gamma^-} f_k\,d\Gamma + \int_{\Gamma^+} f_k\,d\Gamma = 0 \quad \rightarrow$$
$$\int_{\Gamma_A} f_1\,d\Gamma + \int_{\Gamma_B} f_1\,d\Gamma + \int_{\Gamma^-} f_1\,d\Gamma + \int_{\Gamma^+} f_1\,d\Gamma = 0$$

no loading of crack faces : $\qquad n_1 = 0 \quad ; \quad t_i = 0 \quad$ on $\quad \Gamma^+$ and Γ^-

$$\left.\begin{array}{l} \displaystyle\int_{\Gamma_A} f_1\,d\Gamma + \int_{\Gamma_B} f_1\,d\Gamma = 0 \\ \displaystyle\int_{\Gamma_A} f_1\,d\Gamma = J_{1_A} \quad ; \quad \int_{\Gamma_B} f_1\,d\Gamma = -J_{1_B} \end{array}\right\} \rightarrow J_{1_A} - J_{1_B} = 0 \rightarrow \boxed{J_{1_A} = J_{1_B}}$$

10.2.3 Relation $J \sim K$

In LEFM, the stress and displacement components at the crack tip are known as a function of the position relative to the crack tip. For multi-mode loading, they are characterized by the stress intensity factors K_I, K_{II} and K_{III}.

Because the J-integral is path-independent, the integration path can be chosen to be a circle with the crack tip as its center. Integration over this circular path reveals that the J-integral is related to the stress intensity factors.

lin. elast. material : $\qquad W = \frac{1}{2}\sigma_{mn}\varepsilon_{mn} = \frac{1}{4}\sigma_{mn}(u_{m,n} + u_{n,m})$

$$J_k = \int_\Gamma \left(\tfrac{1}{4}\sigma_{mn}(u_{m.n} + u_{n,m})\delta_{jk} - \sigma_{ij}u_{i,k} \right) n_j \, d\Gamma$$
$$= \int_\Gamma \left(\tfrac{1}{2}\sigma_{mn}u_{m,n}\delta_{jk} - \sigma_{ij}u_{i,k} \right) n_j \, d\Gamma$$

Mode I + II + III

$$\sigma_{ij} = \frac{1}{\sqrt{2\pi r}} \left[K_I f_{Iij} + K_{II} f_{IIij} + K_{III} f_{IIIij} \right]$$
$$u_i = u_{Ii} + u_{IIi} + u_{IIIi}$$

substitution and integration over Γ = circle

$$J_1 = \frac{(\kappa+1)(1+\nu)}{4E} \left(K_I^2 + K_{II}^2 \right) + \frac{(1+\nu)}{E} K_{III}^2$$
$$J_2 = -\frac{(\kappa+1)(1+\nu)}{2E} K_I K_{II}$$

For Mode I loading of the crack, it follows immediately that the J-integral is equivalent to the energy release rate G. This means that the J-integral can be used in the crack growth criteria of LEFM as a replacement for K and G.

Mode I $\quad J_1 = J = \dfrac{(\kappa+1)(1+\nu)}{4E} K_I^2 = G$

plane stress $\quad \kappa + 1 = \dfrac{3-\nu}{1+\nu} + \dfrac{1+\nu}{1+\nu} = \dfrac{4}{1+\nu} \quad \rightarrow \quad J = \dfrac{1}{E} K_I^2$

plane strain $\quad \kappa + 1 = 4 - 4\nu \quad \rightarrow \quad J = \dfrac{(1-\nu^2)}{E} K_I^2$

Obviously, J-integral is now also related to the crack tip opening displacement δ_t.

plane stress	Irwin	$J = \dfrac{\pi}{4} \sigma_y \delta_t$
	Dugbale	$J = \sigma_y \delta_t$
plane strain	Irwin	$J = \dfrac{\pi}{4} \sqrt{3} \, \sigma_y \delta_t$
	Dugbale	$J = 2\sigma_y \delta_t$

Based on empirical observations, a better relation is suggested by ASTM, including the influence of the specimen dimensions and the ultimate strength σ_u.

$$J = m \, \sigma_y \delta_t$$
$$m = -0.111 + 0.817 \frac{a}{W} + 1.36 \frac{\sigma_u}{\sigma_y}$$

10.3 HRR crack tip stresses and strains

Hutchinson, Rice and Rosengren (HRR) derived a solution for the crack tip stress and displacement components, when the material behavior is described by the Ramberg-Osgood relation [31, 56].

10.3.1 Ramberg-Osgood material law

Non-linear material behavior can often be described by an exponential relation between (equivalent) stress and (equivalent) strain. A much used relation of this type is the Ramberg-Osgood relation. Although it is a general non-linear material model, we will use it here to describe post-yield behavior. The initial yield stress is σ_{y0} and the initial yield strain is $\varepsilon_{y0} = \sigma_{y0}/E$, where E is Young's modulus, describing the linear elastic behavior. The model has two parameters, a coefficient α and an exponent n, which is the strain hardening parameter. When $n = 1$ the relation describes linear hardening and with $n \to \infty$ we have ideal plastic behavior as is illustrated in the figure for $\alpha = 0.01$.

$$\frac{\varepsilon}{\varepsilon_{y0}} = \frac{\sigma}{\sigma_{y0}} + \alpha \left(\frac{\sigma}{\sigma_{y0}} \right)^n$$

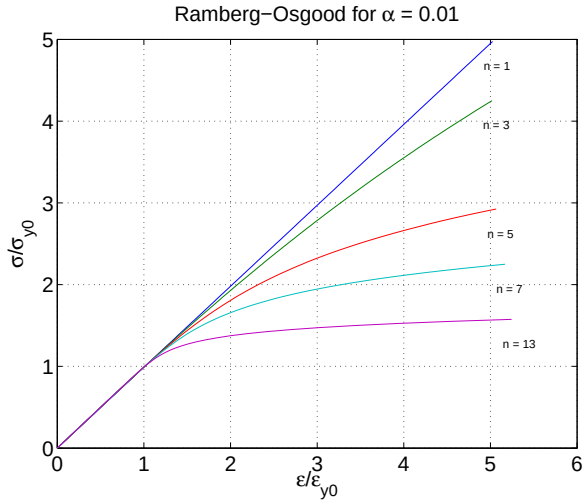

Fig. 10.5 : *Stress-strain relation according to the Ramberg-Osgood material law.*

10.3.2 HRR-solution

The HRR-solution comprises a parameter β, which is directly related to the J-integral. This means that the stress and deformation state at the crack tip is completely characterized by J, just as it is by K in LEFM. The parameter β also depends on a constant I_n, which value is determined numerically as a function of the exponent n, both for plane stress and plane strain.

The solution reveals that the dependency of the distance to the crack tip is determined by the exponent n. For $n = 1$ the singularity of the stresses is $1/\sqrt{r}$, the same as we had in LEFM. For $n > 1$ the singularity is smaller.

$$\sigma_{ij} = \sigma_{y0}\beta\, r^{-\frac{1}{n+1}}\, \tilde{\sigma}_{ij}(\theta) \qquad ; \qquad u_i = \alpha\varepsilon_{y0}\beta^n\, r^{\frac{1}{n+1}}\, \tilde{u}_i(\theta)$$

$$\text{with :} \qquad \beta = \left[\frac{J}{\alpha\sigma_{y0}\varepsilon_{y0}I_n}\right]^{\frac{1}{n+1}} \qquad (I_n \text{ from num. anal.})$$

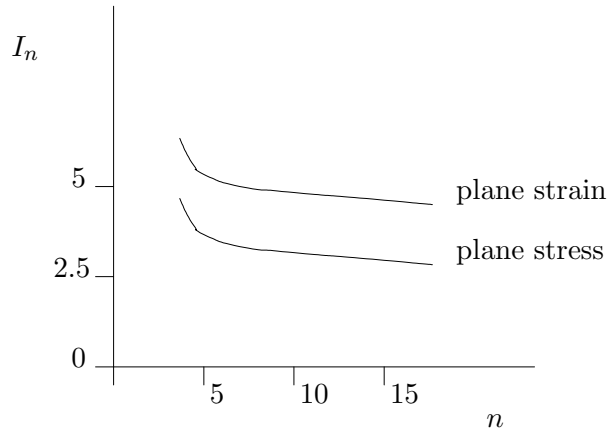

Fig. 10.6 : *Value of the variable I_n for plane strain and plane stress.*

10.3.3 J-integral crack growth criterion

We saw that the J-integral can replace the energy release rate in LEFM and is related to the stress intensity factor. In NLFM, where the material behavior is described by the general Ramberg-Osgood relation, the J-integral characterizes the stress at the crack tip. It is thus obvious that it can be used in a crack growth criterion. Calculation of its value is easily done, due to the fact that the integration path can be chosen arbitrarily. Critical values have to be measured according to normalized experiments.

$$\boxed{J = J_c}$$

Chapter 11

Numerical fracture mechanics

In the crack growth criteria of LEFM and NLFM, a crack growth parameter has to be calculated and compared to a critical value, which is known from experiments. Crack parameters, G, K, δ_t and J, can be calculated analytically, but this is only possible with great mathematical effort and even then for rather simple cases. When such solutions exist, they can often be found in literature. Using numerical methods, it is possible to calculate their values rather straightforwardly, also for practical problems.

Finite element programs are widely available and can be used for the numerical calculation of crack growth parameters. Although special procedures are developed and implemented, the use of standard elements is possible after a minor adaptation of the element mesh. Calculation of the J-integral is often implemented as a standard option.

With the finite element method it is also possible to simulate crack propagation. Several techniques are used and new ones are still under development.

Besides the finite element method, the boundary element method is used in numerical fracture mechanics. Commercial programs for BEM are available although not so widespread as for FEM.

11.1 Quadratic elements

For two-dimensional finite element analyses, the 8-node plane stress or plane strain element gives accurate results for most mechanical problems. The displacement of an internal element point is interpolated quadratically between the nodal displacements. Although initially the element edges are straight lines, after deformation they may become of parabolic shape.

Interpolation or shape functions are used for this purpose, which are a function of two local so-called isoparametric coordinates ξ_1 and ξ_2, which have values between -1 and +1. The ξ_1, ξ_2-coordinate system is not orthonormal, because the axes are not perpendicular.

Strains, which are derivatives of the displacements, are more or less linear in the local coordinates and this is also the case for the stresses, which are proportional to the strains. It has to be said that these statements are not valid when non-linear strain-displacement and stress-strain relations are used.

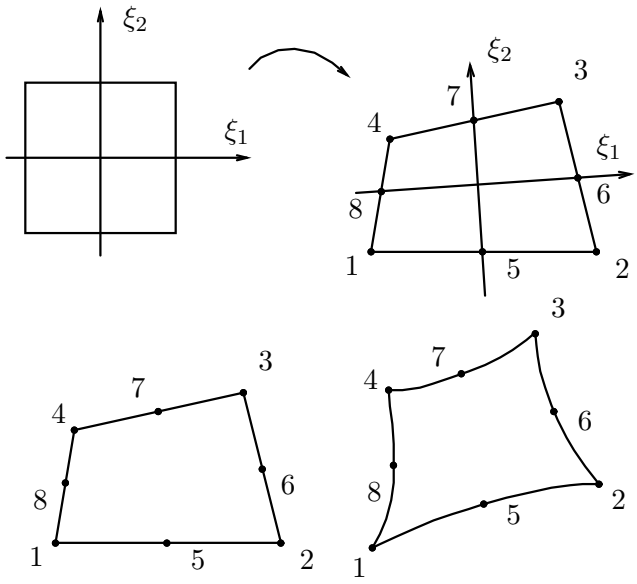

Fig. 11.1 : *Quadratic elements with 8 nodal points.*

11.2 Crack tip mesh

The figure shows part of the element mesh around the crack tip. Where the crack has opened, the nodes of elements above and below the crack may coincide, but must not be connected.

When the material is assumed to be linearly elastic, theory says that the stresses at the crack tip are proportional to $1/\sqrt{r}$, with r the distance to the crack tip. The very steep stress gradient at the crack tip can only be described with a lot of small elements. However, it is found that refining the mesh at the crack tip will not lead to convergence, i.e. further refinement will always render different results. The reason for this unacceptable mesh dependency is the singularity in the stress field, which is not described by the element interpolation functions.

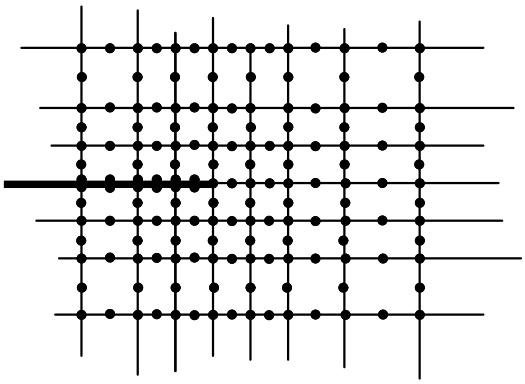

Fig. 11.2 : *Crack tip mesh.*

11.3 Special elements

Solutions to circumvent the shortcomings of the standard 8-node element to describe the crack tip stresses well, are still being sought and found.

One solution is to change the interpolation function of the element in such a way that the crack tip field is included. This results in a so-called *enriched element*, which is only usable at the crack tip.

Another solution may be found in application of a modified variational principle as the basis for the finite element equations. The resulting element is a *hybrid element*, where stresses are unknown nodal variables.

Using enriched or hybrid elements implies implementation of these elements and sometimes new solution techniques in the FEM program, which may be very infeasible, when a commercial program is used. However, there is a possibility to calculate the crack tip stress field very accurately with standard 8-node elements, which are slightly adapted into so-called *quarter point elements*.

11.4 Quarter point elements

Quarter point elements are devised by Barsoum in 1976 [2] as a simple means to describe the stress singularity at the crack tip. They are standard 8-node quadrilateral or 6-node triangular elements, where two mid-side points are repositioned towards one corner node, such that they divide there side in the ratio 1:3. They are used at the crack tip, which is located in the node towards which the mid-side nodes are moved. It can be proved that they describe the $1/\sqrt{r}$-stress field singularity at the crack tip accurately.

Quarter point elements are also referred to as Distorted Quadratic Quadrilateral or Triangle. Another suitable solution is to use a Collapsed Quadratic Quadrilateral, where three points of the 8-node quadrilateral element are situated at the same location, but not connected.

A linear 4-node quadrilateral element can be collapsed into a triangle and it appears to describe a $1/r$ singularity very accurately.

Quarter point elements can be made very easily at the crack tip by replacing some mid-side nodes of the element mesh. The big advantage is that they allow the use of standard finite element packages.

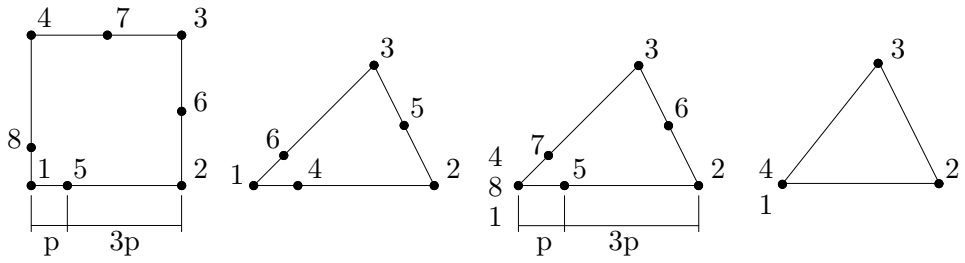

Fig. 11.3 : *Quarter point and collapsed elements.*

The crack tip mesh is often made as a crack tip rozet, with quarter point elements at the crack tip. Lim advised in 1993 [44], to use transition elements between the quarter point elements and the regular mid point elements for better results.

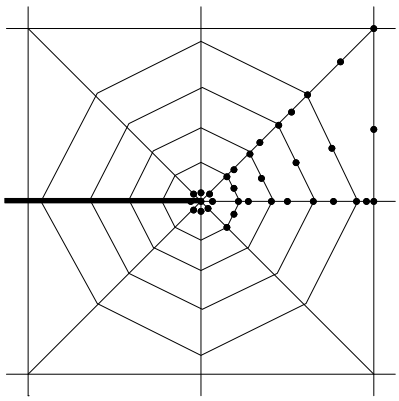

Fig. 11.4 : *Crack tip rozet.*

11.4.1 One-dimensional case

For a one-dimensional case, it will be proved that the quarter point technique indeed renders the $1/\sqrt{r}$ singularity. The figure shows a line element with three nodes and a local coordinate $-1 \leq \xi \leq 1$. The global coordinate x has its origin in node 1, where the crack tip can be seen.

The global position of an element point can be interpolated between the position of the three nodes $\{x_1, x_2, x_3\}$, where $x_1 = 0$ and $x_2 = L$, the length of the element. The displacement u in x-direction is interpolated in the same way between the nodal displacements u_1, u_2 and u_3. The strain of the element is calculated as the derivative of u w.r.t. x, which can be calculated, using the interpolations.

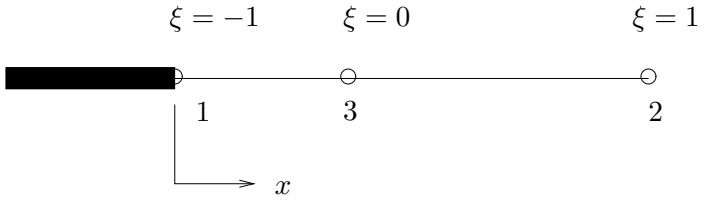

Fig. 11.5 : *One-dimensional three-point element at the crack tip.*

$$\begin{aligned} x &= \tfrac{1}{2}\xi(\xi-1)x_1 + \tfrac{1}{2}\xi(\xi+1)x_2 - (\xi^2-1)x_3 \\ &= \tfrac{1}{2}\xi(\xi+1)L - (\xi^2-1)x_3 \end{aligned}$$

$$u = \tfrac{1}{2}\xi(\xi-1)u_1 + \tfrac{1}{2}\xi(\xi+1)u_2 - (\xi^2-1)u_3$$

$$\frac{du}{d\xi} = (\xi - \tfrac{1}{2})u_1 + (\xi + \tfrac{1}{2})u_2 - 2\xi u_3 \qquad \rightarrow \quad \frac{du}{dx} = \frac{du}{d\xi}\,\frac{d\xi}{dx} = \frac{du}{d\xi} \Big/ \frac{dx}{d\xi}$$

Mid point element

When node 3 is located in the center of the element ($x_3 = \frac{1}{2}L$), the strain in node 1 (at the crack tip) can be evaluated and appears to be a linear function of the local coordinate ξ. The strain at node 1 (the crack tip) is constant.

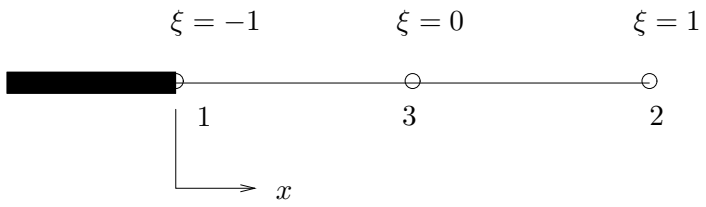

Fig. 11.6 : *One-dimensional mid point element at the crack tip.*

$$x = \tfrac{1}{2}\xi(\xi+1)L - (\xi^2-1)\tfrac{1}{2}L = \tfrac{1}{2}(\xi+1)L \qquad \Rightarrow \qquad \frac{dx}{d\xi} = \tfrac{1}{2}L$$

$$\frac{du}{dx} = \frac{\frac{du}{d\xi}}{\frac{1}{2}L} \quad \rightarrow \quad \left.\frac{du}{dx}\right|_{\xi=-1}^{x=0} = \left(\frac{2}{L}\right)\left\{\left(-\tfrac{3}{2}\right)u_1 + \left(\tfrac{1}{2}\right)u_2 + 2u_3\right\}$$

Quarter point element

When node 3 is positioned at the quarter of the element length ($x_3 = \frac{1}{4}L$), the strain appears to be proportional to $1/\sqrt{x}$ and becomes infinite in node 1.

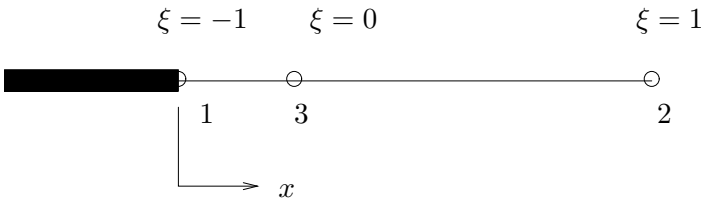

Fig. 11.7 : *One-dimensional quarter point element at the crack tip.*

$$x = \tfrac{1}{2}\xi(\xi+1)L - (\xi^2-1)\tfrac{1}{4}L = \tfrac{1}{4}(\xi+1)^2L \quad \rightarrow \quad \xi+1 = \sqrt{\frac{4x}{L}} \quad \Rightarrow$$

$$\frac{dx}{d\xi} = \tfrac{1}{2}(\xi+1)L = \sqrt{xL}$$

$$\frac{du}{dx} = \frac{\frac{du}{d\xi}}{\sqrt{xL}} \quad \rightarrow \quad \left.\frac{du}{dx}\right|_{\xi=-1}^{x=0} = \infty \quad \rightarrow \quad \text{singularity} \quad \frac{1}{\sqrt{x}}$$

11.5 Virtual crack extension method (VCEM)

One of the variables which can be calculated with a standard finite element package is the energy release rate G. It is defined by differentiation of internal and external work w.r.t. the crack length.

The energy release rate can be calculated following two analyses, with a small difference in crack length Δa. The ratio of the difference in elastic energy and Δa is a good approximation for G, when Δa is indeed very small and when "fixed grips" is used, i.e. when boundary displacements are prescribed.

This procedure is called the Virtual Extension Method or Stiffness Derivation Method.

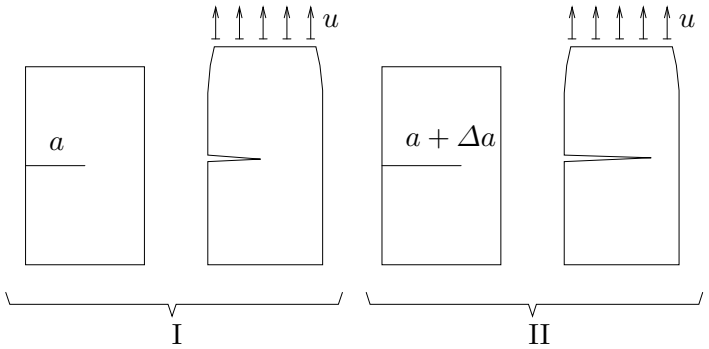

Fig. 11.8 : *Virtual Crack Extension Method.*

$$\text{fixed grips} \quad \rightarrow \quad \frac{dU_e}{da} = 0 \quad \Rightarrow \quad G = -\frac{1}{B}\frac{dU_i}{da} \approx -\frac{1}{B}\frac{U_i(a+\Delta a) - U_i(a)}{\Delta a}$$

stiffness matrix variation

Instead of analyzing the whole structure two times with small difference in crack length, the energy release rate can be calculated directly from the stiffness matrix. Only a small part of the mesh around the crack tip is considered and its contribution to the global stiffness matrix $\underline{C}$ is calculated for crack length a and for crack length $a + \Delta a$, where the outer boundary of the crack tip mesh is fixed. The change in the stiffness matrix can be used directly to evaluate G. Because only a small region around the crack tip is considered, it is important to use quarter point elements at the crack tip.

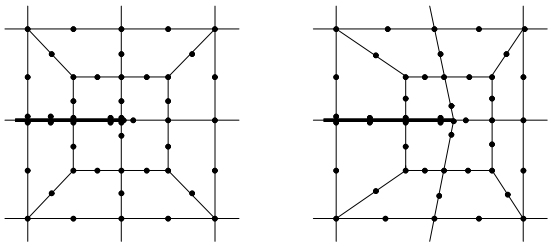

Fig. 11.9 : *VCEM in crack tip mesh.*

$$B\,G = -\frac{dU_i}{da} = -\tfrac{1}{2}\underset{\sim}{u}^T \frac{\Delta \underline{C}}{\Delta a}\,\underset{\sim}{u} \qquad \text{with} \qquad \Delta \underline{C} = \underline{C}(a+\Delta a) - \underline{C}(a)$$

11.6 Stress intensity factor

Calculation of the stress intensity factor is of course possible trough its relation with the energy release rate.

$$\begin{array}{lll} \text{plane stress} & K_I^2 = EG_I \quad ; & K_{II}^2 = EG_{II} \\ \text{plane strain} & K_I^2 = \dfrac{E}{1-\nu^2}\, G_I \quad ; & K_{II}^2 = \dfrac{E}{1-\nu^2}\, G_{II} \end{array}$$

Calculation of the stress intensity factor is also possible through its definition, which relates it to the stress field. Stress components have to be calculated accurately upon which K results from extrapolation to the crack tip. Because stresses are calculated in integration points and the crack tip is located in an element node, this calculation is not exactly according to the definition of K. It always remains to be investigated how the interpolation has to be done to get the best results.

$$K_I = \lim_{r \longrightarrow 0} \left(\sqrt{2\pi r}\ \sigma_{22}|_{\theta=0} \right) \quad ; \quad K_{II} = \lim_{r \longrightarrow 0} \left(\sqrt{2\pi r}\ \sigma_{12}|_{\theta=0} \right)$$

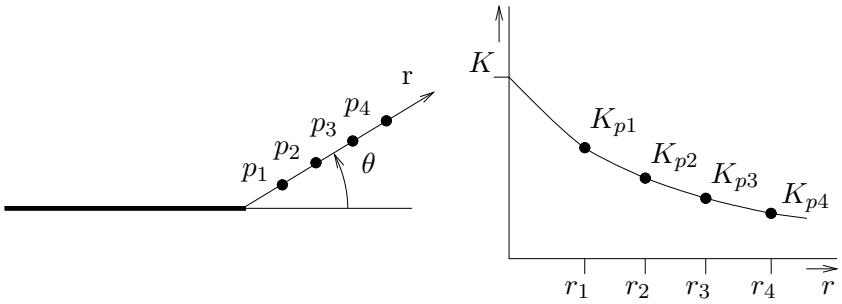

Fig. 11.10 : *Calculation of K by extrapolation.*

Stresses in element integration points are calculated by differentiation, which makes them less accurate then the calculated nodal displacements. It seems logical therefore to calculate the stress intensity factor not from the stress field but from the displacement field.

$$u_y = \frac{4(1-\nu^2)}{E} \sqrt{\frac{r}{2\pi}}\ K_I\ g_{ij}(\theta) \quad \rightarrow \quad K_I = \lim_{r \longrightarrow 0} \left[\frac{E}{4(1-\nu^2)} \sqrt{\frac{2\pi}{r}}\ u_y(\theta = 0) \right]$$

11.7 J-integral

The J-integral can be calculated according to its definition, i.e. by integration along a path around the crack tip. Because stresses and strains are known in integration points, the integration path must preferably pass through these points. In a general crack tip mesh such a path would be difficult to define during post-processing of the results.

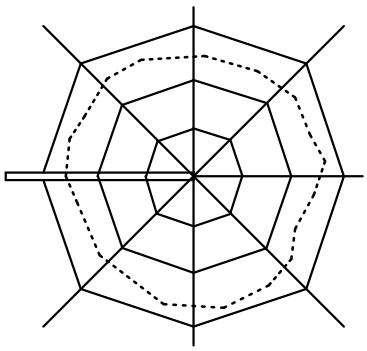

Fig. 11.11 : *J-integral path in crack tip rozet.*

In a regular crack tip mesh, an integration path could be defined as indicated in the figure. It consists of lines in coordinate directions. When symmetry can be considered, only half of the path has to be taken into account. When such a path is taken at a certain distance from the crack tip, there is no need to use quarter point crack tip elements.

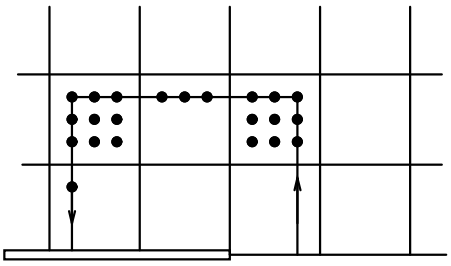

Fig. 11.12 : *J-integral path through integration points.*

11.7.1 Domain integration

In commercial element packages, the J-integral over a curve Γ is transformed to an integral over the domain Ω, enclosed by Γ. Because the path Γ is not a closed path, Stokes theorem cannot be applied directly. In a paper by Li et.al. published in 1985, it is shown that the transformation is possible when a shift function q is introduced, which is 0 at the outer boundary of Ω and 1 at the inner boundary.

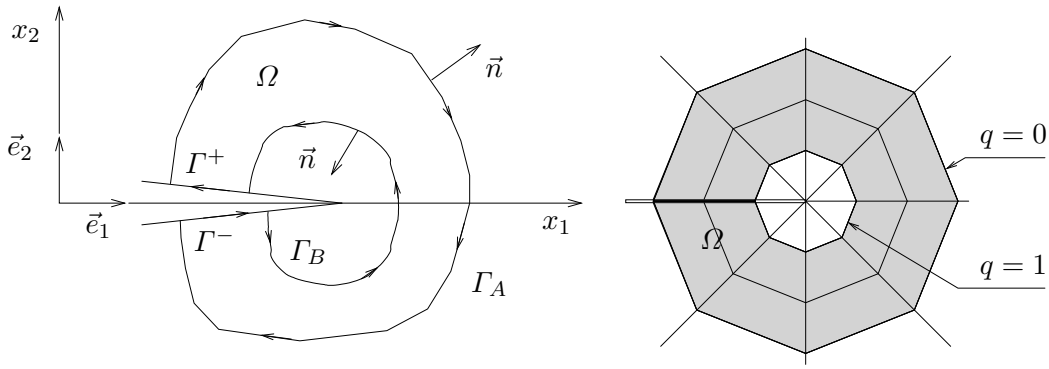

Fig. 11.13 : *J-integral domain.*

$$J = \int_{\Omega} \frac{\partial q}{\partial x_j} \left(\sigma_{ij} \frac{\partial u_i}{\partial x_1} - W \delta_{1j} \right) d\Omega$$

11.7.2 De Lorenzi J-integral : VCE technique

In the Marc/Mentat package a general J-integral is calculated, which includes phenomena like pressure on the crack faces p_i, acceleration effects and initial strains ε^o_{ij}. It is calculated as a domain integral, where the shift function q is defined as the ratio of a displacement Δx_1 of nodes within the domain Ω and the elongation Δa of the crack. The user has to indicate which ring of elements around the crack tip must be moved when the crack is virtually extended. In one analysis several options can be chosen.

Calculating such J-integral values is a default option in major FEA codes. It does not require intensive mesh refinement near the crack tip or the use of quarter point elements.

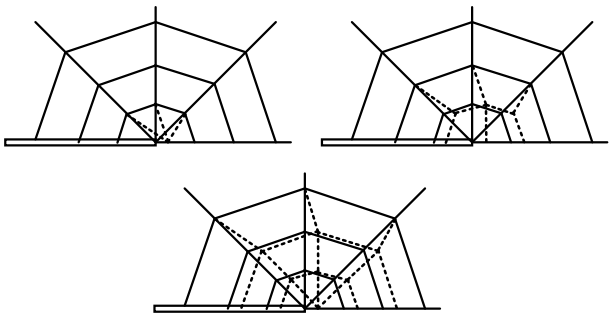

Fig. 11.14 : *J-integral domain with various element rings.*

$$J = \int_{\Omega} \frac{\partial q}{\partial x_j} \left(\sigma_{ij} \frac{\partial u_i}{\partial x_1} - W \delta_{1j} \right) d\Omega - \int_{\Gamma_s} q p_i \frac{\partial u_i}{\partial x_1} \, d\Gamma - \int_{\Omega} q(\rho q_i - \rho \ddot{u}_i) \frac{\partial u_i}{\partial x_1} \, d\Omega + \int_{\Omega} q \sigma_{ij} \frac{\partial \varepsilon^o_{ij}}{\partial x_1} \, d\Omega$$

11.8 Crack growth simulation

Numerical procedures can not only be used to evaluate crack growth criteria. The actual crack propagation can be simulated. Various approaches exist and they are improved in ongoing research.

11.8.1 Node release

One of the techniques to simulate crack propagation is the "node release" method. When a crack growth criterion indicates that a crack will growth, use of a crack growth direction criterion like MTS or SED, reveals in what direction the crack tip wants to move. In the node release approach, a crack can only move along element edges and the movement is realized by splitting one or more nodes in two, which are not connected anymore. The resulting crack path is strongly depending on the mesh geometry. Application is not so easy to accomplish, because the propagation implies that the element mesh topology has to change.

By introducing springs and/or dashpots between the released nodes, ductile crack propagation can be simulated.

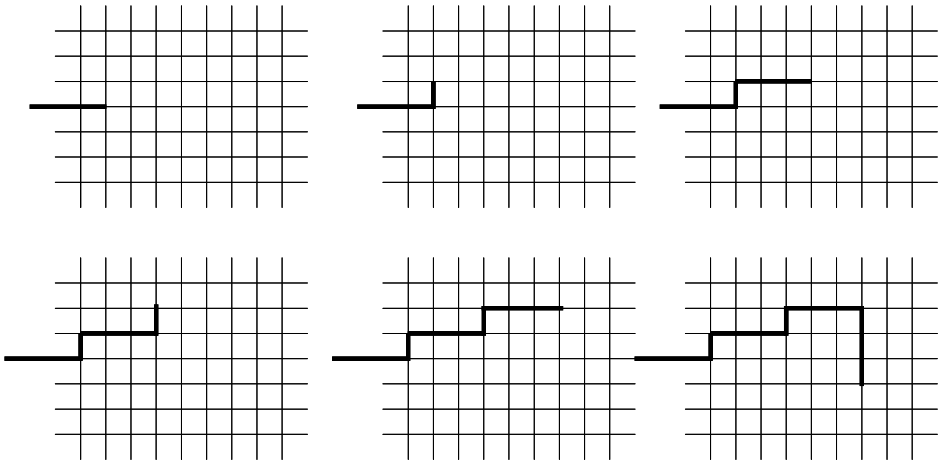

Fig. 11.15 : *Node release method for crack growth simulation.*

11.8.2 Moving Crack Tip Mesh

Because of the high stress gradients at the crack tip, small elements are required there, while elements at a some distance to the crack tip can be considerably larger. It is for this reason that a so-called crack tip mesh (CTM) is often used. When crack propagation is simulated, this CTM can follow the crack tip. The example shows the crack propagation in the interface between fiber and matrix for a plane strain simulation in the transversal plane, where the loading is in the vertical direction. The crack opening is shown with enlarged displacements. It was possible to simulate the crack propagation, which initially was in the fiber-matrix interface but from some point moved into the matrix material. The CTM was moved by hand for each crack advancement, which was a very laborious operation.

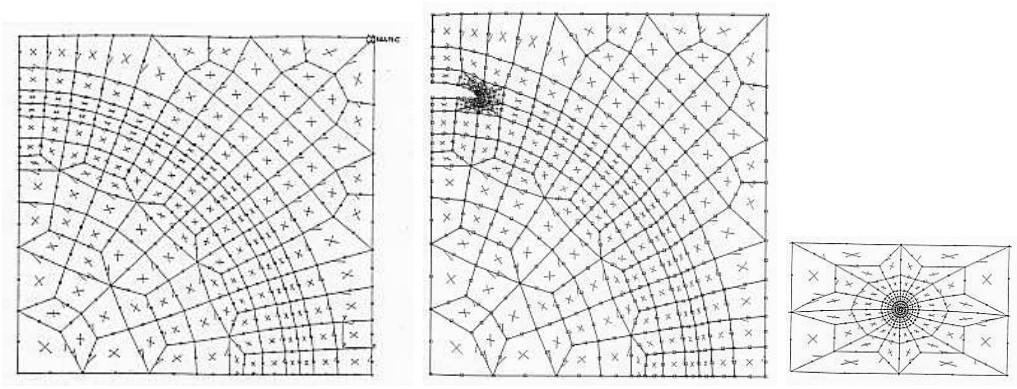

Fig. 11.16 : *Crack tip mesh moves along fiber-matrix interface [42].*

11.8.3 Element splitting

Instead of advancing a crack along element edges, propagation through elements is also an option. It implies the subdivision of an element in two or more smaller elements, which changes the mesh topology. Results are more accurate than those of the node release method. Mesh refinement can be realized in the region of the crack tip.

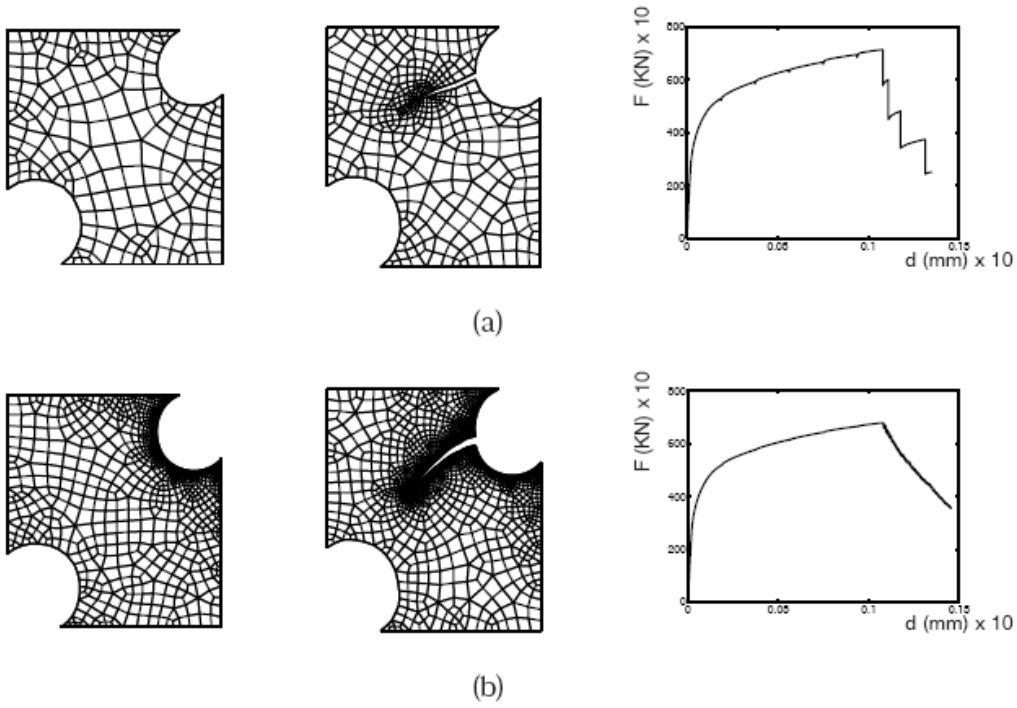

Fig. 11.17 : *Crack propagation by element splitting technique [47].*

11.8.4 Smeared crack approach

The smeared crack approach can be seen as an intermediate between fracture mechanics and continuum damage mechanics. Attention is not focused on one large crack, but the material damage is modeled with small cracks in element integration points. These cracks may initiate and lengthen according to certain loading criteria. The cracks are not really modeled, but simulated with anisotropic material behavior, where in one direction the material stiffness is reduced.

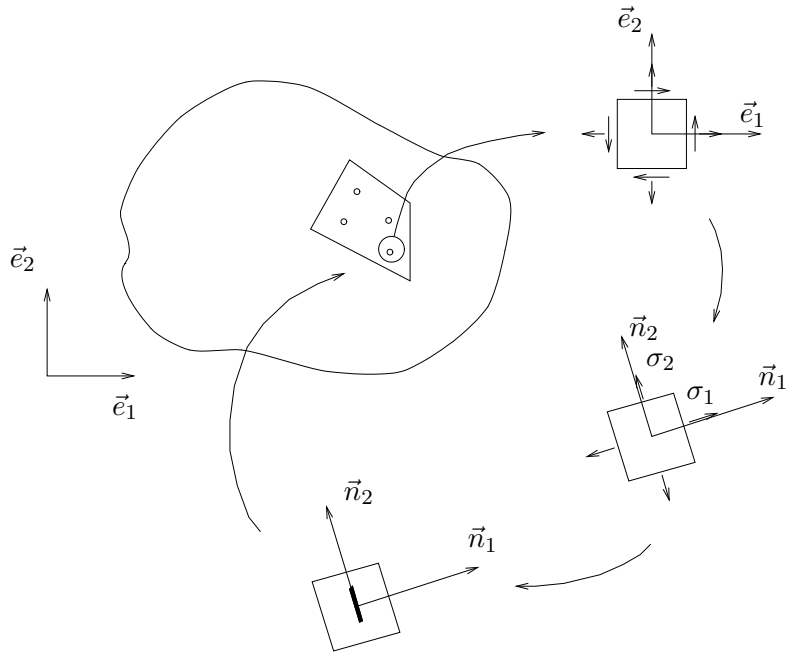

Fig. 11.18 : *Smeared crack approach for crack propagation.*

Chapter 12

Fatigue

Many structures are subjected to cyclic loading, with an amplitude so low that failure due to yielding or crack growth, is never to be expected. However, experience tells a different story. After a large number of load reversals, structural parts fail unexpectedly, often leading to dramatic and overall collapse. This very dangerous phenomenon is the result of fatigue crack growth.

Fatigue failure became an issue when carriages and trains with iron or steel axles began traveling frequently over long distances in the mid 19th century. Axles broke mostly at diameter-jumps and this was explained first as the result of changes in the material's structure. Wöhler was among the first to investigate these phenomena systematically, all of course experimentally. Over many years, a tremendous amount of data was gathered, but theoretical explanation had to wait until Griffith saw the importance of cracks for the failure of materials.

Cyclic loading of structures does not only occur as the result of deliberately applied load reversals. Vibrations (machine(s) (parts)), repeated pressurization en depressurization (airplanes), thermal cycling (switching of electronic devices), random forces (ships, vehicles, planes) occur always and everywhere.

12.1 Crack surface

When fatigue failure has occurred, the crack surface shows two distinct markings on two different scales.

At a macroscopic scale, so-called *clam shell markings* also called *beach marks* can be seen. They are the result of irregularities in the growth of the fatigue crack, due to changes in loading conditions.

When the crack surface is observed with a microscope, the crack displacement during each individual load cycle is seen as a pattern of *striations*. During one cycle, plastic deformation at the crack tip results in sequential blunting and sharpening of the crack tip. This crack growth is very regular.

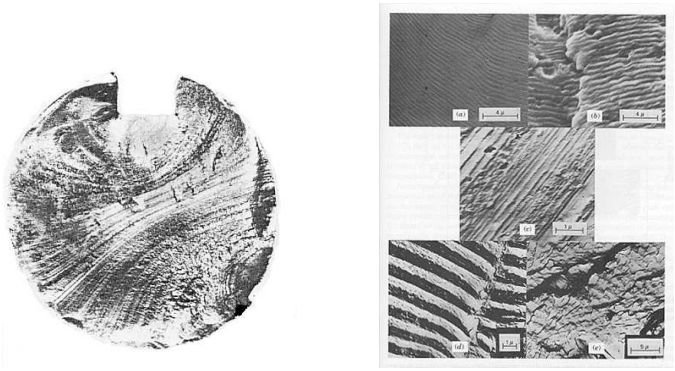

Fig. 12.1 : *Clam shell fatigue crack surface and striations [29].*

12.2 Experiments

Experiments can be done on full-scale structures subjected to real-life loading. This, however, is often not feasible, due to costs and the extremely long times involved before the detection of fatigue damage. Experiments are therefore mostly done on laboratory scale, using small test specimens subjected to high loads varying at high frequencies. Results must be carefully evaluated, because size effects and up-scaling of load amplitude and frequencies may lead to inconsistencies with real-life applications.

12.3 Fatigue load

When fatigue crack growth is studied experimentally, the loading is first taken to be harmonic and is characterized in terms of stresses or strains. For stress controlled loading, the stress range $\Delta\sigma$ is the difference between the maximum and the minimum stress during the cycle. The stress amplitude σ_a is half the stress variation. Average stress σ_m and stress ratio R_σ are used to specify the loading. Also the amplitude ratio σ_a/σ_m is sometimes used.

In strain controlled experiments, all these variables obviously apply to strains.

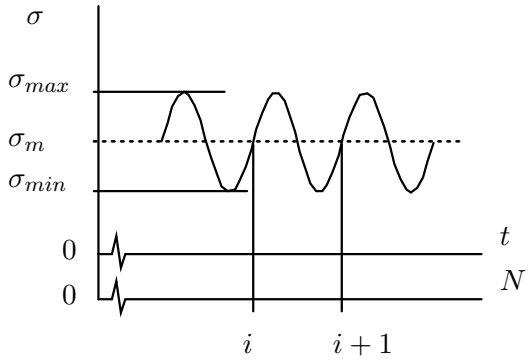

Fig. 12.2 : *Harmonic stress.*

$$\Delta\sigma = \sigma_{max} - \sigma_{min} \quad ; \quad \sigma_a = \tfrac{1}{2}\Delta\sigma$$
$$\sigma_m = \tfrac{1}{2}(\sigma_{max} + \sigma_{min}) \quad ; \quad R_\sigma = \sigma_{min}/\sigma_{max} \quad ; \quad \frac{\sigma_a}{\sigma_m} = \frac{1-R}{1+R}$$

12.3.1 Fatigue limit

Experiments reveal that some materials – e.g. mild steel, low strength alloys, some Ti/Al/Mg alloys – never fail under cyclic loading, when the stress in each cycle is below a certain threshold σ_{th}, also referred to as *fatigue limit*. Other materials – high strength steels, most non-ferro alloys, some austenitic steels, some Ti/Al/Mg alloys – do not have such a fatigue limit: they will always fail no matter how low the stress, although it may take a very large number of load cycles.

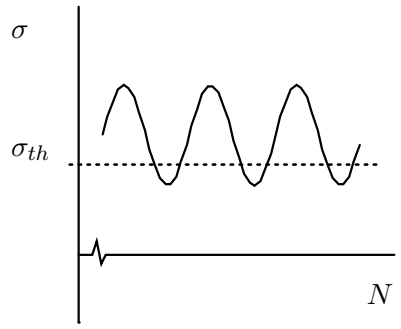

Fig. 12.3 : *Harmonic stress and fatigue limit.*

12.3.2 (S-N)-curve

The experimental data are represented as a (S-N)- or Wöhler curve, where the maximum stress $S = \sigma_{max}$ is indicated along the vertical axis and the logarithm of the number of cycles to failure or *fatigue life* N_f along the horizontal axis. Determination and representation of these data is prescribed in normalization sheet B.S. 3518 part I 1984.

These curves are mostly recorded for zero average stress. For materials with a fatigue limit, the (S-N)-curve will advance towards a horizontal asymptote at the level $\sigma = \sigma_{th}$. When a fatigue limit does not exist, the *fatigue strength* or *endurance limit* is defined as the stress variation for failure after a specified high – typically 10^6 – number of cycles. The ratio of fatigue limit or endurance limit to tensile strength is referred to as endurance ratio.

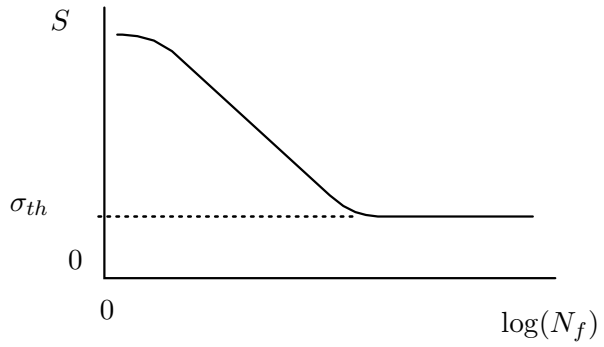

Fig. 12.4 : *S-N-curve with fatigue limit.*

Fatigue data may also be presented in a (S_a-N)-curve, where the vertical axis indicates the stress amplitude : $S_a = \sigma_a = \frac{1}{2}\Delta\sigma$.
For some real materials the (S-N)-curves are shown in the figure.

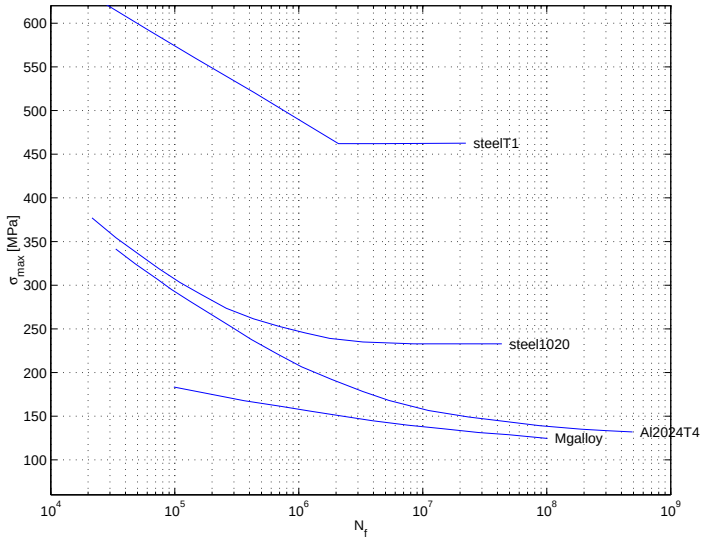

Fig. 12.5 : *S-N-curves for various materials.*

12.3.3 Influence of average stress

When the average stress is positive, a crack will grow faster and the curve will be located at lower stress values, indicating that the fatigue life N_f is reached earlier for the same stress amplitude σ_a. It can also be stated that for the same N_f, σ_a is reduced to σ_a^*.

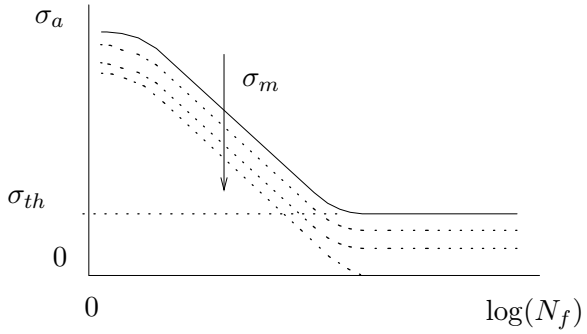

Fig. 12.6 : *Influence of the average stress on the S_a-N-curve.*

Corrections have been proposed to take into account the decrease in σ_a due to $\sigma_m \neq 0$ and to relate it to the tensile strength σ_u or the initial yield stress σ_{y0}. Much used are the empirical formulas of Gerber, Goodman and Soderberg.

Gerber (1874)
$$\frac{\sigma_a^*}{\sigma_a} = 1 - \left(\frac{\sigma_m}{\sigma_u}\right)^2$$

Goodman (1899)
$$\frac{\sigma_a^*}{\sigma_a} = 1 - \frac{\sigma_m}{\sigma_u}$$

Soderberg (1939)
$$\frac{\sigma_a^*}{\sigma_a} = 1 - \frac{\sigma_m}{\sigma_{y0}}$$

12.3.4 (P-S-N)-curve

Variations in experimental fatigue data can be represented in a (P-S-N)-curve, where probability (P) of failure is incorporated. The center curve represents the stress for which 50 % of all specimens will fail after the associated N_f. When the upper curve is reached, 99 % of all specimens will have failed. The lower curve represents the weakest specimens. For the given stress, 1 % of all specimens fail for N_f on this curve.

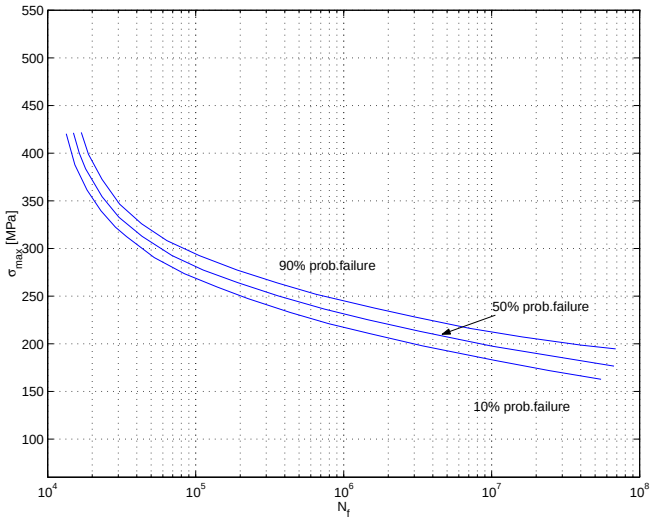

Fig. 12.7 : *P-S-N-curves.*

12.3.5 High/low cycle fatigue

For low stresses and thus long fatigue life (typically $N_f > 50000$), we are in the *High Cycle Fatigue* (HCF) range. Because stresses are very low, the plastic crack tip zone is small and concepts from LEFM (+ SSY) can be applied. We can characterize the crack tip stress field with stress intensity factors.

For high stresses and thus short fatigue life, we are in the *Low Cycle Fatigue* (LCF) range. Crack tip stresses are so high that NLFM has to be applied to study the crack behavior.

For high cycle fatigue the (S-N)-curve can be fitted with the Basquin relation. For low cycle fatigue the Manson-Coffin relation is used for the fit.

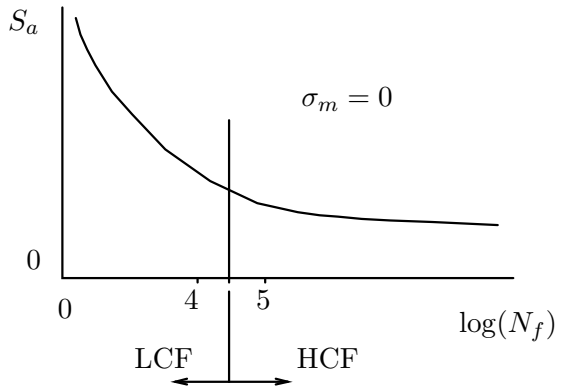

Fig. 12.8 : *Low and High Cycle Fatigue regimes.*

12.3.6 Basquin relation

The Basquin relation relates the stress amplitude to the number of load reversals, which is twice the number of cycles. The relation has two parameters: the *fatigue strength coefficient* σ'_f, and the *fatigue strength exponent* or *Basquin exponent* b.

$$\tfrac{1}{2}\Delta\sigma = \sigma_a = \sigma'_f(2N_f)^b \quad \rightarrow \quad \Delta\sigma N_f^{-b} = \text{constant}$$

Fig. 12.9 : *Basquin fit of S-N-curve.*

12.3.7 Manson-Coffin relation

The Manson-Coffin relation relates the plastic strain amplitude to the number of load reversals, which is twice the number of cycles. The relation has two parameters: the *fatigue ductility coefficient* ε'_f, and the *fatigue ductility exponent* or *Manson-Coffin exponent* c.

$$\tfrac{1}{2}\Delta\varepsilon^p = \varepsilon'_f(2N_f)^c \quad \rightarrow \quad \Delta\varepsilon^p N_f^{-c} = \text{constant}$$

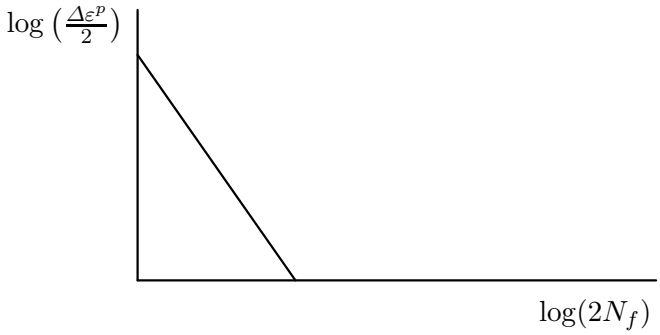

Fig. 12.10 : *Manson-Coffin fit of S-N-curve.*

12.3.8 Total strain-life curve

Basquin and Manson-Coffin relations can be combined. To that purpose, the stress amplitude in the Basquin relation has to be replaced by a strain amplitude, which is easily accomplished, because the low stresses assure linear elastic behavior. The total strain amplitude is the addition of the elastic and plastic strain amplitudes, which is a valid assumption for small deformations.

The resulting *total strain-life curve* can be plotted, using logarithmic axes.

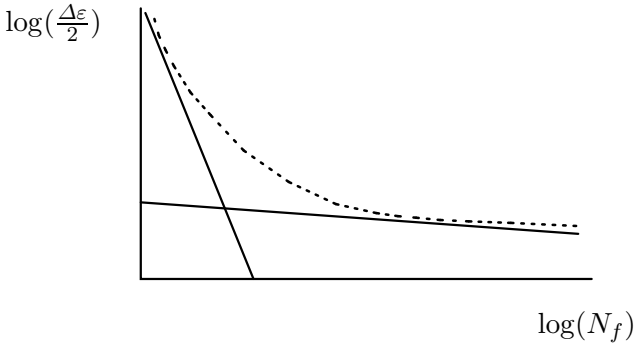

Fig. 12.11 : *Total strain-life curve.*

$$\frac{\Delta\varepsilon}{2} = \frac{\Delta\varepsilon^e}{2} + \frac{\Delta\varepsilon^p}{2} = \frac{1}{E}\sigma'_f(2N_f)^b + \varepsilon'_f(2N_f)^c$$

12.4 Influence factors

Fatigue life of a test specimen is determined by the external load amplitude and frequency, as is experimentally represented in an (S-N)-curve. For real structures, the fatigue life is highly determined by macroscopic shape and dimension, and by microscopic configuration (material microsructure). Manufacturing procedures are also very influential. Environmental influences can have a high impact on the initiation and propagation of fatigue damage as well.

12.4.1 Load spectrum

Fatigue life is experimentally represented in an (S-N)-curve. Until so far we considered tensile loading where S can be the maximum stress or the stress amplitude. The influence of the average stress σ_m is obvious and has been discussed.

Fatigue data are independent of the loading frequency within certain limits. Too low or too high frequencies will result in different fatigue life.

Shear loading experiments result in different (S-N)-curves than the tensile equivalents. Multi-axial loading results in lower fatigue life that uni-axial loading.

12.4.2 Stress concentrations

The shape of structural parts, combined with the external loading, almost always leads to inhomogeneous deformation and non-uniform stress fields. In certain situations local stresses can become much higher than the average or nominal stress and such stress concentrations are mostly found at notches. The *stress concentration factor* K_t is the ratio between the maximum stress and the nominal stress and is a function of the notch radius ρ.

When the specimen is subjected to an harmonic load, the fatigue or endurance limit is theoretically reduced with $1/K_t$. Experiments have shown, however, that the fatigue life is reduced less severely than this: it is reduced by a factor $1/K_f$, where K_f is the *fatigue strength reduction factor*, which is smaller than K_t.

The *notch sensitivity factor* q relates K_f to K_t and is found to be a function of the notch radius and a material parameter. Relations for q have been proposed by Peterson [54] and Neuber [51].

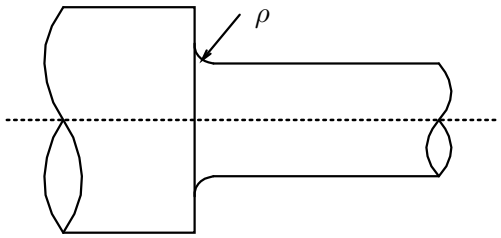

Fig. 12.12 : *Stress concentration at axis diameter reduction.*

$$\Delta\sigma_{th}(\text{notched}) = \frac{1}{K_f}\,\Delta\sigma_{th}(\text{unnotched}) \quad ; \qquad 1 < K_f < K_t$$

$$K_f = 1 + q(\rho)(K_t - 1)$$

Peterson : $q = \dfrac{1}{1 + \frac{a}{\rho}}$ with a = material parameter

Neuber : $q = \dfrac{1}{1 + \sqrt{\frac{b}{\rho}}}$ with b = grain size parameter

12.4.3 Stress gradients

The size of a structural part, e.g. an axis subjected to bending, determines the gradients of stresses at equal external load. Larger specimens show lower gradients than smaller ones, when subjected to the same external load. When the gradient is lower, more material is subjected to a raised stress level than in the case of a higher gradient. This results in a decrease of fatigue life with specimen size. This size effect often necessitates testing in full scale experiments, especially for critical applications like aviation.

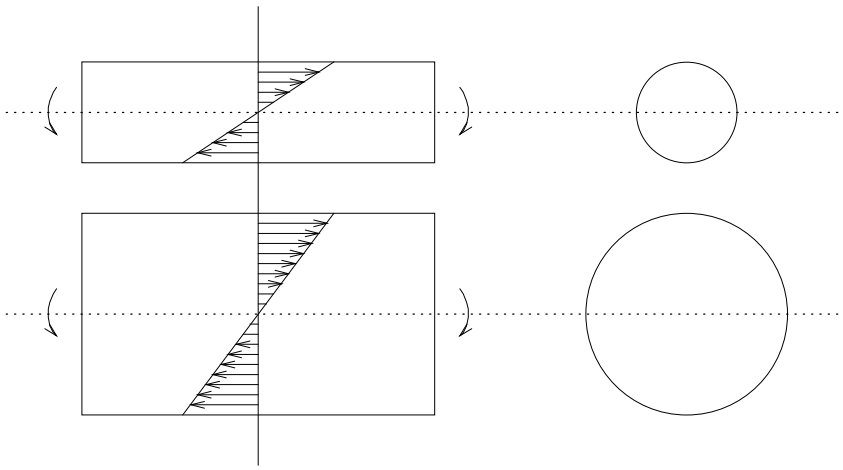

Fig. 12.13 : *Stress gradients in axes of different diameter.*

12.4.4 Material properties

The ease of fatigue crack initiation and growth is obviously influenced by the microstructure of the material. At low temperatures grain boundaries act as a barrier for crack propagation, so fatigue limit is higher for small grain microstructures. At high temperatures, the grain boundaries are weakened by diffusion of atoms (creep), so fatigue limit is lower for small grains. The texture (grain shape) also influences fatigue life and leads to anisotropy. Inhomogeneities – lattice imperfection, voids, particles, fibers – may have a negative (stress concentration $\rightarrow$ initiation of cracks) or positive (crack arrest, dissipation) influence on fatigue life.

12.4.5 Surface quality

Material microstructure determines the growth of a fatigue crack to a high extent. At the external surface of the specimen, crystal lattices may be squeezed out by cyclic plastic deformation. The resulting extrusions (and intrusions) act as a notch, where stress concentrations will easily lead to the initiation of a fatigue crack. They show up at about $0.1\,N_f$.

The surface roughness can be set during manufacturing (or specimen preparation) and will highly influence the surface crack initiation and fatigue life. Surface treatments, like shot peening and carbonizing, can be applied to induce compressive stresses, which will prohibit crack initiation and growth. A coating can be applied to eliminate deteriorating environmental effects. Increasing the yield stress by applying alloying materials, will result in a higher resistance against lattice slip.

Besides the external surface, internal surfaces at bulk defects, are also influencing fatigue life.

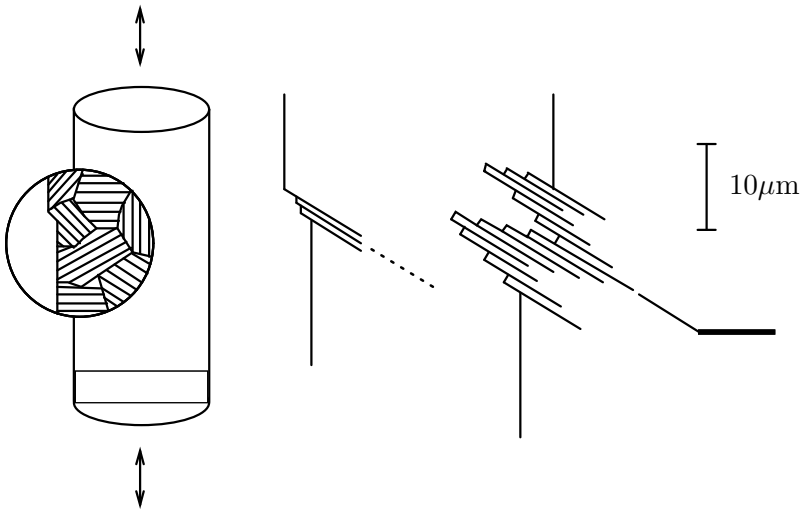

Fig. 12.14 : *In- and extrusion of lattices at the surface.*

12.4.6 Environment

Environmental influences on fatigue life are mostly due to temperature effects and chemical attack.

Low temperatures lead to embrittlement, due to the prevention of plastic deformation. High temperature ($T > 0.5T_m$) facilitates the creep deformation due to diffusion of atoms to and from grain boundaries, dislocation movement and migration of vacancies. Weakening of the grain boundaries leads to loss of inter-granular adhesion. Fatigue cracks will travel more easily between grains or cross grain boundaries. This phenomenon is referred to as *creep fatigue*.

Grain boundaries may also be weakened by chemical influence. Hydrogen and other gasses can diffuse to the grain boundaries and diminish bond strength. Protective surface films may be cracked. This process is called *corrosion fatigue*.

12.5 Crack growth

Detailed experiments have shown that the crack length a is an exponential function of the number of cycles N. This means that crack growth is very slow until the final stage in the fatigue life, where a relative short number of cycles will result in fast crack growth leading to failure. The *initial fatigue crack* length a_i seems to be a very important parameter for the fatigue life N_f.

For an initially undamaged material, it takes N_i cycles to initiate a crack by dislocation movement and void coalescence. At this *fatigue crack initiation life* the initial crack has been formed, but in most cases it is so small that it cannot be detected. In this stage I, crack growth is provoked by shear stresses and involves slip on a single crystallographic slip plane. The crack propagation rate is very low, typically < 0.25 nm/cycle.

After N_i cycles, in stage II of crack growth, crack propagation is faster, typically μm's per cycle. The crack growth is provoked by tensile stresses and involves plastic slip on multiple slip planes at the crack tip, resulting in striations. After a large number of cycles the crack reaches a length a_1, which can be detected by non-destructive techniques. The crack growth is now much faster and after the fatigue life N_f its length is a_f and after a few cycles a_c the critical crack length is reached and failure occurs. For higher loading amplitudes, the crack growth will be faster.

After N cycles, the cycles to go until failure at N_f, is indicated as N_r. The *rest-life* is the ratio of N_r and N_f.

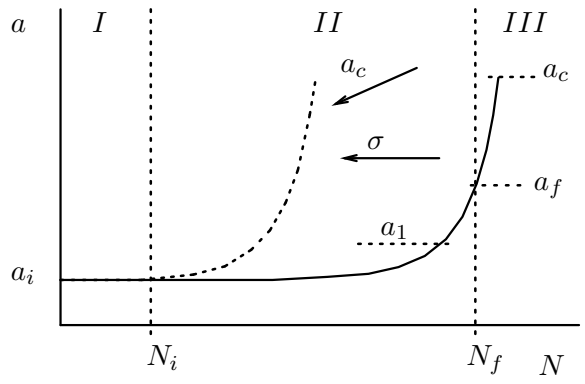

Fig. 12.15 : *Crack length increase with number of cycles.*

$$\frac{N_r}{N_f} = 1 - \frac{N}{N_f}$$

12.5.1 Crack growth models

To predict the fatigue life of structures, *crack growth models* have been proposed, which relate the crack grow rate $\frac{da}{dN}$ to load amplitude or maximum load, which can be expressed in the stress intensity factor K, because we assume to be in the high cycle fatigue regime, where stresses are low.

Microstructural models relate the crack grow rate to microstructural parameters, such as the spacing between the striations. Bates and Clark [3] found that for certain materials this spacing is about 6 times $(\Delta K/E)^2$.

Phenomenological models are formulated and fitted by close inspection of experimental crack growth data. All these relations describe $\frac{da}{dN}$ to be a function of the stress σ and the crack length a. This is generally written as a relation between $\frac{da}{dN}$ and ΔK, where scaling with E improves the generality of the fitted results. However, in LEFM, $\frac{da}{dN}$ is mostly related to ΔK by the so-called *Paris law*, using two parameters : a coefficient and an exponent,

$$\frac{da}{dN} = C(\Delta K)^m$$

12.5.2 Paris law

Paris & Erdogan published the crack grow law, which has become known as the Paris law in 1963 and it is still widely used [52]. On a double-logarithmic axes, the Paris law is represented by a straight line. The two parameters, C and m, can be fitted easily, when two data points are known, as is shown in the example below. Their values depend on material, geometry, load and loading frequency.

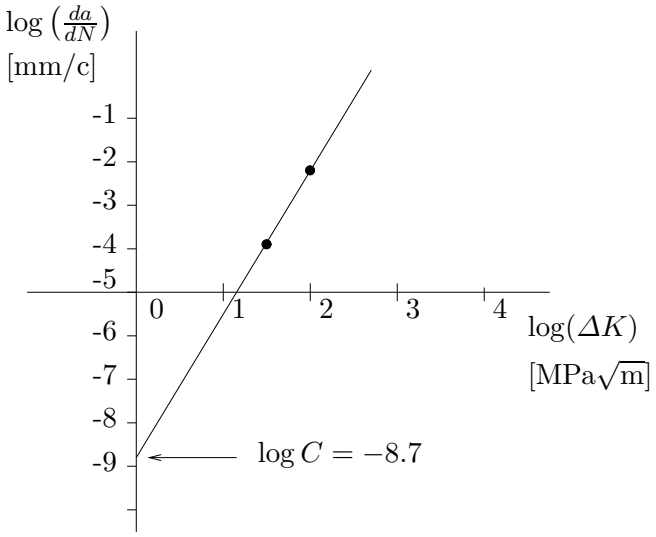

Fig. 12.16 : *Paris law parameter fit.*

$$\frac{da}{dN} = C(\Delta K)^m \quad \rightarrow \quad \log\left(\frac{da}{dN}\right) = \log(C) + m\ \log(\Delta K)$$

$$\log(\Delta K) = 0 \rightarrow\ \log(C) = \log\left(\frac{da}{dN}\right) = -8.7 \quad \rightarrow \quad C = 2 \times 10^{-9}\ \ \frac{[\text{mm}]}{[\text{MPa}\sqrt{\text{m}}]^m}$$

$$m = \frac{(-2) - (-4)}{(2) - (1.5)} = 4$$

Limits of Paris law

For low and high values of ΔK, Paris law will not describe the crack growth rate accurately any more. For $\Delta K \approx K_{th}$, the lower limit, a crack grows extremely slowly, hampered by the roughness of the crack faces. For still smaller values of ΔK, the crack growth is extremely small but not completely zero. For high values of ΔK, crack growth is much faster than predicted by the Paris law.

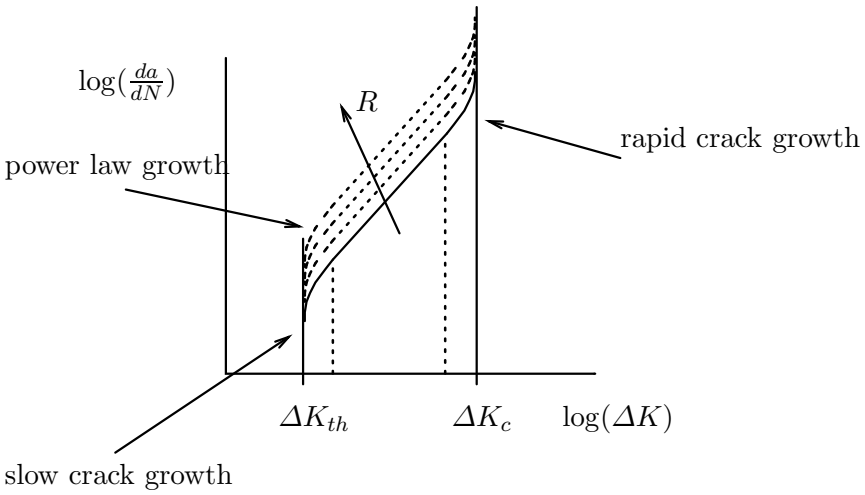

Fig. 12.17 : *Limits of Paris law.*

Paris law parameters

For some materials values of Paris law parameters are listed.

material	ΔK_{th} [MNm$^{-3/2}$]	m[-]	$C\times10^{-11}$[!]
mild steel	3.2 - 6.6	3.3	0.24
structural steel	2.0 - 5.0	3.85 - 4.2	0.07 - 0.11
idem in sea water	1.0 - 1.5	3.3	1.6
aluminium	1.0 - 2.0	2.9	4.56
aluminium alloy	1.0 - 2.0	2.6 - 3.9	3 - 19
copper	1.8 - 2.8	3.9	0.34
titanium	2.0 - 3.0	4.4	68.8

Conversion

Because the dimension of C depends on the value of m, the conversion of units must be done with care. The example shows the conversion from BS to SI units and vice versa.

$$\frac{da}{dN} = C\,(\Delta\sigma\,\sqrt{\pi a})^m \qquad \rightarrow \qquad C = \frac{\frac{da}{dN}}{(\Delta\sigma\,\sqrt{\pi a})^m}$$

[in] and [ksi] $\rightarrow$ [m] and [MPa]

$$1\;\frac{[\,\mathrm{in}\,]}{[\,\mathrm{ksi}\,\sqrt{\mathrm{in}}\,]^m} = \frac{0.0254\,[\,\mathrm{m}\,]}{\{6.86\,[\,\mathrm{MPa}\,]\,\sqrt{0.0254\,[\,\mathrm{m}\,]}\,\}^m} = \left(\frac{0.0254}{(1.09)^m}\right) \quad \frac{[\,\mathrm{m}\,]}{[\,\mathrm{MPa}\,\sqrt{\mathrm{m}}\,]^m}$$

[m] and [MPa] $\rightarrow$ [mm] and [MPa]

$$1\;\frac{[\,\mathrm{m}\,]}{[\,\mathrm{MPa}\,\sqrt{\mathrm{m}}\,]^m} = \frac{10^3\,[\,\mathrm{mm}\,]}{\{[\,\mathrm{MPa}\,]\,\sqrt{10^3}\,[\,\sqrt{\mathrm{mm}}\,]\}^m} = \left(\frac{10^3}{\{\sqrt{10^3}\}^m}\right) \quad \frac{[\,\mathrm{mm}\,]}{[\,\mathrm{MPa}\,\sqrt{\mathrm{mm}}\,]^m}$$

12.5.3 Fatigue life

Paris law can be integrated analytically, where a increases from a_i to a_f while N goes from N_i to N_f. The result $N_f - N_i$ can be represented as a function of a_f with a_i as parameter or vice versa.

Paris law can also be integrated numerically, here, using an explicit integration scheme. The initial crack length is indicated to be a_0 and the final crack length is the critical crack length a_c.

$$N_f - N_i = \frac{(\Delta\sigma)^{-m}}{\beta^m C(\sqrt{\pi})^m(1-\frac{m}{2})}\;a_f^{(1-\frac{m}{2})}\left[1-\left(\frac{a_i}{a_f}\right)^{(1-\frac{m}{2})}\right]$$

numerical procedure

set $\Delta\sigma$, ΔN, a_c
initialize $N = 0$, $a = a_0$
while $a < a_c$
$\Delta K = \beta\,\Delta\sigma\sqrt{\pi * a}$
$\frac{da}{dN} = C * (\Delta K)^m \quad \rightarrow \quad \Delta a = \frac{da}{dN} * \Delta N$
$a = a + \Delta a$
$N = N + \Delta N$
end

Initial crack length

It is now very easy to show that the initial crack length a_0 is of utmost importance for the fatigue life. Results are shown for aluminum and for mild steel for a stress amplitude $\Delta\sigma = 50$ MPa.

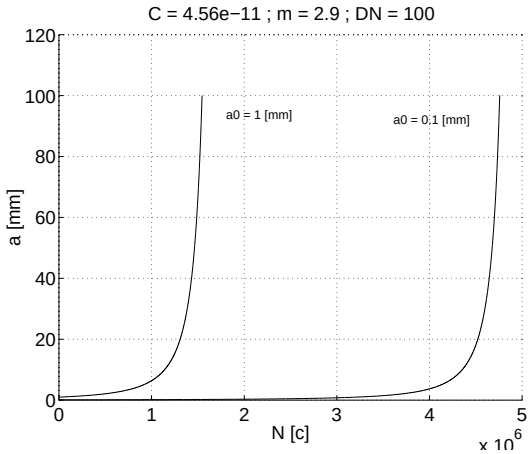

aluminum ; $\Delta\sigma = 50$ [MPa]

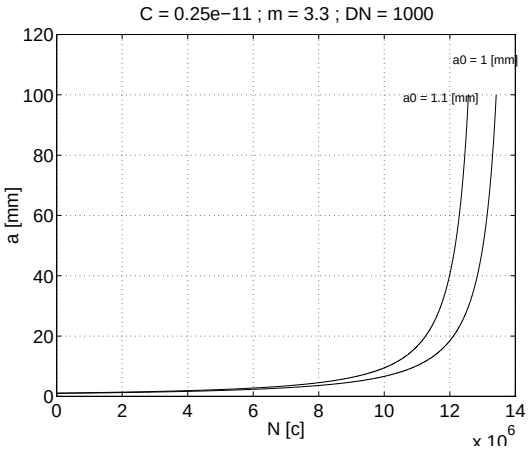

mild steel ; $\Delta\sigma = 50$ [MPa]

Fig. 12.18 : *Fatigue crack length in aluminum and mild steel for two values of the initial crack length.*

Fatigue load

The fatigue life is reached, when the crack length becomes critical ($a = a_c = \frac{2\gamma}{\pi}\frac{E}{\Delta\sigma^2}$). For aluminum, the number of cycles to reach this length has been calculated for various stress amplitudes.

$\Delta\sigma$ [MPa]	25	50	75	100
a_0 [mm]	0.1	0.1	0.1	0.1
a_c [mm]	56	28	12.5	7
N_f [c]	35070000	4610000	1366000	572000

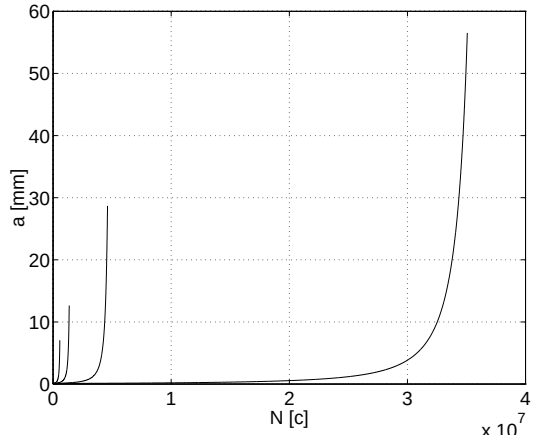

Fig. 12.19 : *Fatigue crack length in aluminum for various load amplitudes.*

12.5.4 Other crack grow laws

Numerous special and extended versions of the basic Paris law have been published.

Erdogan (1963)

$$\frac{da}{dN} = \frac{C(1+\beta)^m(\Delta K - \Delta K_{th})^n}{K_{I_c} - (1+\beta)\Delta K} \qquad \text{with} \quad \beta = \frac{K_{max} + K_{min}}{K_{max} - K_{min}}$$

Broek & Schijve (1963)

$$\frac{da}{dN} = C K_{max}^2 \, \Delta K$$

Forman (1967)

$$\frac{da}{dN} = \frac{C(\Delta K)^n}{(1-R)K_c - \Delta K} \qquad \text{with} \quad R = \frac{K_{min}}{K_{max}}$$

Donahue (1972)

$$\frac{da}{dN} = C(\Delta K - \Delta K_{th})^m \qquad \text{with} \quad \Delta K_{th} = (1-R)^\gamma \Delta K_{th}(R=0)$$

Walker (1970)

$$\frac{da}{dN} = C\left\{\frac{\Delta K}{(1-R)^n}\right\}^m \qquad \text{with} \quad m = 0.4 \quad ; \quad n = 0.5$$

Priddle (1976)

$$\frac{da}{dN} = C\left(\frac{\Delta K - \Delta K_{th}}{K_{I_c} - K_{max}}\right)^m$$

with $\Delta K_{th} = A(1-R)^\gamma$ and $\frac{1}{2} \le \gamma \le 1$ [Schijve (1979)]

McEvily & Gröger (1977)

$$\frac{da}{dN} = \frac{A}{E\sigma_v}(\Delta K - \Delta K_{th})^2 \left(1 + \frac{\Delta K}{K_{I_c} - K_{max}}\right)$$

with $\Delta K_{th} = \sqrt{\frac{1-R}{1+R}}\Delta K_0$

$A, \Delta K_0 \quad \sim$ influence environment

NASA / FLAGRO program (1989)

$$\frac{da}{dN} = \frac{C(1-R)^m \Delta K^n (\Delta K - \Delta K_{th})^p}{[(1-R)K_{Ic} - \Delta K]^q}$$

$m = p = q = 0 \quad \rightarrow \quad$ Paris

$m = p = 0, q = 1 \quad \rightarrow \quad$ Forman

$p = q = 0, m = (m_w - 1)n \quad \rightarrow \quad$ Walker

12.5.5 Crack growth at low cycle fatigue

Paris law and its extended version are valid for the high cycle fatigue regime, where stresses are so low that ΔK characterizes the stress amplitude. For low cycle fatigue this is not the case any more. Crack grow laws for this high stress regime with large plastic crack tip regions, are still under development.

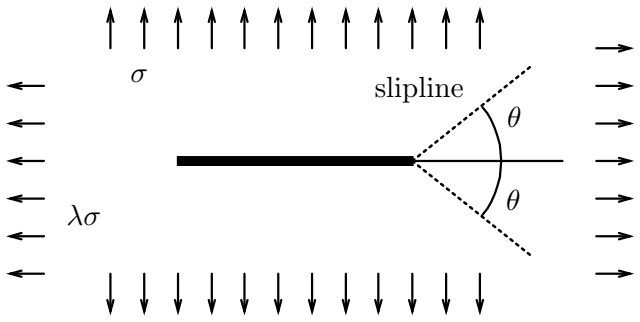

Fig. 12.20 : *Crack under multi-mode fatigue loading.*

$$\frac{da}{dN} = \frac{3 - \sin^{-2}(\theta)\cos^{-2}(\frac{\theta}{2})}{9\sin(\theta)} \frac{K}{E\sigma_v} \left(1 - \beta\gamma^{-\frac{1}{2}}\right) \frac{K_{max}^2}{\{1-(1-\lambda)\frac{\sigma_{max}}{\sigma_v}\}}$$

$$\left.\begin{array}{l} \theta = \cos^{-1}\left(\frac{1}{3}\right) \\ \frac{\beta}{\sqrt{\gamma}} = 0.5 + 0.1R + 0.4R^2 \end{array}\right\} \quad \rightarrow$$

$$\frac{da}{dN} = \frac{7}{64\sqrt{2}} \frac{K}{E\sigma_v} (1 - 0.2R - 0.8R^2) \frac{K_{max}^2}{\{1-(1-\lambda)\frac{\sigma_{max}}{\sigma_v}\}}$$

For high values of crack tip stress and consequently a large plastic zone, the Paris law may be used with ΔJ instead of ΔK. Note that $\Delta J \neq J_{max} - J_{min}$ over a cycle.

$$\frac{da}{dN} = C^* \left(\Delta J\right)^{m^*}$$

$$\text{with} \qquad \Delta J = \int_\Gamma \left\{ W^* n_1 - \Delta t_i \frac{\partial \Delta u_i}{\partial x_1} \right\} d\Gamma \quad ; \qquad W^* = \int_{\varepsilon_{pq_{min}}}^{\varepsilon_{pq_{max}}} \Delta\sigma_{ij}\, d\varepsilon_{ij}$$

12.6 Load spectrum

Until now, we only looked at harmonic loads with constant frequency and amplitude. In practical situations, such loads will almost never be seen. Both loading frequency and amplitude will generally vary over time. Cyclic loading with such a time dependent character is referred to as a load spectrum. It is assumed here that the direction of the load remains the same.

A load spectrum is shown in the figure below. It consists of four ($i = 1..4$) harmonic loads with different frequencies and amplitudes. In the subsequent loads the number of cycles is n_i. For each individual harmonic load the life time N_{if} is known.

Miner has found in 1945 that the fatigue life for the whole spectrum is independent on the actual sequence of the individual loadings [48]. This means that the individual harmonic loadings do not influence the damage growth in the following loading stage with a different character. The final life time is reached, when the summation of $\frac{n_i}{N_{if}}$ becomes one. This so-called *Miner's rule* is approximately valid for a wide range of materials. In reality the ultimate sum of all the ratios is between 0.6 and 2.0, which indicates that there is actual some interaction between the different load cycles.

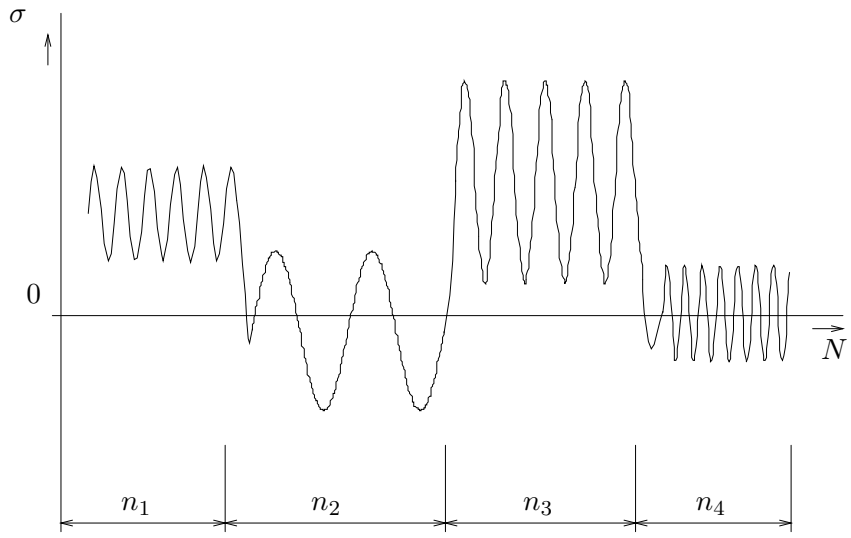

Fig. 12.21 : *Sequence of various harmonic loadings.*

$$\sum_{i=1}^{L} \frac{n_i}{N_{if}} = 1$$

Miner's rule is clearly illustrated by regarding the rest life after each load cycle. When it reaches zero, the summation of the ratio $\frac{n_i}{N_{if}}$ must reach the value one.

$$\begin{aligned}
1 \quad &\rightarrow \quad 1 - \frac{n_1}{N_{1f}} \\
2 \quad &\rightarrow \quad \left(1 - \frac{n_1}{N_{1f}}\right) - \frac{n_2}{N_{2f}} \\
3 \quad &\rightarrow \quad \left(1 - \frac{n_1}{N_{1f}} - \frac{n_2}{N_{2f}}\right) - \frac{n_3}{N_{3f}} \\
4 \quad &\rightarrow \quad \left(1 - \frac{n_1}{N_{1f}} - \frac{n_2}{N_{2f}} - \frac{n_3}{N_{3f}}\right) - \frac{n_4}{N_{4f}} = 0
\end{aligned}$$

12.6.1 Random load

Although the load spectrum is already much more realistic than the harmonic loading with constant frequency and amplitude, practical loading is mostly rather random, as is illustrated in the figure below.

Prediction of fatigue life is only possible after this random load is transferred into a load spectrum, a sequence of harmonic loads, with known frequencies and amplitudes. Various *counting procedures* can be used for this transformation. Literature gives detailed information about *(mean crossing) peak count*, *range pair (mean) count* and *rain flow count* techniques.

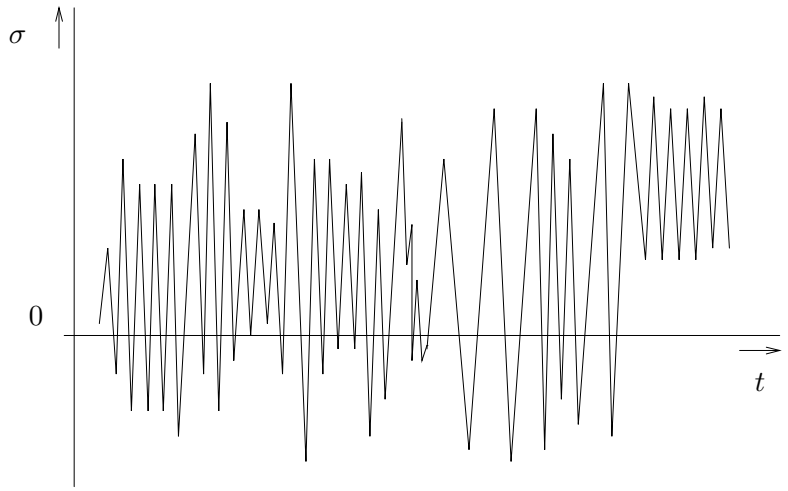

Fig. 12.22 : *Random load.*

Measured load histories

For some applications, random load sequences are measured and used in design. During service life the load can be monitored and the expected fatigue life time can be updated. Typical loadings for a manufacturing machine (a), a sea vessel (b) and an airplane (c) are shown in the figure.

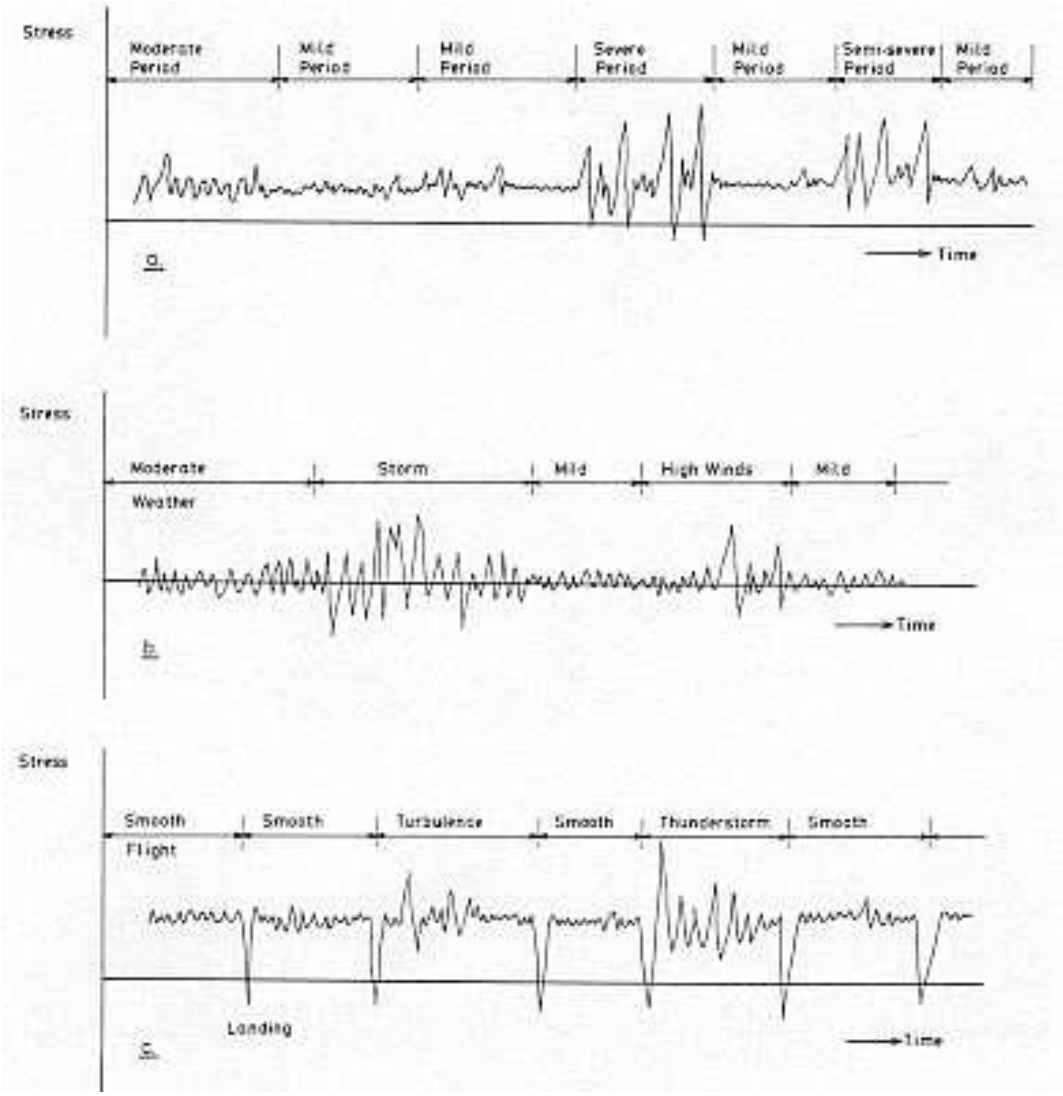

Fig. 12.23 : *Random loads for machine (a), sea vessel (b) and airplane (c).*

12.6.2 Tensile overload

Known random loadings are used to calculate the fatigue life during the design of structures. During service life extreme overloads can occur, which must of course be low enough to cause no direct damage. The question is how they affect the fatigue life.

Although the intuitive feeling is that overload must be bad, practical experience shows that the crack propagation is slowed down by such an overload, at least during a limited number of cycles. This is illustrated in the next figure, where $(K_{max})_{OL}$ is the maximum SIF during the overload.

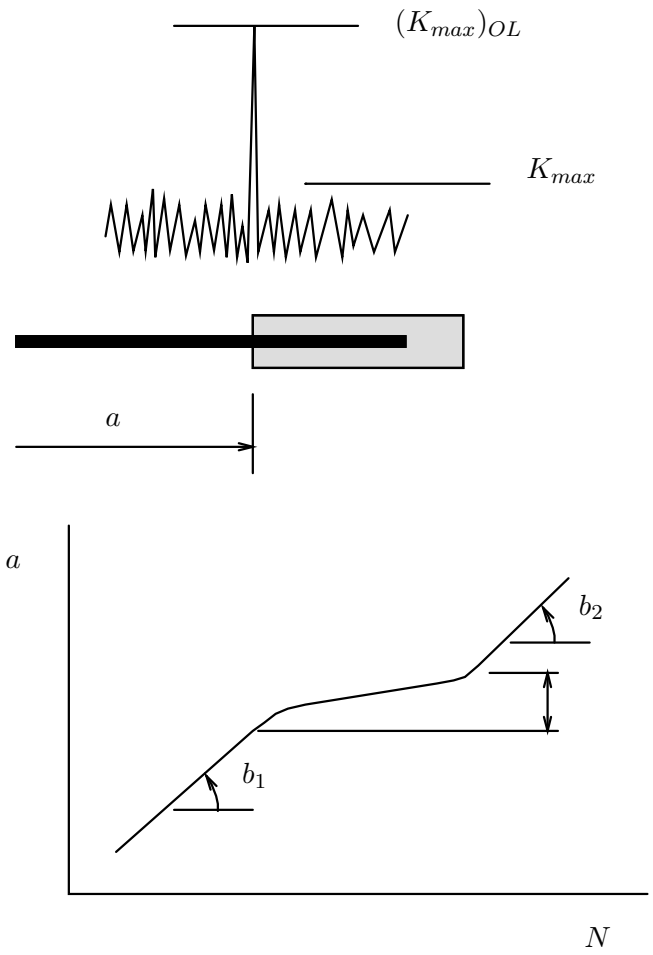

Fig. 12.24 : *Overload and crack retardation.*

The crack retardation is also illustrated quantitatively by the values in the next table (from [29]), which apply to the Mode I loading of specimen made of Al 2024-T3 alloy.

ΔK [MPa$\sqrt{\text{m}}$]	% P_{max} [-]	nr. P_{max} [-]	delay [10^3 cycles]
15	53	1	6
15	82	1	16
15	109	1	59
16.5	50	1	4
16.5	50	10	5
16.5	50	100	9.9
16.5	50	450	10.5
16.5	50	2000	22
16.5	50	9000	44
23.1	50	1	9
23.1	75	1	55
23.1	100	1	245

The crack retardation can be explained by regarding the stress state in a region in front of the crack tip. The figure shows the stress σ_{yy} and the plastic limit stress. In a certain time period, the loading stress is increased to a maximum value σ_1, representing the overload, and decreased again. In two points A and B the stress σ_{yy} is plotted in the figure as a function of the strain ε_{yy}. In point A, the material is plastically deformed, while the deformation in point B remains elastic. After unloading, the strain in A and B is more or less the same, so that it becomes clear from the stress-strain curves that a compressive residual stress remains in point A. This compressive stress inhibits the opening of the crack and thus the crack elongation. When the crack tip has moved through the compressive zone, the normal crack grow rate is again established.

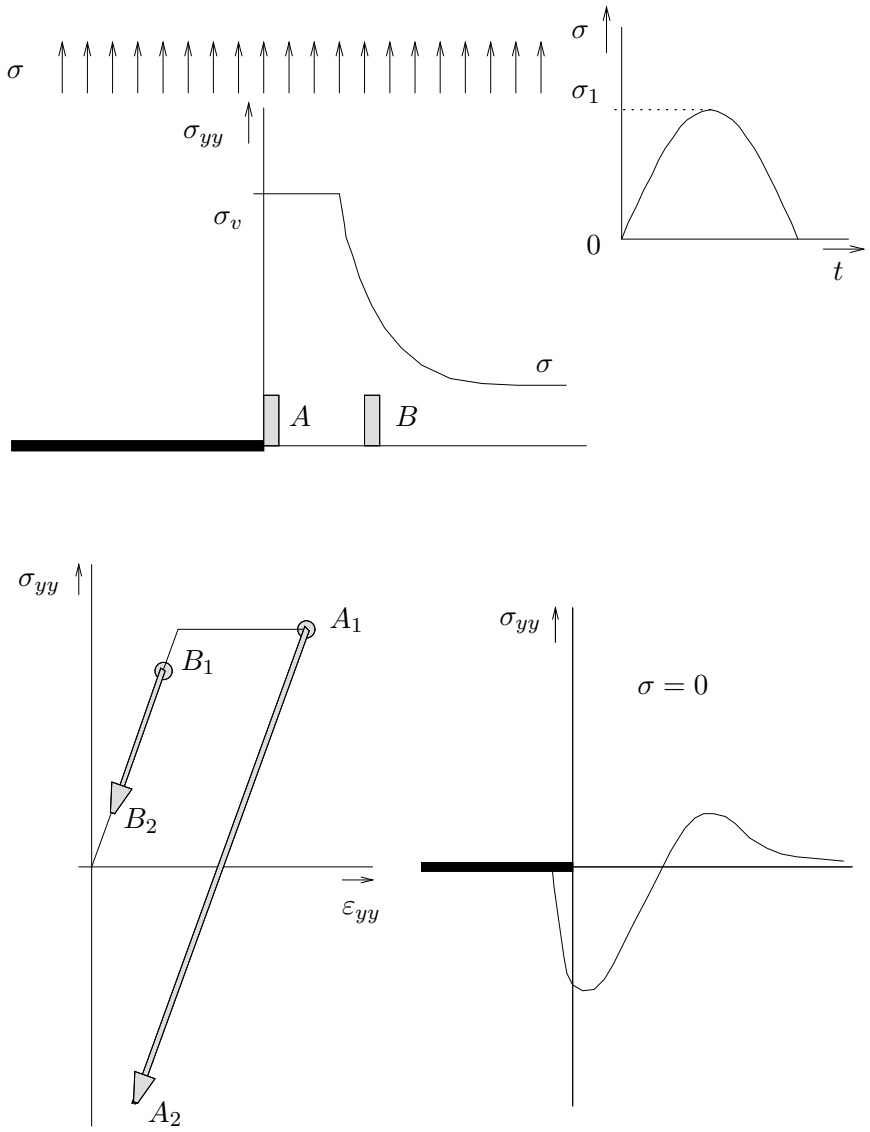

Fig. 12.25 : *Residual stress at the crack tip resulting from overload.*

Crack retardation models

Willenborg (1971) has published a relation for the SIF, K_R, in the crack retardation stage. It has been enhanced by Johnsson [37]. Both relations are taking into account the influence of the compressive stress zone at the front of the crack tip.

Willenborg (1971)

$$K_R = \phi \left[(K_{max})_{OL} \left[\sqrt{1 - \frac{\Delta a}{r_y}} \right] - K_{max} \right] \quad ; \quad \Delta a < r_y$$

$K_R =$ residual SIF ; $K_R = 0 \rightarrow$ delay distance

$\phi = [1 - (K_{th}/K_{max})](S-1)^{-1}$; $S =$ shut-off ratio

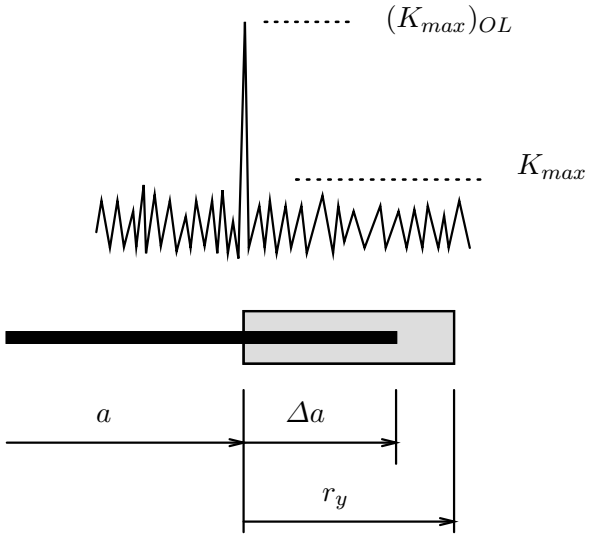

Johnson (1981)

$$R^{eff} = \frac{K_{min} - K_R}{K_{max} - K_R} \quad ; \quad r_y = \frac{1}{\beta\pi} \left(\frac{(K_{max})_{OL}}{\sigma_v} \right)^2$$

$\beta =$ plastic constraint factor

Crack retardation due to crack closure, caused by the compressive stress zone behind the crack tip, have also been devised and published.

Elber (1971) [17] $\Delta K_{eff} = U\,\Delta K \quad ; \quad U = 0.5 + 0.4R \quad$ with $\quad -0.1 \leq R \leq 0.7$

Schijve (1981) [59] $U = 0.55 + 0.33R + 0.12R^2 \quad$ with $\quad -1.0 < R < 0.54$

12.7 Design against fatigue

There are three different strategies which can be followed to prevent that fatigue damage leads to failure, so-called *design against fatigue*.

Infinite life design

For infinite life design, the stress amplitude in the most severely loaded parts of the structure are kept below the fatigue limit. The result is that fatigue crack growth will be practically zero. This strategy will involve the use of much material and thus lead to bulky and heavy structures.

Safe life design

Using the concept of *safe life*, the (S-N)-curve is used to predict when the fatigue life is reached. For this purpose, the loading must be known and the number of cycles must be logged.

When the load is random, statistical counting procedures must be employed to translate the random load spectrum to a sequence of harmonic loads.
Instead of the (S-N)-curve, the fitted Basquin or Manson-Coffin relations can be used. They can be combined in a stress/strain life curve.

When the number of cycles to failure – probable a much lower safe number – is reached, the structur(e)(al) (part) is replaced.

Damage tolerant design

Crack growth can be predicted, using a crack growth relation like Paris law. Periodic inspection is of course needed to check whether predicted crack lengths are correct. The rest life can be calculated, including effects like overloads. When the critical crack length – probable a much smaller value – is reached, the structur(e)(al) (part) is replaced.

Fail safe design

Although safety factors will certainly be used to be within safe margins of the fatigue life, The design must be such that (undetected) fatigue cracks will not lead to global failure.

Chapter 13

Engineering plastics (polymers)

Polymer materials are widely used in functional and structural applications. External loads and other influences lead of course to damage, cracking and failure. Systematic study of these phenomena has brought insight in their behavior and, even more than in the case of metal alloys, has given rise to the development of new materials with better damage resistance.

There are a huge number of different polymer materials, some of which are listed in the table.

ABS	acrylonitrilbutadieenstyreen	EM
HIPS	high-impact polystyrene	TP
LDPE	low-density polythene	TP
Nylon		
PC	polycarbonate	TP
PMMA	polymethylemethacrylate (plexiglas)	TP
PP	polypropylene	TP
PPO	polyfenyleneoxide	TP
PS	polystyrene	TP
PSF	polysulfone	TP
PTFE	polytetrafluorethene (teflon)	TP
PVC	polyvinylchloride	TP
PVF	polyvinylfluoride	TP
PVF2	polyvinylidieenfluoride	TP

13.1 Mechanical properties

For many applications, metal alloys show linear elastic behavior, in which case Linear Elastic Fracture Mechanics can be used to study cracks. Polymers mostly have a lower stiffness and the linear elasticity limit is reached sooner. Polymer materials generally show strain-rate and time-dependent behavior. Temperature effects cannot be neglected in many cases. In fracture analysis of polymers it is therefore often needed to use concepts from Non-Linear Fracture Mechanics. Composite materials are anisotropic, which, even in the linear elastic case, complicates the mechanical behavior.

13.1.1 Damage

Damage in polymers may occur as shear bands or crazes. These can occur both in the same material in regions with different stress states.

Shear bands are associated to shear yielding. In this case no change in density is observed. Crazes are connected to normal yielding. The local density may decrease with 40 - 60 %. In a craze, fibrils are connecting the two craze surfaces. When the craze opens, the fibrils are elongated due to extrusion of macromolecules from the bulk polymer. When the maximum elongation is reached, the fibril snaps.

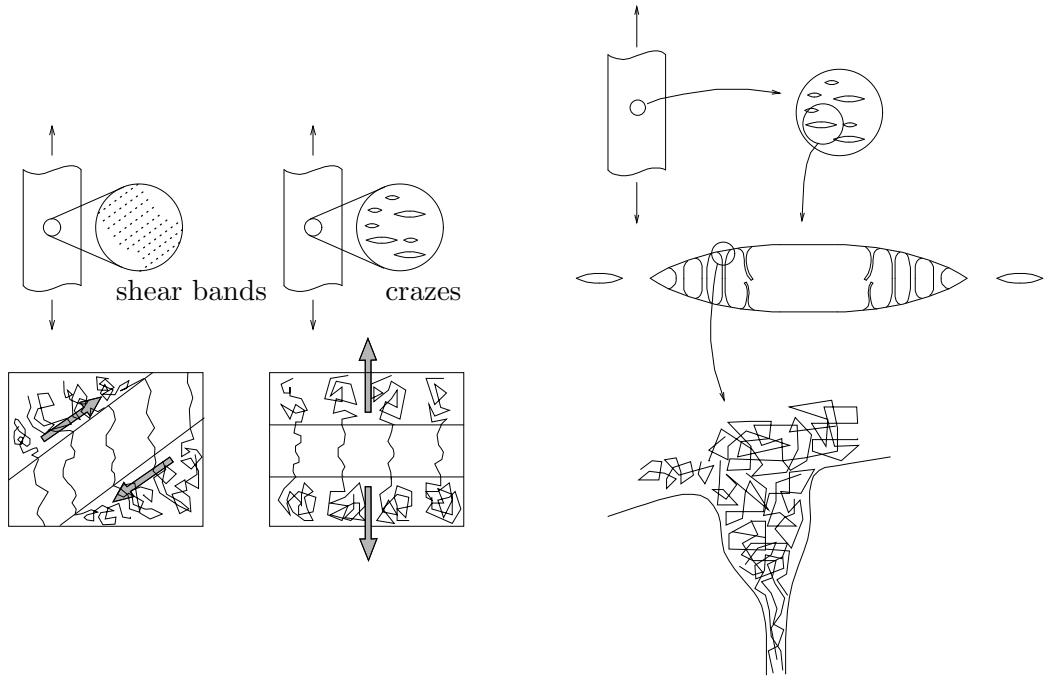

Fig. 13.1 : *Shear bands and crazes in a polymer.*

13.1.2 Properties of engineering plastics

The next table shows some properties of engineering plastics, which are related to their damage behavior. The crystallinity is a very important item, because crystals can stop cracks in an early stage. The occurrence of crazes is also relevant, because crazing is generally associated to brittle behavior.

	AC	CZ	K_{Ic}	
PMMA	a	+	13.2	
PS	a	+	17.6	
PSF	a	-	low	
PC	a	-	high	main chain segmental motions → energy dissipation
Nylon 66	cr	-		main chain segmental motions → energy dissipation
				crystalline regions → crack retardation
PVF2	sc			
PET	sc			amorphous → strain induced crystallization at crack tip
CPLS		-		cross-linked → suppressed crazing
HIPS		+		μ-sized rubber spheres → enhanced crazing
ABS				blending

AC : a = amorphous
AC : c = crystalline
AC : sc = semicrystalline
AC : cr = crystalline regions
CZ = crazing
K_{Ic} = fracture toughness in MPa$\sqrt{\text{m}}$

13.2 Fatigue

Fatigue crack propagation in polymers is strongly affected by properties like molecular weight, cross linking, main chain mobility and crystallinity. Blending one polymer with another polymer or particles to improve ductility and fatigue life is referred to as *toughening*. Data for the next figures are taken from [29].

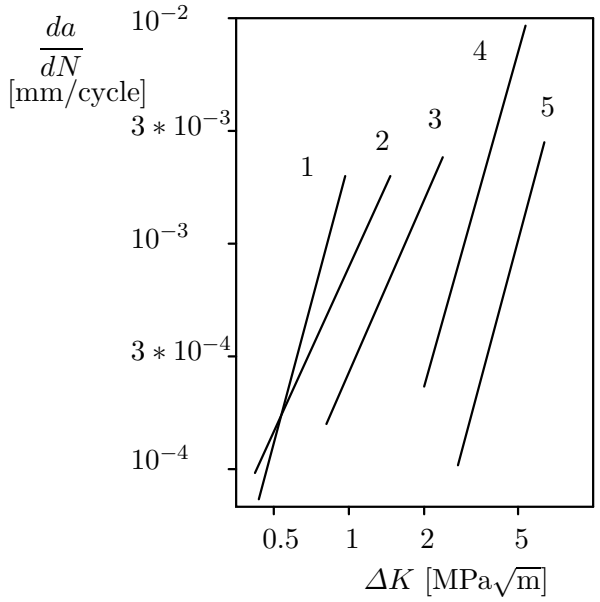

1 : PMMA 5 Hz crazing
2 : LDPE 1 Hz
3 : ABS 10 Hz
4 : PC 10 Hz no crazing
5 : Nylon 10 Hz crystalline regions

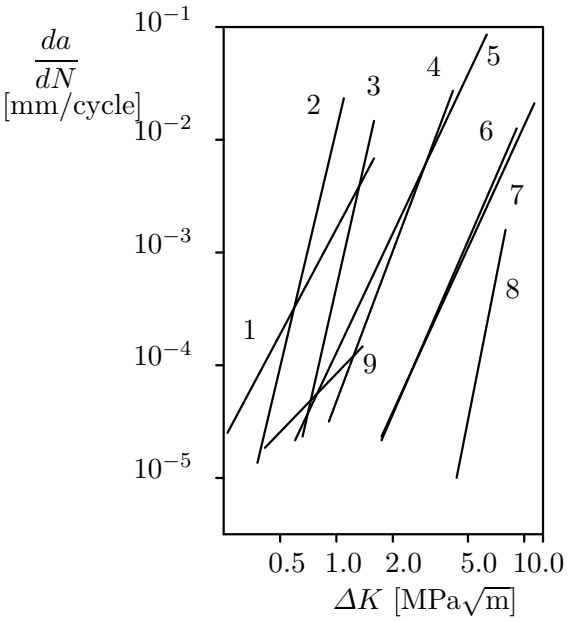

1 : PS
2 : PMMA
3 : PSF
4 : PPO
5 : PC
6 : Nylon 6.6
7 : PVF2
8 : PET
9 : PVC

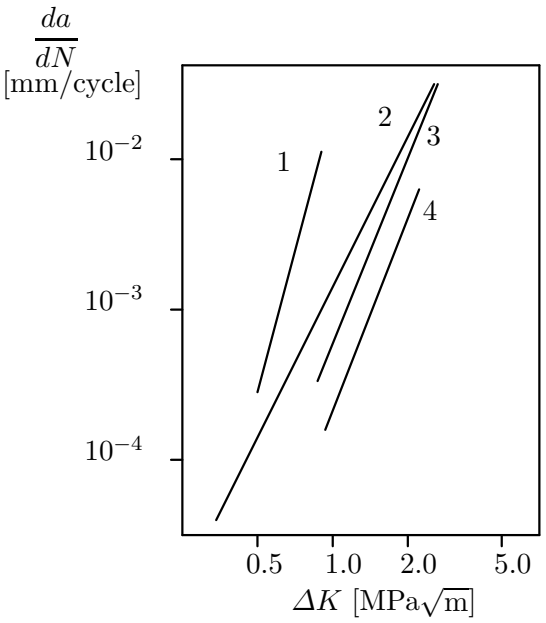

1 : CLPS
2 : PS
3 : HIPS
4 : ABS

Bibliography

[1] Barenblatt, G.I. *The mathematical theory of equilibrium cracks in brittle fracture*. Advances in Applied Mechanics, Vol 7, 1962, pp 55-129.

[2] Barsoum, R.S. *On the use of isoparametric Finite Elements in Linear Fracture Mechanics*. Int. J. Numerical Methods in Engineering, Vol 10, 1976.

[3] Bates, R.C.; Clark, W.G. *Fractography and fracture mechanics*. Trans. ATM, Vol 62, 1969, pp 380-388.

[4] Bijker, S.*Study of the opening behavior of food containers with Easy Peel-Off Lid*. MSc Thesis, MT 08.11, Eindhoven University of Technology, 2008.

[5] Bosch van den, M.J.; Schreurs, P.J.G.; Geers, M.G.D.*An improved description of the exponential Xu and Needleman cohesive zone law for mixed-mode decohesion*. Engineering Fracture Mechanics, Vol 73, 2006, pp 1220-1234.

[6] Bosch van den, M.J.; Schreurs, P.J.G.; Geers, M.G.D.*A cohesive zone model with a large displacement formulation accounting for interfacial fibrillation*. Eur.J.Mech., Vol 26, 2007, pp 1-19.

[7] Bosch van den, M.J.; Schreurs, P.J.G.; Geers, M.G.D.*On the development of a 3D cohesive zone element in the presence of large deformations*. Comp.Mech., Vol 42, 2008, pp 171-180.

[8] Bosch van den, M.J.*Interfacial delamination in polymer coated metal sheet*. PhD Thesis, Eindhoven University of Technology, 2007.

[9] Bosch van den, M.J.; Schreurs, P.J.G.; Geers, M.G.D.; Van Maris, M.P.H.F.L.*Interfacial characterization of pre-strained polymer coated steel by a numerical-experimental approach*. Mech.Mat., Vol 40, 2008, pp 302-314.

[10] Broek, D. *Elementary engineering fracture mechanics; 4thed.*. Martinus Nijhoff Publishers, 1986.

[11] Broek, D. *The practical use of Fracture Mechanics*. Kluwer Academic Publishers, 1989.

[12] Camacho, G.T.; Ortiz, M. *Computational modelling of impact damage in brittle materials*. Int. J. of Solids and Structures, Vol 33, 1996, pp 2899-2938.

[13] Carlson, R.L.; Kardomateas G.A. *An Introduction to Fatigue in Metals and Composites*. Chapman and Hall, 1996.

[14] Donahue, R.J.; Clark H.M.; Atanmo P.; Kumble R.; McEvily A.J. *Crack opening displacement and the rate of fatigue crack growth.* Int. J. of Fracture Mechanics, Vol 8, 1972, pp 209-219.

[15] Dugdale, D.S. *Yielding of steel sheets containing slit.* J. of the Mechanics and Physics of Solids, Vol 8, 1960, pp 100-108.

[16] Elber, W. *Fatigue crack closure under cyclic tension.* Engineering Fracture Mechanics, Vol 2, 1970, pp 37-45.

[17] Elber, W. *The significance of fatigue crack closure.* Damage Tolerance in Aircraft Structures, ASTM STP 486, 1971, pp 230-242.

[18] Erdogan, F,; Sih, G.C. *On the crack extension in plates under plane loading and transverse shear.* J. Basic Eng., Vol 85, 1963, pp. 519-527.

[19] Erdogan, F.; Ratwani M. *Fatigue and fracture of cylindrical shells containing a circumferential crack.* Int. J. of Fracture Mechanics, Vol 6, 1970, pp 379-392.

[20] Erinç, M.E.; Schreurs, P.J.G.; Zhang, G.Q.; Geers, M.G.D.*Microstructural damage analysis of SnAgCu solder joints and an assessment on indentation procedures.* J.Mat.Sc.:Mat.Electr., Vol 16, 2005, pp 693-700.

[21] Erinç, M.; Schreurs, P.J.G.; Zhang, G.Q.; Geers, M.G.D.*Characterization and fatigue damage simulation in SAC solder joints.* Microelectronics Reliability, Vol 44, 2004, pp 1287-1292.

[22] Erinç, M.E.; Schreurs, P.J.G.; Geers, M.G.D.*Integrated numerical-experimental analysis of interfacial fatigue fracture in SnAgCu solder joints.* Int.J. Solids and Structures, Vol 44, 2007, pp 5680-5694.

[23] Erinç, M.E.*Thermo-mechanical fatigue failure of interfaces in lead-free solders.* PhD Thesis, Eindhoven University of Technology, 2007.

[24] Forman, R.G.; Kearney V.E.; Engle R.M. *Numerical analysis of crack propagation in cyclic-loaded structures.* J. of Basic Engineering; Trans. ASME, Vol 89, 1967, pp 459-464.

[25] Gdoutos, E.E. *Fracture Mechanics ; an introduction.* Kluwer Academic Publishers, 1993.

[26] Gordon, J.E. *The new science of strong materials.* Penguin Books, 1976.

[27] Gordon, J.E. *Structures.* Penguin Books, 1978.

[28] Griffith, A.A. Phil. Trans. Roy. Soc., Vol 221, 1921, pp 163.

[29] Hertzberg, Richard W. *Deformation and fracture mechanics of engineering materials.* John Wiley and Sons, 1976.

[30] Hertzberg, Richard W. *Deformation and fracture mechanics of engineering materials; 4th ed..* John Wiley and Sons, Chichester, 1996.

[31] Hutchinson, J.W. *Singular behavior at the end of a tensile crack in a hardening material.* J. of the Mechanics and Physics of Solids, Vol 16, 1968, pp 13-31.

[32] Inglis, C.E. *Stresses in a plate due to the presence of cracks and sharp corners.* Transactions of the Institute of Naval Architects, Vol 55, 1913, pp 219-241.

[33] Irwin, G.R.; Kies, J.A. Welding J. Res. Suppl., Vol 33, 1954, pp 1935.

[34] Irwin, G.R.; Kies, J.A.; Smith, H.L. *Fracture strength relative to onset and arrest of crack propagation.* Proceedings of the American Society for Testing Materials, Vol 58, 1958, pp 640-657.

[35] Irwin, G.R.; *Handbook of physics.* Vol 6, 1958, pp 551-590.

[36] Irwin, G.R. *Plastic zone near a crack and fracture toughness.* Proc. 7th Sagamore Conf., 1960, pp IV-63.

[37] Johnson, Gordon R.; Cook, William H. *Fracture characteristics of three metals subjected to various strains, strain rates, temperatures and pressures.* Engineering Fracture Mechanics, Vol 21, 1985, pp 31-48.

[38] Kanchanomai, C.; et al. *Low cycle fatigue test for solders using non-contact digital image measurement system.* Int.J. of fatigue, Vol 24, 2002, pp 57-67.

[39] Kanninen, M.F.; Popelar, C.H. *Advanced fracture mechanics.* Oxford University TTss, New York, 1985.

[40] Klingbeil, N.W. *A total dissipated energy theory of fatigue crack growth in ductile solids.*, 2003.

[41] Knott, J.F. *Fundamentals of fracture mechanics.* Butterworths, 1973.

[42] Kurz, Wolfgang *Debonding along a fiber/matrix interface in a composite.* WFW 93.109, 1993(jul), pp 34.

[43] Leevers, J.C. *Inherent stress biaxiality in various fracture specimen geometries.* Int. Journ. of Fracture, Vol 19, 1983, pp 311-325.

[44] Lim, I.L.; Johnston, I.W.; Choi, S.K. *Application of singular quadratic distorted isoparametric elements in linear fracture mechanics.* Int. J. for Numerical Methods in Engineering, Vol 36, 1993, pp 2473-2499.

[45] Matous, K.; Geubelle, P. *Multiscale modeling of particle debonding in reinforced elastomers subjected to finite deformations.* International Journal for Numerical Methods in Engineering, Vol 65, 2006, pp 190-223.

[46] McMaster (Ed.). *Nondestructive Testing Handbook....*

[47] Mediavilla, J. *Continuous and discontinuous modelling of ductile fracture.* PhD Thesis TU/e, 2005.

[48] Miner, M.A. *Cumulative damage in fatigue.* Journal of Applied Mechanics, Vol 12, 1945, pp A159-A164.

[49] Murakami, Y. *Stress intensity factors handbook, Vol.1 and Vol.2.* Pergamon, N.Y., 1987.

[50] Murakami, Y. *Stress intensity factors handbook, Vol.3.* Pergamon, N.Y., 1992.

[51] Neuber, H. *Theory of stress concentrations for shear-strained prismatical bodies with arbitrary non-linear stress-strain law.* J. Appl. Mech. ASME Trans., Vol 28, 1961, pp 544-550.

[52] Paris, P.; Erdogan, F. *A critical analysis of crack propagation laws.* J. of Basic Engineering; Trans. ASME, Vol 85, 1963, pp 528-534.

[53] Peterson, R.E. *Stress concentration design factors.* John Wiley, 1953.

[54] Peterson, R.E. *Stress concentration factors.* Wiley, New York, 1974.

[55] Rice, J.R. *A path independent integral and the approximate analysis of strain concentrations by notches and cracks.* J. of Applied Mechanics, Vol 35, 1968, pp 379-386.

[56] Rice, J.R.; Rosengren, G.F. *Plane strain deformation near a crack tip in a power-law hardening material.* J. of the Mechanics and Physics of Solids, Vol 16, 1968, pp 1-12.

[57] Roberts, D.K.; Wells, A.A. *The velocity of brittle fracture.* Engineering, Vol 171, 1954, pp 820-821.

[58] Rooke, D.P.; Cartwright, D.J. *Compendium of stress intensity factors.* Her Majesty's Stationary Office, London, 1976.

[59] Schijve, J. *Some formulas for the crack opening stress level.* Engineering Fracture Mechanics, Vol 14, 1981, pp 461-465.

[60] Sih, G.C.; Chen, E.P. *Fracture analysis of unidirectional composites.* J. of composite materials, Vol 7, 1973, pp 230-244.

[61] Sih, G.C. *Handbook of stress intensity factors.* Lehig University, Bethlehem, Pennsylvania 18055, 1973.

[62] Sih, G.C. *Strain energy density factor applied to mixed mode crack problems.* Int. J. of Fracture, Vol 10, 1974, pp 305-322.

[63] Tada, H.; Paris, P.C.; Irwin, G.R. *The stress analysis of cracks handbook.* Del Research, 1973.

[64] Tada, H.; Paris, P.C.; Irwin, G.R. *The stress analysis of cracks handbook; 2nd Ed.* Paris Productions, Inc., St. Louis, 1985.

[65] Tvergaard, V. *Effect of fibre debonding in a whisker-reinforced metal.* Materials Science and Engineering A, Vol 125, 1990, pp 203-213.

[66] Tvergaard, V.; Hutchinson, J.W. *The relation between crack growth resistance and fracture process parameters in elastic-plastic solids.* J. Mech. Phys. Solids, Vol 40, 1992, pp 1377-1397.

[67] Vinals, J. *High performance fracture approach to fatigue crack analysis and life prediction.* In: WCCM-5, 2002, 2002.

[68] Wasiluk, B.; Hoshide, T. *The fracture process in elastic-plastic materials under biaxial cyclic loading.*, 2003.

[69] Wells, A.A. *Application of fracture mechanics at and beyond general yielding.* British Welding Research Ass. Rep., MI3, 1963.

[70] Xu, X.P.; Needleman, A. *Void nucleation by inclusions debonding in a crystal matrix.* Model Simul Mater Sci Engng, VOL 1, 1993, pp 111-132.

[71] Yoffe, E.H. *The moving Griffith crack.* Philosophical Magazine, Vol 42, 1951, pp 739-750.

External sources of figures and other data

			Source
fig	1.7	:	Copied from Internet
fig	1.8	:	Copied from Internet (MaTe website)
fig	1.10	:	Copied from Kanninen [39]
fig	1.12	:	Unknown source
fig	2.1	:	Copied from Hertzberg [30]
fig	2.3	:	Copied from Hertzberg [30]
fig	2.4	:	Copied from Internet : Google Books : Derek Hull "Fractography: observing, measuring, and interpreting fracture surface topography"
fig	3.1	:	Copied from Internet : www.venti-oelde.de (2009)
fig	3.2	:	Copied from Internet : Univ. of Strathclyde (2006)
fig	8.3	:	Copied from Kanninen [39]
fig	9.5	:	Copied from Hertzberg [30], Gdoutos [25], Kanninen [39]
fig	11.16	:	Copied from Kurz [42]
fig	11.17	:	Copied from Mediavilla [47]
fig	12.1	:	Copied from Hertzberg [30]
fig	12.5	;	Unknown source
fig	12.7	;	Unknown source
fig	12.23	:	Unknown source
chp	13	:	Data taken from Hertzberg [29]

Appendix A

Laplace equation

The derivatives of the complex function f w.r.t. x_1 and x_2 are calculated first. After using the Cauchy-Riemann equations and a second derivation w.r.t. x_1 and x_2, it follows that the real part of the complex function f satisfies the Laplace equations. The same can be derived for the imaginary part of f.

$$\left.\begin{aligned} \frac{\partial f}{\partial x_1} &= \frac{\partial f}{\partial z}\frac{\partial z}{\partial x_1} = \frac{\partial f}{\partial z} = f'(z) \\ \frac{\partial f}{\partial x_2} &= \frac{\partial f}{\partial z}\frac{\partial z}{\partial x_2} = i\frac{\partial f}{\partial z} = if'(z) \end{aligned}\right\} \quad \rightarrow \quad f'(z) = \frac{\partial f}{\partial x_1} = -i\frac{\partial f}{\partial x_2} \quad \rightarrow$$

$$\frac{\partial \phi}{\partial x_1} + i\frac{\partial \zeta}{\partial x_1} = -i\left(\frac{\partial \phi}{\partial x_2} + i\frac{\partial \zeta}{\partial x_2}\right) = \frac{\partial \zeta}{\partial x_2} - i\frac{\partial \phi}{\partial x_2}$$

Cauchy-Riemann equations

$$\frac{\partial \phi}{\partial x_1} = \frac{\partial \zeta}{\partial x_2} \qquad \text{and} \qquad \frac{\partial \zeta}{\partial x_1} = -\frac{\partial \phi}{\partial x_2} \quad \rightarrow \quad \frac{\partial \phi}{\partial x_2} = -\frac{\partial \zeta}{\partial x_1} \quad \rightarrow$$

$$\frac{\partial^2 \phi}{\partial x_1^2} = \frac{\partial \zeta}{\partial x_1 \partial x_2} \qquad ; \qquad \frac{\partial^2 \phi}{\partial x_2^2} = -\frac{\partial \zeta}{\partial x_1 \partial x_2} \quad \rightarrow$$

$$\frac{\partial^2 \phi}{\partial x_1^2} + \frac{\partial^2 \phi}{\partial x_2^2} = 0$$

Appendix B

Derivatives of Airy function

The general solution of the complex bi-harmonic equation is an expression for the Airy function in terms of complex functions.

$$\psi = \tfrac{1}{2}\left[\bar{z}\Omega + z\bar{\Omega} + \omega + \bar{\omega}\right]$$

The derivatives w.r.t. the complex variables z and $\bar{z}$ can be determined.

$$\begin{aligned}
\frac{\partial\psi}{\partial z} &= \tfrac{1}{2}\left[\bar{z}\Omega' + \bar{\Omega} + \omega'\right] \\
\frac{\partial\psi}{\partial \bar{z}} &= \tfrac{1}{2}\left[\Omega + z\bar{\Omega}' + \bar{\omega}'\right] \\
\frac{\partial\psi}{\partial z\partial \bar{z}} &= \tfrac{1}{2}\left[\Omega' + \bar{\Omega}'\right] \\
\frac{\partial^2\psi}{\partial z^2} &= \tfrac{1}{2}\left[\bar{z}\Omega'' + \omega''\right] \\
\frac{\partial^2\psi}{\partial \bar{z}^2} &= \tfrac{1}{2}\left[z\bar{\Omega}'' + \bar{\omega}''\right]
\end{aligned}$$

The derivatives w.r.t. the coordinates x_1 and x_2 can now be calculated.

$$\begin{aligned}
\psi_{,1} &= \frac{\partial\psi}{\partial z}\frac{\partial z}{\partial x_1} + \frac{\partial\psi}{\partial \bar{z}}\frac{\partial \bar{z}}{\partial x_1} = \frac{\partial\psi}{\partial z} + \frac{\partial\psi}{\partial \bar{z}} \\
\psi_{,11} &= \frac{\partial}{\partial z}\left(\frac{\partial\psi}{\partial z} + \frac{\partial\psi}{\partial \bar{z}}\right)\frac{\partial z}{\partial x_1} + \frac{\partial}{\partial \bar{z}}\left(\frac{\partial\psi}{\partial z} + \frac{\partial\psi}{\partial \bar{z}}\right)\frac{\partial \bar{z}}{\partial x_1} = 2\frac{\partial\psi}{\partial z\partial\bar{z}} + \frac{\partial^2\psi}{\partial z^2} + \frac{\partial^2\psi}{\partial \bar{z}^2} \\
\psi_{,12} &= \frac{\partial}{\partial z}\left(\frac{\partial\psi}{\partial z} + \frac{\partial\psi}{\partial \bar{z}}\right)\frac{\partial z}{\partial x_2} + \frac{\partial}{\partial \bar{z}}\left(\frac{\partial\psi}{\partial z} + \frac{\partial\psi}{\partial \bar{z}}\right)\frac{\partial \bar{z}}{\partial x_2} = i\left(\frac{\partial^2\psi}{\partial z^2} - \frac{\partial^2\psi}{\partial \bar{z}^2}\right) \\
\psi_{,2} &= \frac{\partial\psi}{\partial z}\frac{\partial z}{\partial x_2} + \frac{\partial\psi}{\partial \bar{z}}\frac{\partial \bar{z}}{\partial x_2} = \frac{\partial\psi}{\partial z}i - \frac{\partial\psi}{\partial \bar{z}}i \\
\psi_{,22} &= \frac{\partial}{\partial z}\left(\frac{\partial\psi}{\partial z}i - \frac{\partial\psi}{\partial \bar{z}}i\right)\frac{\partial z}{\partial x_2} + \frac{\partial}{\partial \bar{z}}\left(\frac{\partial\psi}{\partial z}i - \frac{\partial\psi}{\partial \bar{z}}i\right)\frac{\partial \bar{z}}{\partial x_2} = 2\frac{\partial\psi}{\partial z\partial\bar{z}} - \frac{\partial^2\psi}{\partial z^2} - \frac{\partial^2\psi}{\partial \bar{z}^2}
\end{aligned}$$